NATIONAL ADVISORY COMMITTEE
FOR AERONAUTICS

TECHNICAL NOTE

No. 1040

WAKE STUDIES OF EIGHT MODEL PROPELLERS

By Elliott G. Reid
Stanford University

N A C A

Washington
July 1946

NATIONAL ADVISORY COMMITTEE FOR AERONAUTICS

TECHNICAL NOTE NO. 1040

WAKE STUDIES OF EIGHT MODEL PROPELLERS

By Elliott G. Reid

SUMMARY

The influences of shank form and pitch distribution upon the charac-
teristics of constant-speed propellers have been investigated by exploring
the wakes of eight model propellers in the Guggenheim Aeronautic Labo-
ratory of Stanford University.

The experiments show the improvement of efficiency which results
from the substitution of faired shanks for round ones to be caused by
disproportionate local augmentations of thrust and torque. It was also
found that blade shank stalling at reduced advance ratios caused adverse
effects which were amplified as the power coefficient increased.

Analysis of previous force tests in the light of wake characteristics
reveals that, for constant-speed operation, pitch should be so distributed
that no element will operate at a negative lift coefficient in high-speed
flight, that shank stalling during take-off and climb will be minimized,
and that substantial uniformity of the section lift coefficients will
prevail in normal cruising and high-speed flight. A blade twist curve
of the "envelope" type appears most suitable to these requirements.

In addition to the foregoing conclusions and the provision of a
large mass of data for strip method prediction of operating character-
istics, the investigation led to the following noteworthy findings.
The radial variation of section lift coefficient is in qualitative
accord with that of the geometric angle of attack, and the average
section lift coefficient at which maximum efficiency is attained in-
creases with pitch. Abnormally large lift coefficients are attained
by slightly cambered shank elements; this is ascribed to the action
of a highly favorable radial pressure gradient upon their boundary
layers. Finally, Glauert's prediction of the independence of blade
elements is substantially confirmed in so far as twist is concerned,
but his momentum-vortex theory is found unsatisfactory for the accu-
rate prediction of propeller characteristics from airfoil section data.

INTRODUCTION

The investigation covered by this report was carried out under a contract with the National Advisory Committee for Aeronautics, "...to determine, by means of wake surveys, the nature of the influence of shank form and pitch distribution upon the characteristics of constant-speed propellers, and to provide data for strip method prediction of operating characteristics."

More specifically, it was directed toward determination of the underlying causes of significant differences between the operating characteristics of previously tested model propellers (reference 1) which differed only in shank form and pitch distribution. Further, it extended the range of propeller wake measurements to pitch angles greater than any heretofore explored, enable correspondingly extensive determination of the lift coefficients at which blade elements operate and, through analysis of the results, shed new light upon some basic concepts of modern propeller theory.

SYMBOLS

B number of blades

D diameter, feet

R tip radius, feet

r radius of element, feet (See also a below.)

x radius ratio, r/R

b chord of element, feet

h maximum thickness of element, feet

β pitch angle of element, degrees (reference - chord line)

β' pitch angle of element, degrees (reference - lift axis)

β_T' pitch angle of tip element, degrees

Φ effective angle of advance, degrees (See diagram B, p. 14.)

Φ_o geometric angle of advance, degrees ($\Phi_o = \tan^{-1} V/2\pi nr$)

2

α effective angle of attack, degrees $(\alpha = \beta - \Phi)$

α' geometric angle of attack, degrees   (reference - lift axis; $\alpha' = \beta' - \Phi_o$)

α_{LO} angle of zero lift, degrees

ψ angle of yaw, degrees

V velocity, feet per second

V_s slipstream velocity, feet per second

V_r resultant velocity of element, feet per second

u axial component of V_s

w tangential component of V_s

a coefficient of induced axial velocity   (Note: $1 + a = r$)

a' coefficient of induced tangential velocity

ρ air density, slugs per cubic foot

σ relative air density, ρ/ρ_o

M mass flow per unit time, slugs per second

$q = \rho V^2/2$ $q_s = \rho V_s^2/2$ $q_r = \rho V_r^2/2$ $q_w = \rho w^2/2$ $E = q_w/q$

ω angular velocity, radians per second

n rotative speed, revolutions per second

V/nD advance ratio

p_o static pressure at upstream face, lb/ft^2

p_1 static pressure at downstream face, lb/ft^2

Δp increase of static pressure $(p_1 - p_o)$, lb/ft^2

p_{to} total pressure in undisturbed stream, lb/ft^2

p_{t1} total pressure at downstream face, lb/ft^2

3

Δp_t increase of total pressure $(p_{t1} - p_{to})$, lb/ft^2

$P_{TO} = p_{to}/q$ $\qquad\qquad$ $P_{T1} = p_{t1}/q$ $\qquad\qquad$ $\Delta P_T = P_{T1} - P_{TO}$

p_u total pressure on upstream[1] tube of yaw head, lb/ft^2

p_d total pressure on downstream[1] tube of yaw head, lb/ft^2

p_y yaw head pressure difference $(p_u - p_d)$, lb/ft^2

$P_U = p_u/q$ $\qquad\qquad$ $P_D = p_d/q$ $\qquad\qquad$ $P_Y = p_y/q$

K yaw head constant $(K = P_Y/\sin 2\psi)$

S.P. static plate pressure difference, lb/ft^2 $\quad$ $(q = 1.0525$ S.P.$)$

T thrust, pounds

Q torque, pounds feet

P power input, foot-pounds per second

C_T thrust coefficient, $T/\rho n^2 D^4$ $\quad$ $(C_T = C_{TO} - \Delta C_T)$

C_{TO} integrated thrust coefficient $\left(C_{TO} = \int_{0.15}^{1.0} (dC_T/dx)\, dx\right)$

ΔC_T spinner thrust coefficient (negative) $\quad$ (Also used to denote error
$\qquad$ in thrust coefficient - fig. 11)

C_Q torque coefficient, $Q/\rho n^2 D^5$ $\left(C_Q = \int_{0.15}^{1.0} (dC_Q/dx)\, dx\right)$

η efficiency $(C_T V/C_P n D)$

dT thrust of all elements at radius r, pounds

dQ torque of all elements at radius r, pounds feet

dT' thrust of element, pounds

---

[1]With reference to tangential velocity normally imparted to slip-
stream.

dF_Q' tangential force on element, pounds

dL' lift of element, pounds

dD' drag of element, pounds

dR' resultant force on element, pounds

c_L section lift coefficient, $dL'/q_r b d r$

MODELS

Eight of the previously tested series of thirteen models[1] were selected for wake survey studies. All of them have adjustable-pitch, duralumin blades of 2.80-foot diameter. Their geometric characteristics are defined by figures 1 to 4; the following particulars are worthy of note:

Four-Blade Models

Model P.- A conventional type blade of uniform geometric design pitch $(\beta_{0.75R} = 24°)$ with relatively wide tip and so-called round shank. Attention is called to the measurement of β with reference to the nominal chord line and to the fact that degeneration of the airfoil profile into a circular cylinder is complete only at the innermost section of the blade (see figs. 1 and 2).

Model P_C represents Model P equipped with a cuff of Clark Y profile; the geometric pitch of the cuff is the same as that of the outer portion of the blade.

Model P_{CH} represents Model P equipped with a refined Clark Y cuff which has smaller radial and chordwise dimensions than those of P_C and incorporates a washout of 12°. (Note: Washout specified is that at spinner surface.)

Model P_{C2} has the same plan form and profiles, outboard of the cuff, as Model P, but has a larger design pitch $(\beta_{0.75R} = 30°)$, and an unusually thin cuff in which NACA series 16 profiles and a washout of 10° are incorporated.

---

[1] Force tests reported in reference 1.

Three-Blade Models

Model U-24 has the same plan form and profiles as Model P_{C2}. Its uniform design pitch (measured with reference to the lift axes, or "no lift lines" of the profiles) is characterized by $\beta'_{0.75R} = 24^\circ$.

Model U-60 is also of uniform design pitch and differs from U-24 only in having $\beta'_{0.75R} = 60^\circ$.

Model 0.4E has the same plan form and profiles as the U-models but is of non-uniform design pitch. The ordinates of its twist curve (see fig. 4) are 0.4 times those of the "envelope twist curve."[1]

Model 0.8E is also of non-uniform design pitch and differs from Model 0.4E only in having a twist curve whose ordinates are 0.8 times those of the envelope curve.

The hubs of all models were enclosed within a spinner of the form illustrated by figure 5.

APPARATUS AND TECHNIQUE

The experiments were carried out in the 7.5-foot wind tunnel of the Guggenheim Aeronautic Laboratory at Stanford University where the models were driven by the dynamometer ordinarily used for force tests. A description of this equipment will be found in reference 2.

The wake survey apparatus installed in the wind stream consisted of the two banks of yaw heads shown in figure A. Details of the heads are illustrated by figure B and the manometer used to record the pressures may be seen in figure C.

To make the obstruction offered by the supporting structure symmetrical, the yaw heads were arranged in two banks which extended vertically above and below the propeller axis. The dimensions and locations of the heads may be seen in figure 5 where it will be noted that they are numbered in the order of increasing radii. Those numbered 1 to 10 were located at the mean radii of annular rings of equal area;

---

[1] Note: The envelope of the twist curves of all uniform design pitch blades is defined by the equation

$$\beta' - \beta_T' = \cot^{-1}\sqrt{r/R} - \tan^{-1}\sqrt{r/R}$$

those numbered 0 and 11 were arbitrarily located close to the spinner and just outside the blade tips. As shown in figure 5, the tips of all yaw heads were 0.05D aft of the plane of the blade axes; this location was fixed by the necessity of providing a small clearance for Model P_C - which has the widest cuff.

Except for the incorporation of shielded total head tubes, the yaw heads used in this investigation closely resemble the British type whose development is described in reference 3. Although this type has been used in at least one previous American investigation (reference 4), it was found impossible to obtain satisfactorily linear yaw calibration characteristics when the tips of the tubes were beveled to sharp edges; the final calibration data shown in the left-hand chart of figure 6 were obtained only after the tips had been blunted to the extent illustrated by the enlarged section of figure 5. It will be noted that although the yaw characteristics are substantially unaffected by changes of airspeed, the calibration constants (K) for the various heads differ somewhat. Since these differences bear no evident relation to the local variations of total pressure (P_{TO} - see right-hand chart of fig. 6), they are believed to reflect minute differences between the forms of individual heads.

The calibration curves for the total head tubes (fig. 6) represent, actually, the results of total pressure surveys along the vertical diameter of the stream. These were carried out in the presence of the dynamometer and spinner and the blade apertures in the spinner were, of course, covered while the surveys were being made. If it be assumed that the variations of total and dynamic pressures are identical, these results indicate variations of approximately ±1.1 percent V ($\pm$ 2.2 percent q) at all but the lowest speeds where a slightly greater variation is evident. Yaw tests of the total head tubes were extended only to ± 45° but, within that range, no measurable variation of the registered total pressures was observed. (It may be worth noting that isolated tubes of this kind are entirely reliable up to ± 60°.)

The yaw and total head tubes were connected to a multiple manometer (with common cistern) whose column heights were recorded by means of a 35-millimeter camera. Additional connections enabled the recording of a pressure difference (SP) proportional to the dynamic pressure and of a predetermined pressure difference (usually 10 lb/sq ft) which was imposed by a double bell-jar balance. The former had the effect of making the records non-dimensional by defining q as a head of the same liquid as that used to measure the yaw and total pressures while the latter provided a dimensional pressure scale which enabled checking of the photographically recorded values of SP against those observed by the tunnel operator. Damping sufficient to make the meniscus velocity proportional to the applied pressure difference - rather than to the square root of that quantity - was incorporated in each pressure transmitting line and uniformity was obtained by the adjustment of individual dampers.

Specially constructed projection and measuring apparatus eliminated several steps from the usual process of reducing film records to pressure ratios. The records were projected upon a ground glass screen and measured by means of a vernier height gage which could be traversed along a precision straightedge. Convenient control of the enlargement ratio made it possible to use fixed scales for direct measurement and recording of the heads as multiples of the dynamic pressure, regardless of the absolute value of q.

Only one at all serious inconvenience was encountered in the use of this apparatus; it arose out of the sensitivity of the yaw heads. After the initial adjustment, slight inequalities of the pressures experienced by the two tubes of a given yaw head were sometimes detected in the preliminary run made without model before each test. To re-establish balance, the tube shanks were bent by hand — but the deformations required were so small that a dial indicator had to be used for their measurement. Early detection and constant surveillance precluded appreciable errors from this cause but it is mentioned as a basis for the recommendation that construction of the same type be avoided in the assembly of future yaw heads because it is believed that temperature and vibration effects upon unrelieved stresses in the soldered assemblies probably contributed substantially the unbalance developed by the heads used in this investigation.

TEST PROGRAM

In this wake investigation, all models were tested under the same conditions which prevailed during their previous force tests (reference 1). A constant rotative speed was maintained throughout each test and the advance ratio was varied by altering the airspeed. Listed below are the blade angles[1] and corresponding rotative speeds at which each model was tested:

Four-Blade Models

$\beta_{0.75R}$ (deg)	20	30	40	50	60
Revolutions per minute	2100	1740	1314	996	744

Three-Blade Models

$\beta_{0.75R}$ (deg)	12	24	36	48	60
Revolutions per minute	2100	2100	1470	1056	744

[1] Nominal angles, β ; reference - arbitrary chord line.

The number of advance ratios at which wake survey records were
taken varied with the pitch setting; only 6 or 7 records were taken
when $\beta_{0.75R} = 12°$ but 13 to 15 were made at the 60° settings.

Preliminary tests were made to determine the effect of presence
of the survey apparatus upon the performance characteristics of the
models; none was found. After completion of the test program, auxiliary
experiments were made with the yaw heads moved farther downstream to
explore the possibility of making dependable surveys under conditions of
stalled blade operation.

REDUCTION OF DATA

A sample record is reproduced as figure D. The datum with reference
to which all pressures were measured was the level of the column actuated
by the pressure at the upstream (higher pressure) static orifice in the
tunnel entrance cone. As previously stated, pressures were read directly
from the projected records as multiples of the dynamic pressure. From
the total pressures in the slipstream, P_{T1}, the corresponding free
stream values, P_{TO} (from fig. 6), were subtracted to obtain the changes
of total pressure, ΔP_T, due to propeller action. Since the yaw head
pressures were balanced in the free stream, the pressure differences due
to obliquity of the slipstream were obtained directly as $P_U - P_D = P_Y$.
These recorded values and differences, for the record shown in figure D,
will be found in the upper part of the sample computation form which is
reproduced as figure 7.

Torque Coefficients

The method used for evaluating the elementary torque coefficients, al-
though described elsewhere (reference 3), is developed here for the sake
of completeness and for convenience of reference in the subsequent treat-
ment of thrust. If the elements of a propeller at radius r impart the
tangential velocity w to the mass of air dM which, in unit time, passes
through the annulus swept by these elements, they experience the torque

$$dQ = rw\,dM \qquad (1)$$

If u is the axial velocity through the propeller

$$dM = 2\pi \rho u r\,dr \qquad (2)$$

whence

$$dQ = 2\pi\rho uwr^2 dr \tag{3}$$

Introducing $x = r/R$ and $R = D/2$,

$$r = Dx/2 \qquad dr = Ddx/2 \tag{4}$$

Substitution of these values in (3) gives

$$dQ = \frac{\pi}{4}\rho uwD^3 x^2 dx \tag{5}$$

Now, the pressure difference experienced by a yaw head of the type used in these experiments is proportional to the dynamic pressure of the slipstream, $\rho V_s^2/2$, and to the sine of twice the angle of yaw; that is,

$$p_y = K\left(\rho V_s^2/2\right)\sin 2\psi \tag{6}$$

(Note: The calibration of such heads is accomplished by measuring p_y at a series of angles of yaw in a stream of known direction and dynamic pressure. Thus K is determined as $K = p_y/q \sin 2\psi$).

By substituting $2 \sin\psi \cos\psi$ for $\sin 2\psi$, (6) may be written as

$$\rho\left(V_s \sin\psi\right)\left(V_s \cos\psi\right) = \frac{p_y}{K} \tag{7}$$

If the axis of the yaw head is parallel to the direction of undisturbed flow and if u and w are, respectively, the axial and tangential components of the slipstream velocity to which the yaw head is exposed,

$$u = V_s \cos\psi \quad \text{and} \quad w = V_s \sin\psi \tag{8}$$

whence

$$\rho uw = \frac{p_y}{K} \tag{9}$$

The substitution of this relationship in (5) yields the result

$$dQ = \frac{\pi}{4}\left(\frac{p_y}{K}\right)D^3 x^2 dx \tag{10}$$

The corresponding torque coefficient is

$$dC_Q = \frac{dQ}{\rho n^2 D^5} = \frac{\pi x^2}{4\rho n^2 D^2}\left(\frac{p_y}{K}\right)dx \qquad (11)$$

Multiplying numerator and denominator by twice the square of the undisturbed stream velocity, $2V^2$, yields

$$dC_Q = \frac{\pi x^2}{8}\left(\frac{2}{\rho V^2}\right)\left(\frac{V}{nD}\right)^2\left(\frac{p_y}{K}\right)dx \qquad (12)$$

If, now, the yaw head pressure difference is expressed in terms of the dynamic pressure of the undisturbed stream - that is, $P_Y = p_y/(\rho V^2/2)$ - the expression for the elementary torque coefficient assumes the form

$$\frac{dC_Q}{dx} = \frac{\pi x^2}{8}\left(\frac{V}{nD}\right)^2\left(\frac{P_Y}{K}\right) \qquad (13)$$

which was used in the computation. (See fig. 7.)

Thrust Coefficients

In developing an expression for the elementary thrust coefficient, it should be remembered that the accepted concept of screw propeller action is that as the air passes through the plane of the blades, it experiences a change of static pressure and undergoes tangential acceleration while its axial velocity remains unchanged. Therefore, if the blade elements which have the radius r change the static pressure of the air upon which they act by the amount Δp, they experience the thrust

$$dT = 2\pi r \Delta p \, dr \qquad (14)$$

Substituting for r and dr in accordance with (4) gives

$$dT = \left(\frac{\pi D^2 x}{2}\right)\Delta p \, dx \qquad (15)$$

The corresponding thrust coefficient is

$$dC_T = \frac{dT}{\rho n^2 D^4} = \left(\frac{\pi x}{2\rho n^2 D^2}\right)\Delta p \, dx \qquad (16)$$

Multiplying and dividing by twice the square of the undisturbed velocity, $2V^2$, gives

$$dC_T = \frac{\pi x}{4} \left(\frac{V}{nd}\right)^2 \left(\frac{2\Delta p}{\rho V^2}\right) dx \qquad (17)$$

and if ΔP is now substituted for $\Delta p/(\rho V^2/2)$, the elementary thrust coefficient is

$$\frac{dC_T}{dx} = \frac{\pi x}{4} \left(\frac{V}{nD}\right)^2 \Delta P \qquad (18)$$

In previous slipstream investigations which involved only propellers of relatively low pitch (e.g., references 3, 4, and 5) it has been customary to neglect the difference between the increases of static and total pressures, that is, to accept the approximation

$$\Delta P_T \doteq \Delta P \qquad (19)$$

for use in equation (18). The errors inherent in this method were, in these earlier experiments, minimized somewhat by failure of the unshielded total head tubes to experience full total pressure when exposed to oblique flow. In the present studies, however, it was feared that the larger tangential velocities created by the high-pitch models might lead to serious errors if this approximation were retained and it was therefore decided to use shielded total head tubes for reliable determination of the total pressures and to calculate ΔP from these and other available data.

In appendix A, it is shown that

$$\Delta P = \Delta P_T - E \qquad (20)$$

in which

$$E = \frac{1}{4r^2} \left(\frac{P_Y}{K}\right)^2 \qquad (21)$$

and, if uniform axial inflow is assumed, that

$$r = \frac{1 + \sqrt{1 + \frac{8C_T}{\pi} \left(\frac{nD}{V}\right)^2}}{2} \qquad (22)$$

12

(It should be noted that in these equations $r = 1 + a.$) Application of these relationships to the slipstream survey data, alone, would have made calculation of the elementary thrust coefficients prohibitively laborious because a process of successive approximations would have been required for the evaluation of r.[1] This method was actually applied to the results of a few tests but, fortunately, it was found that the values of r so obtained differed negligibly, if at all, from those computed by substituting in (22) values of C_T (for the same advance ratios) taken from the force test data of reference 1.

The values of r used in the routine calculations of dC_T/dx were therefore determined by the substitution of force-test values of C_T in equation (22). (Actually they were read from a curve of r versus $C_T (nD/V)^2$ which was prepared for the purpose.) The values of E, ΔP and dC_T/dx were then calculated by means of equations (21), (20), and (18), respectively. These steps are summarized at the bottom of the computation form, figure 7.

Section Lift Coefficients

To supplement mere provision of the specified "data for strip method prediction of operating characteristics," the scope of this investigation was voluntarily expanded to include calculation, from these data, of values of the section lift coefficients for elements of several models under various operating conditions. As the results of these calculations are presented and discussed later in this report, the method of their evaluation is outlined below.

---

[1] Procedure: Obtain first approximations of dC_T/dx by accepting (19) for solution of (18); plot and integrate to obtain first approximation of $C_T\left(C_T = \int_{0.15}^{1.0} \frac{dC_T}{dx}\ dx\right)$ and substitute this value in (22) to get first approximation of r. Use approximate value of r in (21) to evaluate E for each station, calculate corresponding ΔP's according to (20) and substitute them in (18) to obtain second approximations of dC_T/dx. Repeat process until no change in r is found.

The following analysis is made in accordance with the basic form of Glauert's momentum-vortex theory (reference 6), in which a propeller of finite solidity is assumed to have infinitely numerous blades. Accordingly, the induced velocities at a given radius are assumed to be one-half the final (far downstream) values of the axial and tangential velocities which would be imparted by the blade elements at that radius to the cylindrical shell of air upon which they act. Finite induced angles of attack therefore arise from the two-dimensional[1] motion of a finite mass of air, that is one whose dimension normal to the span[1] is equal to the circumference of the cylindrical shell. Thus the influences of elements at one radius upon those at another, as well as those of the finite number of blades and of flow around the blade tips, are excluded from consideration.
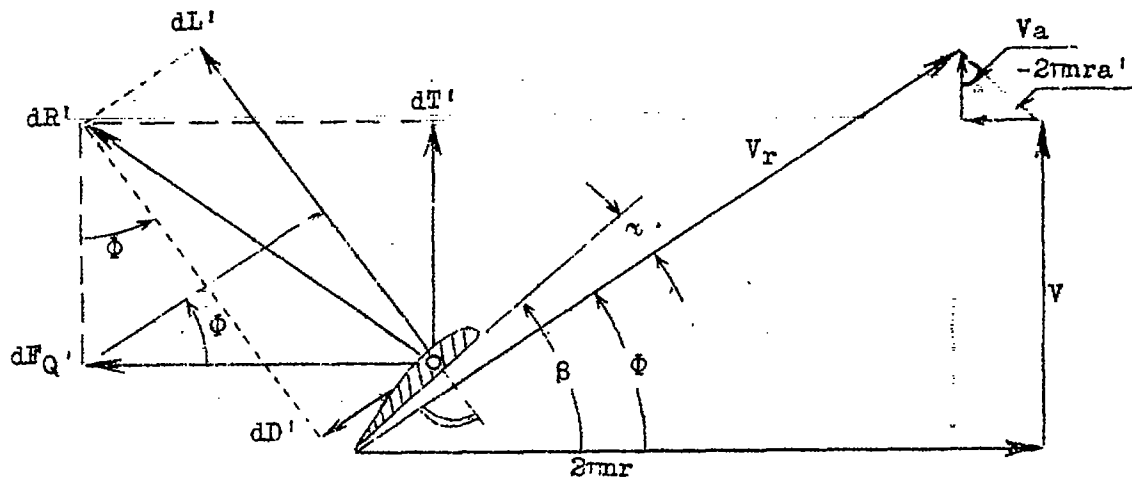

Diagram E

The lift of the blade element illustrated above is

$$dL' = dT' \cos \Phi + dF_Q' \sin \Phi \tag{23}$$

or

$$\frac{dL'}{dr} = \frac{dT'}{dr} \cos \Phi + \frac{dF_Q'}{dr} \sin \Phi \tag{24}$$

Primes are used to distinguish the forces which act upon an element of a single blade from the sums of such forces for all elements which have the same radius. The section lift coefficient is

$$c_L = \frac{dL'}{q_r dS} = \frac{2}{\rho V_r^2 b} \left(\frac{dL'}{dr}\right) = \frac{2}{\rho V_r^2 b} \left[\frac{dT'}{dr} \cos \Phi + \frac{dF_Q'}{dr} \sin \Phi \right] \tag{25}$$

wherein dS is the elementary area, q_r the dynamic pressure corresponding to V_r, and b the blade width. According to (4), $dr = Ddx/2$, whence

$$\frac{dT'}{dr} = \frac{dT'}{dx} \times \frac{2}{D} \quad \text{and} \quad \frac{dF_Q'}{dr} = \frac{dF_Q'}{dx} \times \frac{2}{D} \tag{26}$$

The substitution of these values in (25) gives

$$c_L = \frac{4}{\rho V_r^2 bD} \left[\frac{dT'}{dx} \cos \Phi + \frac{dF_Q'}{dx} \sin \Phi \right] \tag{27}$$

Remembering, now, that the elementary thrust and torque coefficients dC_T/dx and dC_Q/dx are deduced from slipstream pressures produced by the action of all the blade elements located at the radius x, it will be evident that, in the case of a propeller which has B blades, the forces on a single element are

$$\frac{dT'}{dx} = \frac{dC_T}{dx} \frac{\rho n^2 D^4}{B} \quad \text{and} \quad \frac{dF_Q'}{dx} = \frac{dC_Q}{dx} \frac{\rho n^2 D^5}{rB} \tag{28}$$

Thus (27) may be rewritten as

$$c_L = \frac{4}{\rho V_r^2 bD} \times \frac{\rho n^2 D^4}{B} \left[\frac{dC_T}{dx} \cos\Phi + \frac{dC_Q}{dx} \times \frac{D}{r} \sin\Phi \right] \qquad (29)$$

The substitution of $V(1 + a)/\sin\Phi$ for V_r and of $2/x$ for D/r now yields the equation

$$c_L = \frac{4}{B} \frac{\sin^2\Phi}{(b/D)(1 + a)^2 (V/nD)^2} \left[\frac{dC_T}{dx} \cos\Phi + \frac{dC_Q}{dx} \times \frac{2}{x} \sin\Phi \right] \qquad (30)$$

which was used for the calculation of section lift coefficients.

Given the number of blades (B), the location and width of the element $(x, b/D)$, and the corresponding reduced test data $(V/nD, dC_T/dx, dC_Q/dx)$, calculation of the section lift coefficient by means of (30) becomes possible upon the determination of a and Φ. The methods used to evaluate these quantities are described in appendix B.

RESULTS

The results of the entire program of tests, comprising some four hundred separate surveys, were plotted, first, in the form illustrated by figures 8, 9, and 10. When curves of dC_T/dx and dC_Q/dx versus x were faired through the individual sets of points obtained from the upper (odd numbered) and lower (even numbered) banks of yaw heads, it became apparent that the two groups of data exhibited systematic differences which increased with the pitch angle. As it appeared that such differences could logically be ascribed only to slight non-uniformity of velocity of the undisturbed stream, mean curves were constructed as the best possible representation of the average radial distributions of the elementary thrust and torque coefficients. Space limitations prevent the reproduction of more than these samples of the individual grading curves but the ordinates of all the mean curves are presented later in condensed charts.

A comparison of the results of wake surveys and force tests is prefaced by figure 11 which illustrates the importance of taking tangential velocities into account when evaluating the elementary thrust coefficients and also reveals the remarkable sensitivity of the survey-determined thrust to small errors of total pressure measurement.

16

"In figures 12 to 19, the results of the wake surveys are compared with those of previous force tests of the same models. The point values shown on these charts were determined by mechanical integration of the areas under the mean thrust and torque grading curves and correction of the thrust coefficients for spinner drag. (Method of correction and experimental data on spinner drag will be found in appendix C.)

The basic data from which these summary charts were prepared are presented in figures 20 to 35. Each even-numbered figure in this group contains curves of dC_T/dx versus V/nD for all stations and all pitch settings of a particular model; the following odd-numbered figures present the corresponding torque data. The spotted ordinates are those of the mean thrust and torque grading curves. Because the scales of these figures are necessarily such as to preclude very accurate reading of the ordinates of the torque curves for the smaller pitch settings, numerical values of dC_Q/dx for all advance ratios at which tests were made with pitch settings of 12°, 20°, and 24° have been tabulated in table I.

From the basic data, thrust and torque grading curves for various models have been prepared for purposes of comparison under different conditions of operation; these, along with other deduced curves (figs. 36 to 49) will be introduced in the discussion which follows.

The results of preliminary and auxiliary tests are presented in figures 50 and 51.

DISCUSSION

General Features - Comparison with Force Tests

The general character of the results may best be appreciated by following through the development of a typical set. For this purpose the data and calculations tabulated in figure 7 will serve as a starting point; these results were obtained by testing Model 0.8E, with blades set at 36°, at an advance ratio of 0.985.

The thrust and torque grading curves defined by the calculated values of dC_T/dx and dC_Q/dx appear in figure 9 as the charts designated "$V/nD = 0.985$"; in the same figure are similar curves for other advance ratios. Figures 8 and 10 are analogous illustrations for pitch angles of 12° and 60°. The point values of C_T and C_P shown in figure 19 were obtained by the integration of "mean line" grading curves such as those of figures 8, 9, and 10.

17

In figures 8 to 10, it will be noted that discrepancies between the data obtained from heads of the upper and lower groups grow larger as the pitch and, consequently, the advance ratio for unstalled operation, increase. It is this fact which points to non-uniformity of tunnel velocity distribution as the cause of divergence. Lest it be imagined that such discrepancies reflect excessive irregularity of stream velocity, the following analysis, based on simple blade element theory, is presented to demonstrate the fallacy of such an inference.

Taking the value of $\beta'_{0.75R}$ as 63° and the advance ratio for peak efficiency as 3.50 when the nominal pitch setting is 60°, the corresponding values of ϕ_0 and α' are found to be 56.08° and 6.92°, respectively. (Induced velocities have been ignored in making these calculations.) If it is also assumed that at opposite points on the path of this element the local stream velocities are 0.99 and 1.01 times the mean value, the corresponding angles of attack are found to be 7.18° and 6.65°. Since the elementary forces and, therefore, the gains of total pressure in the wake may be expected to vary proportionally, it is seen that a velocity variation of ± 1 percent may be expected to result in a discrepancy of the order of $(7.18/6.65 = 1.08)$ 8 percent between the elementary forces deduced from head measurements made on opposite radii.

It is also worth noting that if a constant mean angle of attack is maintained by simultaneously varying the pitch angle and advance ratio, the discrepancy between the two sets of observations - made on opposite radii and in the presence of a velocity difference of fixed percentage - may be expected to become larger as the advance ratio increases. This is true because the deviation of the instantaneous angle of attack from its mean value is, under these conditions, roughly proportional to the angle of advance.

Another related consideration of equal, if not greater, consequence is illustrated by the curves (B) of figure 11. Reference to the formula used for computing the values of dC_T/dx (fig. 7) shows that if the increase of total pressure were to remain a fixed multiple of q, that is, $\Delta P_T = $ constant, the elementary thrust coefficient would vary with $(V/nD)^2$. Therefore, with fixed accuracy of manometer record measurement (in percent q), the total thrust becomes increasingly sensitive to sensitive to least count errors as the advance ratio increases. The curves of figure 11 illustrate the changes in apparent thrust coefficient (ΔC_T) which would result from errors in location of the total pressure datum (ϵ) which amount to only $0.005q$ and $0.01q$, the accuracy with which the records could be measured at the pitch settings indicated along the curves. The overlapping ranges result from the use

of the different rotative speeds for tests at different pitches and the fact that the limits of measurement were fixed by the absolute values of the dynamic pressure.

This situation obviously presents a serious obstacle to the attainment of high accuracy in surveys made behind propellers of high pitch and, in view of the magnitude of ΔC_T shown in figure 11, the degree of agreement between force and survey results actually attained under such conditions (figs. 12 to 18) appears gratifying rather than disappointing. In fact, the absence of serious scattering among the survey thrust points in the unstalled ranges of high V/nD operation is believed to indicate that the effective accuracy of total pressure determination must have been considerably superior to that which would correspond to an average error equal to the least count of the record measuring apparatus. However, this very fact directs attention to certain systematic differences between force and wake survey test results which will be discussed later.

Reference to figures 12 to 18 will reveal that the agreement between the results of wake surveys and force tests is excellent for pitch settings up to about 36° but that it begins to deteriorate as this angle is exceeded. The greatest divergence occurs in the case of the thrusts of fully stalled blades; it will be noted that although the surveys account for only a small part of the thrust measured under this condition, the corresponding power coefficients are erroneously large. As incipient divergence may be seen in the lowest V/nD range even when the pitch angles are as small as 20°, it is evident that angle of attack rather than pitch angle is the controlling factor. It is thus quite clear that the apparatus and methods used in this investigation yield seriously erroneous results under the conditions of stalled operation.

At this point, attention is called to the results of preliminary tests which are presented in figure 51. There it may be seen that not even the stalling characteristics of a very high-pitch model are appreciably influenced by the presence of the survey apparatus.

Since the values of $d\,c_p/dx$ calculated from given wake data vary with $1/K$ (see equation 13), the erroneously large power coefficients deduced from stalled-blade data probably reflect a substantial augmentation of the yaw head calibration constants at large angles of yaw. This explanation is suggested by the upward trend of the values of K which may be seen in several of the charts of figure 6 and by the fact that if P_y were to remain finite and positive until $\psi = 90°$, K would then become infinite because $\sin 2\psi = 0$. More extensive calibration data would be required to verify this hypothesis but the occurrence of very large instantaneous values of ψ in the wakes of stalled models has been demonstrated by the behavior of tufts.

Supplementary tests made in an effort to determine the cause of the thrust discrepancies indicate that even heads of the shielded type are incapable of measuring the true mean total pressures when the survey tubes are installed at very small distances behind a stalled propeller. This is deduced from the data presented in figure 51; the improved agreement, in the case of torque as well as thrust, obtained by moving the heads downstream is interpreted as the result of rapid decay of the pressure and directional disturbances which are, of course, most intense immediately behind the blades (see figs. 2 and 3, reference 3). Previous investigators (references 3 and 4) have stressed the importance of locating survey heads as close to the propeller as possible; it now appears that, except for the slight uncertainty introduced by slipstream contraction, such close proximity is highly undesirable.

Method of Comparing Performance Characteristics

As the merits of various blade forms are to be appraised from the viewpoint of the constant-speed propeller, which necessarily operates over broad ranges of pitch, power coefficient, and advance ratio, it will be necessary to define, at the outset, the conditions under which comparisons of performance characteristics are to be made. Typical high-speed and climbing flight conditions are defined by Lines I and II, respectively, in figure 36.

Line I is actually a rectilinear approximation of the (very slightly curved) curves of C_p versus V/nD for the condition of maximum efficiency for all of the blade forms tested. The parallel Line II defines values of V/nD which, at equal values of C_p, are 0.6 of those for Line I. These are the same conditions of comparison which were utilized in discussion of the previous force tests reported in reference 1; definitive coordinates of the two lines are:

	C_p	V/nD	C_p	V/nD
Line I	0.05	0.90	0.50	2.85
Line II	.05	.54	.50	1.71

Most of the comparisons to be discussed below involve combinations of pitch angle and advance ratio which did not occur in the test program. Therefore, the thrust and torque grading curves for such conditions were determined by a process of interpolation which was, necessarily, somewhat involved; its principal features are illustrated by figure 36(a). The ordinates of the thrust grading curves in the

lower part of this figure were taken from figure 28; the advance ratios
at which they were read correspond to the intersections of Line I with
the C_p versus V/nD curves for the several test pitch settings as
determined by the force tests of reference 1. The contour chart
which constitutes the upper part of the figure was constructed from
these grading curves and reconciled with the cross-faired curves
(not shown) of dC_T/dx versus β for fixed values of x. The thrust
grading curves for the desired intermediate pitch settings and advance
ratios - which correspond to the attainment of predetermined values
of C_p under the conditions defined by Line I - were constructed
by simply plotting the values of the contours at their intersections
with proper lines of β = constant (broken lines). The values of β
used for such interpolation were also taken from previous force test
data (see figs. 34 and 35, reference 1). The same method was applied
to the torques.

Effects of Shank Form

The changes of thrust and torque caused by enclosing round blade
shanks with cuffs of airfoil profile are illustrated by figures 37 and
38. In examining these curves, it should be noted that they represent
the effect of adding cuffs while the pitch and advance ratio remain
unchanged; in the case of such a basic change of form, this is be-
lieved to give a more significant portrayal of the results than would
a comparison predicated upon the absorption of given amounts of power
at equal values of V/nD.

It will be seen at once that the addition of cuffs has little or
no effect upon the forces experienced by the unmodified outer portions
of the blades so long as stalling does not occur. Such discrepancies
as are apparent in the outer portions of the grading curves for pitch
settings less than 60° are small and generally consistent; it seems
likely that they are due to minor differences of blade form and chance
experimental errors. This evidence tends to verify the substantial
independence of operation of the blade elements - a simplifying
assumption of modern propeller theory which has, until now, had rather
scant experimental verification (see reference 5). It should be noted,
however, that the 60° curves of figures 38 indicate a marked influence
of cuffs upon the stalling behavior of the whole blade; while it is
recognized that these grading curves are quantitatively inaccurate,
the qualitative differences which they exhibit are too marked to admit
reasonable doubt that the stalling characteristics of the two types of
blade are quite dissimilar.

The principal effect of the addition of a cuff is seen to be a marked increase of both the thrust and torque of the inner portion of the blade. The negative thrust which characterizes the round shank is minimized when not entirely eliminated. And it requires only brief inspection to see that the thrust is augmented in considerably greater proportion than is the torque. Thus the improvement of efficiency in the unstalled range, which was demonstrated by previous force tests, is now shown to be the result of localized, rather than extensive, modifications of the thrust and torque grading curves.

The force tests of reference 1 have shown that the thickness of the cuff profile - within the range incorporated in these models - has very little effect upon efficiency in the normal operating range[1] and that the thicker cuff enjoys only a slight superiority at reduced advance ratios. There is, therefore, little cause for surprise in the absence of marked differences between the thrust and torque grading curves for such models.

In figures 39 and 40, the radial distributions of thrust and torque over thick- and thin-shank blades $(P_{CH}$ and $P_{C2})$ which have identical plan forms (but somewhat different pitch distributions - see fig. 3) are compared under six typical operating conditions, that is, at three values of C_P and at advance ratios which correspond to representative high speed (Line I) and climb (Line II) conditions of flight. These grading curves were obtained by the method illustrated by figure 36(a); the pitch settings for which the interpolations were carried out were deduced from the force test data of reference 1 by the use of an auxiliary chart similar to figure 34 of the report on that work. To enable the reader to compare the blade angles of the two models under these conditions, the deduced pitch settings are tabulated below:

<center>β at 0.75R (deg)</center>

		Line I			Line II	
C_P	(V/nD)	P_{CH}	P_{C2}	(V/nD)	P_{CH}	P_{C2}
0.1	(1.27)	29.8	29.8	(0.76)	22.2	22.3
.2	(1.80)	39.9	39.8	(1.08)	32.0	32.2
.5	(2.85)	53.7	53.4	(1.71)	48.0	48.1

---

[1]At the small Mach numbers of these tests. However, it should be appreciated that if resultant velocities at shank radii become sufficiently large, thick profiles will suffer earlier shock stalling than will similar thin ones of equal design lift coefficient.

It will be apparent, upon reference to the blade twist curves of figure 3, that the differences between the grading curves of figures 39 and 40 are in qualitative agreement with the pitch distributions of the two models, that is, larger forces are experienced by the elements which have the larger pitch angles. Thus the survey results are consistent with those of the force tests in the indication of no significant differences between the performance of models with thick and thin cuffs in the unstalled range.

Examination of the elementary thrust and torque curves for these models (figs. 24 to 27) fails to reveal significant differences of shank characteristics in the stalled range of operation. Particularly, there is little evidence of the marked difference between the stalling characteristics of thick and thin shanks to which the greater merit of the model incorporating the thick type was tentatively ascribed in reference 1. Only one set of shank element curves, those for station No. 2 $(x = 0.253)$ at $\beta_{0.75R} = 60°$, furnish definite corroboration; in this instance the thrust of the thick element (P_{CH}) substantially exceeds that of the thin one (P_{C2}) at small values of V/nD whereas their torque curves are practically indistinguishable. However, this isolated bit of evidence is so scant that such advantage as Model P_{CH} enjoys at reduced advance ratios cannot be fairly credited in greater measure to shank profile effects than to the influence of pitch distribution. It is unfortunate that two models differing only in thickness of cuff profiles were not available for test so that this question might have been definitely settled. Nevertheless, in view of the adverse effects of shank stalling which are brought out in the following section, the recommendation that shank profiles having small maximum lift coefficients be avoided would still appear warranted.

Effects of Pitch Distribution

The models selected for wake survey studies of the effects of pitch distribution were the extreme members of the uniform and non-uniform pitch series, that is, U24, U60, 0.4E, and 0.8E. Thrust and torque grading curves for these models, when operating under the six conditions selected for analysis in reference 1, appear in figures 41 and 42.

The qualitative agreement between these curves and the corresponding curves of angle of attack (figs. 37 and 38 of reference 1) would appear to have considerable significance. Comparison will reveal that the elementary thrust and torque vanish under the conditions characterized by zero values of the angle of attack and that they do so at values of x which correspond very closely to those indicated by the curves

referred to above. (It should be recalled that the angles of attack plotted in figures 37 and 38 of reference 1 are measured with reference to the lift axes (no lift lines) of the profiles and that induced velocities were ignored in their evaluation.) Further examination shows that the elementary thrust and torques of the different models attain equality under the various conditions at values of x which very closely approximate those at which the corresponding geometric angles of attack are equal. Additional evidence of correspondence will be found in the relative magnitudes of the elementary thrusts and torques at fixed values of x: they are in excellent general agreement with the magnitudes of the corresponding angles of attack.

Attention is now directed to those features of figures 41 and 42 which reveal the underlying sources of the superiority and inferiority of the various pitch distributions. The grading curves for Model 0.4L stand apart from those for the other three; they indicate that the tips are very heavily loaded and that the inner elements produce negative thrust under all conditions of normal flight operation. That both the negative loading of the shanks and excessive loading of the tips preclude the attainment of high efficiency is, of course, apparent from the viewpoint of momentum theory. The lack of sufficient twist to avoid these objectionable characteristics is thus seen to be the origin of the generally poor performance demonstrated in previous force tests of this model (see fig. 31, reference 1).

The force tests show, however, that in operation at high power input (large C_p) and reduced advance ratios, Model 0.4E is more efficient than any of the types which incorporate greater total angles of blade twist. Although the effects of such superiority would be confined to take-off and low-speed climb performance, the source of even these limited advantages deserves investigation.

None of the six sets of grading curves in figures 41 and 42 depicts a condition in which Model 0.4E outperforms the other types because the smaller of the two selected sets of advance ratios corresponds to normal, rather than to very low-speed, climb. However, it will be seen in figure 42 that as C_p increases along Line II (normal climb) the distributions of thrust and torque over the outer portions of the 0.4E blades approach those of the more conventional types while no such coalescence occurs in the inner region. This fact is even more clearly illustrated by the section lift coefficient curves of figure 47 and it is worth noting that these curves conform well with the corresponding angle of attack curves, figures 37 and 38 of reference 1.

The section lift curves for $C_p = 0.5$ and $V/nD = 1.71$ clearly indicate that the shank of Model U24 has already stalled and that those of U60 and 0.8E may be expected to do so shortly. It therefore appears reasonable to believe that as the advance ratio is reduced still more

24

and the pitch settings are further augmented as required for the main-
tenance of a constant value of C_p, the efficiencies of the conventional
shanks will deteriorate much more rapidly than will that of Model 0.4E,
while the behavior of the outer portions of all the blades will differ
very little. It thus appears that the prevention of shank stalling by
the incorporation of a relatively small angle of twist in the 0.4E blades
is responsible for the superiority of this type in the low-speed, high-
power range.

Returning, now, to consideration of the other three pitch distri-
butions for which grading curves are shown in figures 41 and 42, it
appears that under comparable operating conditions, Models 0.8E, U24,
and U60 experience loadings which differ only by small amounts and that
the mutual relationship between these differences is altered very slightly
by large changes in the conditions of operation, that is, the grading
curves are closely grouped and the spacing varies only slightly. This
is due, chiefly, to the smallness of the ordinates which necessarily
characterize small values of x. In this case, also, the section lift
coefficient curves of figure 47 give a much clearer picture of the con-
ditions which actually prevail. These curves show that under typical
high-speed operating conditions (Line I) the inner elements of Models
0.8E and U60 work at much smaller lift coefficients than do those of
Model U24. This is also true - although to a smaller degree - in climb,
so long as the advance ratio and pitch setting are not large. These
facts are in accord with the angle of attack curves of reference 1.

Since the operation of blade elements at negative lift coefficients
cannot fail to have an unfavorable effect upon efficiency, figure 47
warrants the expectation that Model U60 will be less efficient than
Models U24 and 0.8E in the high-speed (Line I) conditions which corre-
spond to $C_p = 0.05$ and 0.2. This is confirmed by the force test results
(see figs. 30 and 32, reference 1). The same criterion would indicate
the superiority of Model U24 over Model 0.8E when $C_p = 0.05$ and
$V/nD = 0.90$; the force test results in this case differ imperceptibly, al-
though a difference of the predicted sense appears at slightly greater
values of V/nD with $C_p = 0.05$ (see fig. 32, reference 1). With
$C_p = 0.2$ and $V/nD = 1.80$, the section lift coefficients of Model U24
are more nearly uniform than those of Model 0.8E but force tests show
that the efficiency of the former is negligibly superior under this con-
dition. In view of the still considerable differences between the section
lift coefficients for the shanks of the three models when $C_p = 0.50$ and
$V/nD = 2.85$, it is interesting to note that force tests revealed no ap-
preciable differences between the over-all efficiencies actually devel-
oped.

Clear-cut reasons for the relative merits of these three models (U24, U60, and 0.8E) under typical climbing conditions are obvious in only one case: that for which $C_p = 0.50$ and $V/nD = 1.71$. There it is apparent in both figures 42 and 47 that the shanks of the highly twisted blades, U24, are stalled whereas those of Models 0.8E and U60 are still operating at high lift coefficients.

In the intermediate power condition for Line II ($C_p = 0.2$), the three sets of grading curves (figs. 41 and 42) and the corresponding section lift curves (fig. 47) differ very slightly except in their innermost portions. However, the section lift curves for Models 0.8E and U24 exhibit protruding, rounded peaks which do not conform with the previously deduced curves of geometric angle of attack. It appears probable that this discrepancy is the result of incipient stalling of the outer blade elements of these two models. If so, it might be expected that their efficiencies would be adversely affected with reference to that of Model U60. Nevertheless, force tests have shown Model U24 to be definitely superior to the other two under this condition. The only explanation which would appear to be reconcilable with these facts is that the adverse effects of outer blade stalling in the case of Model 0.8E, and of reduced shank loading in the cases of both 0.8E and U60, are greater than that due to the (probably) less severe stalling of the outer portions of Model U24. The fact that the angles of attack of the outer elements of Model U24 are smaller than those of 0.8E lends support to this conjecture.

Analysis of the climbing condition characterized by $C_p = 0.05$ and $V/nD = 0.54$ is no less difficult. In this case, the loading of the shanks of Model U24 is heavier, and that of the outboard portions somewhat lighter, than is the case for the other two models. However, the section lift coefficients for the cuff elements differ widely while those for the outer elements are of the same order. The relative importance of these differences practically defies appraisal - particularly when it is realized that under this condition all three models develop approximately 90 percent of the ideal efficiency predicted by simple momentum theory (see fig. 33, reference 1; $(V/nD)\,C_p^{1/3} = 1.43$).

From the foregoing comparisons, confusing though they seem in certain instances, it is possible to deduce some facts of considerable significance. It is quite evident that for efficient constant-speed operation, blade twist should be such that shank elements will not operate at negative section lift coefficients in high-speed flight, that stalling of the shanks in take-off and low-speed climb will be minimized in so far as possible, and that substantial uniformity of section lift coefficients will prevail over the whole blade in normal cruising and high-speed flight. The desirability of uniformity is indicated by the Line I

comparisons which give evidence that the adverse effects of non-uniformity are most pronounced when the average section lift coefficient is small.

The recommendation of a blade twist curve of the "envelope" type as best suited to fulfillment of these requirements is thus in full agreement with the conclusion drawn from the force tests of reference 1.

Independence of Blade Elements

The data obtained in this investigation offer an opportunity for more extensive and thorough verification of the concept of blade element independence than has been accomplished heretofore. The results of the experiments made by Lock, Bateman, and Townend about twenty years ago (reference 5) were summarized in the statement, "The agreement with theory was good except in certain cases near the tip and boss of the airscrew," - and little or no further attention appears to have been given to the question since then. It is worth noting that these early experiments were made with blades whose twist curves deviated only slightly ($7.8°$) within the range of radii explored ($x = 0.45, 0.6, 0.75, 0.9$) and that the tests were made at small pitch settings and advance ratios ($\beta_{0.75R} = 23°$ to $33.5°$; $V/nD = 0.437$ and 0.570). Moreover, the reference to elements "near the...boss of the airscrew" is somewhat misleading because the location of the innermost element investigated was $x = 0.45$.

As all of the three-blade models involved in the present investigation were tested at the same pitch settings at $0.75R$, verification was begun by plotting the mean curve values of dC_T/dx and dC_Q/dx for station 6 ($x = 0.752$) against V/nD. The resulting curves are reproduced in figure 43. It will be seen that agreement within the unstalled range is excellent for pitch settings of $12°$ to $48°$ and that deviations among the $60°$ curves do not greatly exceed the probable limits of experimental errors. Thus, the forces which act upon the $0.75R$ element of any of these blades can be safely said to be substantially unaffected by the forces on the other elements.

To extend the verification to corresponding elements which were not set at equal pitch angles during the tests, a more complicated procedure had to be adopted. First, the values of V/nD at which certain values of dC_T/dx were attained by four elements of each of the three-blade models were read from figures 28, 30, 32, and 34 and plotted against the pitch angles of the elements in the upper charts of figure 44. (The abscissas are designated "β_e" to avoid possible confusion with nominal pitch settings at $0.75R$.) To make the comparisons complete, the

corresponding values of dC_Q/dx were read from figures 29, 31, 33, and 35 and plotted against V/nD, as shown in the lower charts of figure 44. The plotted data have been taken entirely from the unstalled ranges of operation to avoid the complication of double values. The absence of serious scattering among the points of figure 44 makes it unmistakably clear that the forces on a particular element of one of these propellers are practically unaffected by the forces on the remainder of the blade.

In this connection, however, it should be remembered that in both these and the earlier British experiments, only the effect of altering the twist, and not that of varying the plan form, has been investigated. In the somewhat analogous case of the wing, the relative influence of twist diminishes as the average section lift coefficient increases, and it would appear that a similar influence might be expected in the case of a propeller blade. If so, the interaction between adjacent elements would assume relatively large proportions only when their angles of attack were small and the resultant effects would, therefore, be of small absolute magnitude. On the other hand, the effects of plan form variations are still unexplored and, to judge by the wing analogy, it would not be surprising if verification of the concept of independent action of blade elements were to be found impossible when attempted with blades having different chord distributions.

Section Lift Characteristics

Because the data obtained in these experiments were seen to afford an unique opportunity to clarify some hitherto controversial questions of fundamental importance, the somewhat laborious task of calculating section lift characteristics for several models was undertaken with the following objectives in view:

(a) To compare the variations, with advance ratio and angle of attack, of the section lift coefficients for corresponding elements of models which differ only as regards pitch distribution and number of blades.

(b) To determine the values of the section lift coefficients which prevail under operating conditions representative of normal climbing and high-speed flight.

(c) To test the validity of Glauert's basic momentum-vortex theory by using it to deduce the values of the "effective" lift curve slopes and, by comparing them with accepted two-dimensional values, to appraise the necessity of greater theoretical refinement for the accurate prediction of propeller characteristics from airfoil section data.

28

In connection with the selection of Glauert's simplified theory as the basis for the section lift calculations, it should be noted that although this theory is strictly applicable only to the propeller with infinitely numerous blades, its adaptation to the case of one with a finite number is stated to require only very small corrections (reference 6, pp. 268, 269). It is also pointed out that while the accuracy of the deduced angles of attack may be open to some doubt (as result of the approximate method of evaluating induced velocities), no such uncertainty exists with reference to the values of the section lift coefficients themselves.[1]

The formulas required for the evaluation of the section lift characteristics have been developed in a preceding section of this report; the tabular form used for routine calculation is reproduced as table II. Illustrated there are the computations necessary for the determination of a single section lift coefficient and the corresponding angle of attack.

Calculations were made, first, for four elements $(x = 0.253, 0.520, 0.752,$ and $0.928)$ of the two three-blade models which differ most as regards pitch distribution (U24 and 0.4E); the calculations were then repeated for similarly located elements of one four-blade model (P_{C2}).[a] The results are tabulated in table II and presented as charts of c_L versus V/nD and c_L versus α in figures 45 and 46, respectively.

The section lift coefficients plotted in figures 45 were derived from wake data limited to those ranges of advance ratio within which there is reasonably close agreement between the results of force and wake survey tests. Perhaps the most striking feature of this chart is the similarity between corresponding sets of curves for the various models.[3] The close agreement between the maximum lift coefficients attained by corresponding elements, regardless of number of blades, is quite evident in the two lower rows of charts. Lack of similarity between the curves for the innermost elements $(x = 0.253)$ is, of course, the result of differences

---

[1] Because the magnitude of the resultant velocity is negligibly affected by small variations of induced velocity and the correspondingly small changes in the direction of V_r can have little influence upon the value of dL', the component of dR' which is perpendicular to V_r (see diagram E, p. 14).

[a] These three models have identical developed plan forms and incorporate the same profiles at equal radii.

[3] The use of different pitch settings in tests of three- and four-blade models should be noted.

between the distributions of pitch which diverge widely only in this region. The very peculiar shape of the 60° curve for the innermost element of Model U24 arises from the attainment of the critical angle of attack while the local pitch angle exceeds 80°.

The absence of peaks in the curves for the inner elements (x = 0.520 and 0.253) not only indicates that stalling occurs first on the outer parts of the blades but, also, that some peculiarly favorable condition must exist to permit the attainment of such abnormally large values of c_L by these sections which are not distinguished by unusual camber. All evidence points to the operation of an automatic boundary layer removal mechanism, probably the pumping of the boundary layer of the inner elements toward the region of lower pressure which exists farther outboard.

In figure 46, the section lift coefficients have been plotted against the angle of attack. Examination reveals no identifiable segregation of the points for three- and four-blade models, and the only recognizable general trend appears to be one toward slight reduction of the lift curve slope with increasing pitch. The marked increase of $dc_L/d\alpha$ from tip toward root is evident in the groups of points for the three outer stations but the values for x = 0.253 are so scattered as to make estimation difficult in that case. Maximum values of c_L (some of which are too great to permit inclusion in this chart) appear to depend markedly on pitch setting - and increasingly so as the element under consideration moves toward the hub. This fact tends to substantiate the boundary layer hypothesis previously suggested.

Another set of section lift coefficients have been calculated from the typical grading curves of figures 41 and 42; computations were made for nine stations in order that curves of c_L versus x might be well defined near the root, tip, and outer limit of the cuff. The numerical values are given in table IV and they have been plotted against radial location in figure 47, a chart which has been the subject of previous discussion. These curves are of particular interest, now, because they so clearly illustrate a basic propeller characteristic which is not generally recognized: It is the increase with pitch angle of the average section lift coefficient at which a given propeller attains maximum efficiency. Remembering that Line I very closely approximates the condition for maximum efficiency at all pitch settings, the "high speed" charts of figure 47 reveal that when $C_P = 0.05$ ($\beta_{0.75R} \doteq 23°$) the section lift coefficients average about 0.4, that with $C_P = 0.2$ ($\beta_{0.75R} \doteq 43°$) the average value increases to approximately 0.6, and that when $C_P \doteq 0.5$ ($\beta_{0.75R} \doteq 57°$) it is approximately 0.7.

It is emphasized that the foregoing values correspond to maximum efficiency and that the majority of the normal working range involves still larger angles of attack and greater values of c_L. It should therefore not be surprising to see, in the Line II charts, that section lift coefficients as great as 1.4 to 1.6 may occur in normal climb at high power. Attention is consequently called to the desirability of incorporating profiles which have relatively large design lift coefficients in the blades of propellers intended for operation at high pitch angles.

The section lift coefficients which were derived from figures 41 and 42 (table IV) and used to define the curves of figure 47 have been re-plotted against angle of attack in figure 48. Values for corresponding elements of all four of the three-blade models (U24, U60, 0.4E, and 0.8E) appear in each of the nine charts of this figure.[1] It is evident that the points for all but the two inner elements define at least the lower portions of the lift curves so well that their slopes and the angles of zero lift can be determined with considerable certainty. The values of $dc_L/d\alpha$ and of α_{LO} are plotted against x in figure 49.

In figure 49 it will be seen that, despite the similarity of shape, the differences between the calculated and experimentally determined values of α_{LO} are considerably greater than those ordinarily revealed by tests of model airfoils. Although such differences could arise entirely from profile malformations, two other potential sources of discrepancy exist in the present case; they are inaccuracies of blade twist and such errors as may be inherent in the necessarily indirect method used to determine α_{LO}. The apportioning of responsibility for these discrepancies must therefore await further analysis.

The question of the practical applicability of Glauert's theory of the idealized propeller remains to be examined. Since that analysis bases the prediction of blade element forces upon the infinite aspect ratio characteristics of the profiles, verification of its applicability would require that reversal of the process, that is, deduction of "section" lift characteristics from wake survey data, yield lift curves characterized by slopes appropriate to two-dimensional flow. The failure of the theory to yield this result will be seen in figure 49 where the lift curve slopes from figure 48 have been plotted against x. The ordinates of this curve are not only non-uniform but, with limited exception, they

---

[1]Light lines which extend from clusters of spots carry at their outer ends reference dots and small "flags" which enable the identification of points whose distinguishing symbols are obscured.

fall far short of normal infinite aspect ratio lift curve slopes
(approx. 0.10/deg). The finding of such large discrepancies clearly
demonstrates that a considerable refinement of Glauert's elementary
theory would be required for the accurate prediction of propeller
characteristics from airfoil section data.

The character and distribution of the discrepancies of lift curve
slope revealed by figure 49 indicate underestimation of the induced
velocities at nearly all radii and continuous increase of the de-
ficiency with radial distance over the outer portion of the blade.[1]
The principal source of these errors appears to be Glauert's assumption
of uniform induced velocities at all points of the annulus swept by a
given element. Such a concept cannot be reconciled with the local
augmentation of induced velocity in the neighborhood of one of the wings
of a multiplane, and it is emphasized that local augmentation would persist
even though the number of the multiplane's wings were to be increased
indefinitely while the total wing area and front view dimensions re-
mained unchanged. This analogy would lead to the anticipation of
deficiency of the induced velocities calculated by Glauert's method -
even in the case of the propeller with infinitely numerous blades.
Moreover, the deficiency might be expected to increase with radius, for
blades of normal plan form, as a result of augmentation of the analogue
of the multiplane's gap/chord ratio. The severe deficiencies of lift
curve slope (and induced velocity) near the root and tip can be logically
ascribed only to the concentration of trailing vortices in those regions.
Glauert takes cognizance of this in his "tip corrections" (for the effect
of a finite number of blades) but the application of such corrections
cannot be expected to accomplish more than elimination of the sharp
decline of lift curve slope near the tip.

In view of the evident shortcomings of Glauert's method, it would
appear logical to examine the existing discrepancies against the back-
ground of Goldstein's more elaborate theory (reference 7). This analy-
sis of the ideally loaded propeller with a finite number of blades
yields induced velocities which, over a large part of the blade - and
increasingly so toward the tip, exceed those calculated by the momentum
method of Glauert. As the deficiencies of lift curve slope revealed
by figure 49 also increase toward the tip, it is apparent that application
of the Goldstein theory to these wake survey data would have the effect
of reducing the discrepancies. And although extensive recalculation would
be required to obtain quantitative verification of the Goldstein theory

---

[1]The fact that the outer portion of this particular curve of
$dc_L/d\alpha$ versus x is quite accurately defined by the equation
$dc_L/d\alpha = 0.65 \, x^{-1/2}$ is noted, but its significance, if any, is not
apparent.

8. A more exact theory than that of Glauert is required for the accurate prediction of propeller characteristics from airfoil section data.

Stanford University,
    Stanford University, Calif., May 9, 1945.

REFERENCES

1. Reid, Elliott G.: Studies of Blade Shank Form and Pitch Distribution for Constant-Speed Propellers. NACA TN No. 947, 1945.

2. Lesley, E. P.: Tandem Air Propellers. NACA TN No. 689, 1939.

3. Douglas, G. P. and Coombes, L.P.: The Measurement of Torque Grading Along an Airscrew Blade. R. & M. No. 992, British A.R.C., 1925.

4. Stickle, George W.: Measurement of the Differential and Total Thrust and Torque of Six Full-Scale Adjustable-Pitch Propellers. NACA TN No. 421, 1932.

5. Lock, C. N. H., Bateman, H., and Townend, H. C. H.: Experiments to Verify the Independence of the Elements of an Airscrew Blade. R. & M. No. 953, British A.R.C., 1925.

6. Glauert, H.: Airplane Propellers. The Vortex Theory. Vol. IV, div. L, ch. VI of Aerodynamic Theory, W. F. Durand, ed., Julius Springer (Berlin), 1935.

7. Lock, C. N. H., and Yeatman, D.: Tables for Use in an Improved Method of Airscrew Strip Theory Calculation. R. & M. No. 1674, British A.R.C., 1935.

8. Crigler, John L.: Comparison of Calculated and Experimental Propeller Characteristics for Four-, Six-, and Eight-Blade Single-Rotating Propellers. NACA ACR No. 4B04, 1944.

APPENDIX A

Evaluation of ΔP

For the evaluation of ΔP, use is made of the relationship usually credited to Joukowski

$$p_{t1} - p_{to} = p_1 - p_0 + \rho w^2/2 \qquad (A1)^{[1]}$$

in which p_{t1} and p_{to} are, respectively, the total pressures immediately behind and in front of the propeller, p_1 and p_0 are the corresponding static pressures and w is the tangential velocity of the air just behind the propeller. Substituting

$$\Delta p_t = p_{t1} - p_{to}; \; \Delta p = p_1 - p_0; \; \text{and} \quad q_w = \rho w^2/2 \qquad (A2)$$

equation (20) becomes

$$\Delta p_t = \Delta p + q_w \qquad (A3)$$

Dividing by the dynamic pressure of the undisturbed stream and substituting

$$\Delta P_T = \Delta p_t/q \quad \Delta P = \Delta p/q \text{ and } E = q_w/q \qquad (A4)$$

yields

$$\Delta P = \Delta P_T - E \qquad (A5)$$

Thus, the (thrust-producing) change of static pressure differs from the change of total pressure by the quantity E, which represents the rotational energy imparted to the slipstream.

Although the use of shielded total head tubes enables accurate measurement of ΔP_T (which is not true of the plain tubes used in previous work), no method is known for the direct determination of q_w or E.

---

[1]See reference 6, p. 233, equation (2.3).

However, if the axial velocity through the propeller disk is known, the value of E can be deduced from the yaw head pressure difference as outlined below. According to (9)

$$w = p_y/\rho u K \qquad (A6)$$

whence

$$q_w = \frac{\rho\,w^2}{2} = \frac{1}{2\rho u^2}\left(\frac{p_y}{K}\right)^2 \qquad (A7)$$

and

$$E = \frac{q_w}{q} = \frac{1}{\rho u^2 \rho V^2}\left(\frac{p_y}{K}\right)^2 \qquad (A8)$$

If there is introduced $(rV = u)$ and $P_Y = p_y/(\rho V^2/2)$

$$E = \frac{1}{4r^2}\left(\frac{P_Y}{K}\right)^2 \qquad (A9)$$

The problem which now remains is that of evaluating r, the ratio of the axial velocity through the propeller disk to the velocity of the undisturbed stream. The average value of r is implicitly defined by Froude's equation

$$T = 2A\rho V^2 a(1 + a) \qquad (A10)$$

wherein T is the total thrust, A the disk area, V the velocity of advance and $1 + a = r$. Substituting $\pi D^2/4$ for A and dividing by $\rho n^2 D^4$ to obtain the thrust coefficient

$$C_T = \frac{\pi}{2}\left(\frac{V}{nD}\right)^2 a(1 + a) \qquad (A11)$$

whence

$$a^2 + a - \frac{2C_T}{\pi}\left(\frac{nD}{V}\right)^2 = 0 \qquad (A12)$$

Now, since $r = 1 + a$,

$$r = \frac{1 \pm \sqrt{1 + \dfrac{8C_T}{\pi}\left(\dfrac{nD}{V}\right)^2}}{2} \qquad (A13)$$

APPENDIX B

Evaluation of a

The method of evaluating a which is described in the preceding appendix involves the implicit assumption that the thrust is uniformly distributed over the propeller disk. As such is never the case, the values so computed are of approximate character but are satisfactory for the intended purpose of improving the accuracy with which the elementary thrust coefficients are determined from wake survey data. However, the use of such approximate values of a in the evaluation of section lift coefficients would jeopardize the accuracy of those results and, since the value of a for each element can be rigorously determined from knowledge of the corresponding value of dC_T/dx, that procedure was followed. The development of the equation used for this purpose is outlined below.

According to the momentum theory, the thrust of the blade elements located at the radius r is

$$dT = 4\pi \rho r dr V^2 a(1 + a) \qquad (B1)$$

in which V is the velocity of advance and $V(1 + a)$ is the velocity through the plane of rotation. Substituting $xD/2$ for r and $Ddx/2$ for dr

$$dT = \pi \rho D^2 V^2 a(1 + a)x dx \qquad (B2)$$

The corresponding elementary thrust coefficient is

$$\frac{dC_T}{dx} = \frac{dT/dx}{\rho n^2 D^4} = \pi \left(\frac{V}{nD}\right)^2 a(1 + a)x \qquad (B3)$$

If this equation is rewritten as

$$a^2 + a - \frac{dC_T/dx}{\pi x(V/nD)^2} = 0 \qquad (B4)$$

the value of a is found to be

$$a = \frac{-1 \pm \sqrt{1 + \dfrac{4(dC_T/dx)}{\pi x(V/nD)^2}}}{2} \qquad (B5)$$

For the calculation of section lift coefficients, values of a were

read from a curve of $a = f\left[(dC_T/dx)(nD/V)^2\right]$.

<div align="center">Evaluation of Φ</div>

The effective angle of advance of the blade element in diagram E (p. 14) is

$$\Phi = \tan^{-1}\left[\frac{V(1+a)}{2\pi rn(1-a')}\right] \qquad (B6)$$

in which aV and $2\pi rna'$ are the magnitudes of the induced axial and tangential velocities. When r is replaced by Dx/2

$$\Phi = \tan^{-1}\left[\frac{1}{\pi x}\left(\frac{V}{nD}\right)\left(\frac{1+a}{1-a'}\right)\right] \qquad (B7)$$

and the equation becomes non-dimensional. Since x and V/nD will be known, and as a can be calculated as outlined above, the only additional information required for the determination of Φ is the value of a'.

The general momentum theory postulates the tangential velocity of the air in the plane of rotation as one-half that immediately behind the blades. If the latter is ωr, the former - the induced tangential velocity - is

$$2\pi rna' = \omega r/2 \qquad (B8)$$

whence

$$4\pi na' = \omega \qquad (B9)$$

The torque required to accelerate a cylindrical shell of air (length V(1 + a), mean radius r, radial thickness dr) from rest to the tangential velocity ωr in unit time is

$$dQ = \rho V(1+a)2\pi rdr \times \omega r^2 \qquad (B10)$$

Substituting Dx/2 for r, Ddx/2 for dr and 4πna' for ω,

$$dQ = \frac{\rho}{2}V(1+a)\pi^2 na'D^4 x^3 dx \qquad (B11)$$

The corresponding elementary torque coefficient is

$$\frac{dC_Q}{dx} = \frac{dQ}{dx} \times \frac{1}{\rho n^2 D^5} = \frac{\rho V(1+a)\pi^2 na'D^4 x^3}{2\rho n^2 D^5} \doteq \frac{\pi^2 x^3 (1+a)a'}{2}\left(\frac{V}{nD}\right) \tag{B12}$$

whence

$$a' = \frac{2}{\pi^2 x^3 (1+a)(V/nD)}\left(\frac{dC_Q}{dx}\right) \tag{B13}$$

Thus the calculation of Φ is accomplished by the substitution in (B7) of the values of a and a' which are evaluated in accordance with (B5) and (B13), respectively. It will be noted that the only data required are the values of x, V/nD, dC_T/dx, and dC_Q/dx.

APPENDIX C

Spinner Drag Corrections

As the spinner surface constituted the inner limit of the region covered by these surveys, the apparent thrusts determined by integration necessarily exceed the true net values, which are obtained in dynamometer tests, by the amounts of the spinner drag. Since spinner torque - if appreciable - would be detected by the yaw heads, the survey results need only be corrected for spinner drag in order to be made fully comparable with those of routine force tests on the same combination of propeller and spinner.

To obtain the data required for these corrections, spinner drag was measured - as negative thrust - on the dynamometer. With the blade apertures smoothly covered, the spinner was driven at speeds ranging from 700 to 2100 rpm while dynamic pressure was varied throughout the range utilized in the surveys. The effect of rotative speed was found to be negligible. This enabled definition of the spinner drag coefficient as a function of dynamic pressure only; coordinates of the resulting curve are tabulated below:

q (lb/ft^2)	2	8	14	20
C_{Ds}	0.00200	0.00191	0.00183	0.00176

It should be noted that $C_{Ds} = D_s/q\,D^2$, in which D_s is the drag of the spinner and D the propeller diameter. Had the coefficients been based upon frontal area of the spinner (diam. = 5 in.) instead of D^2 ($D = 33.6$ in.), their values would have been 57.5 times those listed above; that is, they would have ranged from 0.115 to 0.101.

The following relationship indicates the reason for selection of the foregoing form of drag coefficient

$$\Delta C_T = -\frac{D_s}{\rho n^2 D^4} = -\frac{C_{Ds}\,\rho\,V^2 D^2}{2\rho n^2 D^4} = -\frac{C_{Ds}}{.2}\left(\frac{V}{nD}\right)^2 \tag{C1}$$

It will be seen that, as the value of C_{Ds} is fixed by that of q, the direct evaluation of ΔC_T requires only knowledge of the values of q and V/nD. The substantial constancy of C_{Ds} and consequent approximate proportionality of ΔC_T to $(V/nD)^2$ thus indicate the importance of the spinner drag correction at large advance ratios.

TABLE I

Model P $\beta_{0.75R} = 20°$

V/nD = 0.33	0.5	0.7	0.8	0.92
Sta.		dC_Q/dx		
0 +0.0016	+0.0010	+0.0002	-0.0001	+0.0004
1 .0036	.0025	.0015 +	.0010	.0020
2 .0131	.0128	.0110	.0090	.0070
3 .0232	.0225	.0186	.0155	.0107
4 .0299	.0278	.0224	.0182	.0120
5 .0335	.0304	.0242	.0185	.0107
6 .0345	.0311	.0252	.0180	.0091
7 .0349	.0310	.0252	.0169	.0068
8 .0343	.0299	.0235	.0153	.0049
9 .0314	.0254	.0187	.0110	.0027
10 .0031	.0041	.0075	.0048	.0010

Model P_C $\beta_{0.75R} = 20°$

V/nD = 0.3	0.5	0.7	0.8	0.92
Sta.		dC_Q/dx		
0 +0.0025	+0.0024	+0.0015	+0.0012	+0.0002
1 .0056	.0051	.0035	.0030	.0012
2 .0179	.0170	.0139	.0111	.0069
3 .0261	.0249	.0205	.0164	.0110
4 .0302	.0280	.0231	.0183	.0115
5 .0330	.0297	.0245	.0187	.0109
6 .0350	.0301	.0250	.0182	.0095
7 .0355	.0303	.0257	.0177	.0075
8 .0345	.0293	.0238	.0159	.0062
9 .0300	.0245	.0189	.0121	.0040
10 .0081	.0075	.0072	.0060	.0019

Model P_{CH} $\beta_{0.75R} = 20°$

V/nD = 0.33	0.5	0.7	0.8	0.89
Sta.		dC_Q/dx		
0 +0.0020	+0.0019	+0.0009	-0.0002	-0.0015
1 .0040	.0037	.0020 +	.0008 -	.0005
2 .0160	.0152	.0123	.0101 +	.0070
3 .0249	.0235	.0191	.0160	.0115
4 .0300	.0273	.0226	.0185	.0120
5 .0330	.0295	.0241	.0193	.0116
6 .0350	.0306	.0245	.0187	.0105
7 .0360	.0310	.0249	.0182	.0096
8 .0355	.0300	.0242	.0155	.0060
9 .0280	.0230	.0174	.0113	.0020
10 .0049	.0065	.0090	.0065 -	.0015

Model P_{C2} $\beta_{0.75R} = 20°$

V/nD = 0.34	0.5	0.7	0.8	0.92
Sta.		dC_Q/dx		
0 +0.0023	+0.0024	+0.0015	+0.0002	-0.0020
1 .0045	.0046	.0035	.0018 -	.0013
2 .0141	.0142	.0124	.0100 +	.0065
3 .0236	.0230	.0195	.0161	.0105
4 .0305	.0283	.0235	.0193	.0124
5 .0339	.0305	.0262	.0204	.0119
6 .0351	.0314	.0263	.0190	.0096
7 .0345	.0308	.0250	.0165	.0062
8 .0323	.0288	.0211	.0130	.0026
9 .0270	.0224	.0142	.0087	.0002
10 .0080	.0059	.0058	.0042 -	.0007

TABLE I - Cont'd

Model U-24

$\beta_{0.75R} = 12°$			

V/nD = 0.305	0.4	0.5	0.615
Sta.	dC_Q/dx		
0	+0.0014	+0.0015	+0.0015	+0.0011
1	.0027	.0028	.0026	.0021
2	.0071	.0065	.0055	.0040
3	.0098	.0088	.0072	.0045
4	.0114	.0097	.0076	.0041
5	.0118	.0095	.0071	.0032
6	.0109	.0089	.0060	.0020
7	.0095	.0075	.0047	.0007
8	.0078	.0060	.0035	- .0005
9	.0056	.0043	.0024	- .0010
10	.0020	.0015	.0010	- .0011

$\beta_{0.75R} = 24°$				

V/nD = 0.325	0.55	0.75	0.95	1.135
Sta.	dC_Q/dx			
0	+0.0030	+0.0027	+0.0028	+0.0021	+0.0003
1	.0060	.0055	.0054	.0041	.0007
2	.0154	.0152	.0124	.0095	.0041
3	.0245	.0213	.0186	.0138	.0063
4	.0333	.0260	.0256	.0178	.0083
5	.0397	.0305	.0273	.0206	.0095
6	.0436	.0334	.0290	.0225	.0095
7	.0457	.0351	.0305	.0223	.0082
8	.0464	.0340	.0305	.0214	.0064
9	.0524	.0290	.0260	.0157	.0045
10	.0132	.0102	.0124	.0080	.0023

Model U-60

$\beta_{0.75R} = 12°$			

V/nD = 0.31	0.4	0.5	0.575
Sta.	dC_Q/dx		
0	+0.0010	+0.0006	-0.0001	-0.0007
1	.0022	.0016	+ .0008	- .0004
2	.0059	.0051	.0038	+ .0026
3	.0091	.0078	.0061	.0048
4	.0109	.0096	.0072	.0055
5	.0112	.0100	.0068	.0049
6	.0103	.0083	.0057	.0033
7	.0086	.0063	.0041	.0012
8	.0068	.0045	.0025	- .0008
9	.0042	.0026	.0007	- .0022
10	.0015	.0008	- .0005	- .0012

$\beta_{0.75R} = 24°$				

V/nD = 0.33	0.5	0.7	0.9	1.075
Sta.	dC_Q/dx			
0	+0.0015	+0.0020	+0.0009	-0.0010	-0.0039
1	.0033	.0039	.0026	- .0005	- .0044
2	.0112	.0116	.0105	+ .0069	+ .0014
3	.0218	.0195	.0185	.0136	.0063
4	.0335	.0263	.0244	.0190	.0100
5	.0443	.0318	.0277	.0224	.0123
6	.0457	.0352	.0293	.0235	.0120
7	.0432	.0357	.0300	.0233	.0098
8	.0410	.0329	.0301	.0211	.0068
9	.0375	.0268	.0251	.0146	.0038
10	.0121	.0116	.0060	.0065	.0008

TABLE I - Cont'd

$\beta_{0.75R} = 12°$ Model 0.4E $\beta_{0.75R} = 24°$

V/nD =	0.35	0.41	0.47	0.53		V/nD =	0.325	0.45	0.65	0.85	1.02
Sta.		dC_Q/dx				Sta.		dC_Q/dx			
0	+0.0002	-0.0002	-0.0005	-0.0010		0	+0.0015	+0.0013	-0.0002	-0.0025	-0.0042
1	.0004	0	- .0005	- .0009		1	.0025	.0025	+ .0005	- .0027	- .0060
2	.0030	+ .0025	+ .0015	+ .0007		2	.0095	.0085	.0071	+ .0022	- .0030
3	.0054	.0046	.0034	.0022		3	.0179	.0162	.0142	.0087	.0015
4	.0076	.0065	.0050	.0035		4	.0255	.0230	.0208	.0148	.0065
5	.0091	.0078	.0062	.0045		5	.0342	.0298	.0264	.0206	.0110
6	.0100	.0086	.0066	.0047		6	.0435	.0354	.0308	.0250	.0161
7	.0100	.0086	.0067	.0043		7	.0515	.0416	.0346	.0290	.0190
8	.0092	.0079	.0063	.0039		8	.0580	.0455	.0365	.0305	.0190
9	.0069	.0060	.0053	.0029		9	.0567	.0385	.0332	.0280	.0165
10	.0028	.0028	.0029	.0017		10	.0220	.0110	.0242	.0196	.0112

$\beta_{0.75R} = 12°$ Model 0.8E $\beta_{0.75R} = 24°$

V/nD =	0.31	0.4	0.5	0.595		V/nD =	0.35	0.5	0.7	0.9	1.1
Sta.		dC_Q/dx				Sta.		dC_Q/dx			
0	+0.0012	+0.0010	+0.0008	+0.0002		0	+0.0020	+0.0020	+0.0019	+0.0005	-0.0028
1	.0024	.0022	.0015	.0004		1	.0040	.0040	.0036	.0015	- .0029
2	.0060	.0059	.0044	.0029		2	.0119	.0120	.0112	.0077	+ .0013
3	.0091	.0087	.0065	.0041		3	.0199	.0200	.0185	.0139	.0057
4	.0110	.0100	.0075	.0045		4	.0322	.0254	.0246	.0187	.0095
5	.0116	.0104	.0075	.0041		5	.0410	.0510	.0285	.0222	.0107
6	.0111	.0096	.0062	.0028		6	.0426	.0344	.0301	.0244	.0113
7	.0096	.0080	.0045	.0014		7	.0425	.0356	.0315	.0254	.0099
8	.0076	.0063	.0032	0		8	.0423	.0347	.0311	.0242	.0080
9	.0052	.0041	.0017	- .0015		9	.0386	.0296	.0246	.0187	.0051
10	.0014	.0014	.0006	- .0019		10	.0185	.0136	.0135	.0090	.0024

TABLE II

Model U-24 $\beta_{0.75R} = 36°$

Element: $x = 0.752$, $b/D = 0.0678$, $\beta = 35.95°$.

$$\phi = \tan^{-1}\left[\frac{V/nD}{\pi x}\left(\frac{1+a}{1-a'}\right)\right]$$

$$c_L = \left[\frac{dC_T}{dx}\cos\phi + \frac{dC_Q}{dx}\cdot\frac{2}{x}\cdot\sin\phi\right]$$

$$c_L = \frac{4}{B\,(b/D)(1+a)^2(V/nD)^2}\cdot\sin^2\phi$$

Quantity	Operation	Line	Value
V/nD	Data	①	1.200
dC_T/dx	Data	②	0.275
dC_Q/dx	Data	③	0.0590
$(V/nD)^2$	①²	④	1.440
$m\ \left(=\dfrac{dC_T/dx}{2x(V/nD)^2}\right)$	②/(2④x)	⑤	0.1268
$1 + a$	Chart: (1+a) vs. m	⑥	1.075
$2/\pi^2 x^3$	$0.2026/x^3$	⑦	0.4764
$\dfrac{2}{\pi^2 x^3(1+a)(V/nD)}$	⑦/(⑥ · ①)	⑧	0.3670
a'	⑧ · ③	⑨	0.0217
$1 - a'$	1 - ⑨	⑩	0.9783
$(1+a)/(1-a')$	⑥ / ⑩	⑪	1.099
$(V/nD)/\pi x$	① /(πx)	⑫	0.5077
$\tan\phi$	⑪ · ⑫	⑬	0.5580
$\sin\phi$	From tables	⑭	0.4873
$\cos\phi$	From tables	⑮	0.8733
$\sin^2\phi$	⑭²	⑯	0.2375
$4/[B(b/D)]$	$1.333/(b/D)$	⑰	19.660
$(1+a)^2$	⑥²	⑱	1.156
A	(⑯ · ⑰)/(⑱ · ④)	⑲	2.803
B	② · ⑮	⑳	0.2402
C	(2 · ③ · ⑭)/x	㉑	0.0765
$B + C$	⑳ + ㉑	㉒	0.3167
c_L	⑲ · ㉒	㉓	0.8877
β	Data	㉔	35.95
ϕ	arctan ⑬	㉕	29.16
α_0	㉔ - ㉕	㉖	6.79

TABLE III

SECTION LIFT COEFFICIENTS

Model U-24   x = 0.253   b/D = 0.0623

(Data from Figures 28,29)

V/nD	dC_T/dx	dC_Q/dx	C_L	a
	$\beta_{0.75R} = 12°$		$\beta = 40.7°$	
0.6	+0.019	+0.0022	+0.558	+ 0.7
.5	.028	.0027	.861	3.7
.4	.035	.0029	1.147	7.1
.3	.039	.0027	1.409	11.6
	$\beta_{0.75R} = 24°$		$\beta = 52.7°$	
1.1	.007	.0016	.168	− 2.1
1.0	.018	.0034	.425	− .6
.9	.028	.0047	.693	+ 1.2
.8	.035	.0054	.936	3.4
.6	.038	.0052	1.237	9.6
.4	.048	.0065	2.075	15.1
	$\beta_{0.75R} = 36°$		$\beta = 64.7°$	
1.8	.012	.0024	.122	− 1.9
1.6	.025	.0075	.433	− .5
1.4	.038	.0099	.720	+ 1.6
1.2	.045	.0100	.944	4.6
1.0	.045	.0094	1.154	8.6
.8	.053	.0096	1.612	12.8
.6	.068	.0103	2.401	17.0
	$\beta_{0.75R} = 48°$		$\beta = 76.7°$	
2.5	.048	.0253	.641	2.1
2.3	.052	.0245	.728	3.3
2.1	.067	.0225	.804	4.6
1.9	.059	.0205	.873	6.3
1.7	.054	.0187	.962	8.3
1.5	.047	.0159	1.006	10.9
1.3	.045	.0152	1.202	13.7
	$\beta_{0.75R} = 60°$		$\beta = 88.7°$	
3.7	.036	.0700	.835	8.0
3.5	.071	.0655	.873	8.5
3.3	.080	.0600	.898	9.2
3.1	.069	.0535	.901	10.0
2.9	.030	.0445	.841	11.2
2.7	− .102	.0315	.618	13.1
2.5	− .103	.0275	.606	14.3
2.3	− .102	.0235	.573	15.8

TABLE III - Cont'd

SECTION LIFT COEFFICIENTS

Model U-24 $x = 0.520$ $b/D = 0.0699$

(Data from Figures 28,29)

V/nD	dC_T/dx	dC_Q/dx	C_L	α
	$\beta_{0.75R} = 12°$		$\beta = 19.7°$	
0.6	+0.046	+0.0050	+0.315	- 1.9
.5	.071	.0073	.501	+ .1
.4	.095	.0088	.687	1.9
.3	.118	.0099	.871	3.7
	$\beta_{0.75R} = 24°$		$\beta = 31.7°$	
1.1	.044	.0083	.267	- 3.0
1.0	.073	.0121	.450	- 1.2
.9	.100	.0154	.638	+ .7
.8	.125	.0178	.823	2.6
.6	.157	.0202	1.115	6.8
.4	.165	.0243	1.330	11.2
	$\beta_{0.75R} = 36°$		$\beta = 43.7°$	
1.8	.029	.0075	.132	- 4.3
1.6	.079	.0215	.417	- 1.7
1.4	.127	.0300	.708	+ 1.3
1.2	.170	.0350	1.008	4.6
1.0	.177	.0347	1.161	8.6
.8	.197	.0382	1.444	12.6
.6	.212	.0431	1.768	16.6
	$\beta_{0.75R} = 48°$		$\beta = 55.7°$	
2.5	.083	.0425	.391	- 1.9
2.3	.128	.0540	.585	- .1
2.1	.165	.0595	.760	+ 1.9
1.9	.194	.0630	.944	4.3
1.7	.200	.0640	1.093	7.0
1.5	.230	.0620	1.289	9.9
1.3	.195	.0600	1.338	13.7
1.1	.167	.0595	1.403	17.8
	$\beta_{0.75R} = 60°$		$\beta = 67.7°$	
3.7	.135	.1255	.583	.5
3.5	.185	.1345	.703	1.4
3.3	.222	.1350	.795	2.5
3.1	.249	.1340	.892	3.8
2.9	.267	.1305	.978	5.1
2.7	.250	.1210	1.014	6.8
2.5	.258	.1160	1.247	8.6
2.3	.243	.1115	1.353	10.6

TABLE III - Cont'd

SECTION LIFT COEFFICIENTS

Model U-24   x = 0.752   b/D = 0.0678

(Data from Figures 28,29)

V/nD	dC_T/dx	dC_Q/dx	C_L	α
	$\beta_{0.75R} = 12°$		$\beta = 12°$	
0.6	+0.011	+0.0025	+0.041	− 2.5
.5	.057	.0060	.194	− 1.1
.4	.100	.0089	.353	+ .2
.3	.139	.0111	.496	1.4
	$\beta_{0.75R} = 24°$		$\beta = 24°$	
1.1	.060	.0122	.198	− 1.6
1.0	.105	.0195	.350	− .2
.9	.149	.0250	.503	+ 1.5
.8	.187	.0278	.638	3.0
.6	.244	.0320	.861	6.2
.4	.272	.0383	1.016	9.4
	$\beta_{0.75R} = 36°$		$\beta = 36°$	
1.8	.050	.0160	.146	− 1.6
1.6	.138	.0375	.411	+ .9
1.4	.213	.0520	.662	3.8
1.2	.275	.0590	.888	6.8
1.0	.324	.0695	1.123	9.9
.8	.311	.0730	1.173	13.5
.6	.283	.0750	1.158	17.3
	$\beta_{0.75R} = 48°$		$\beta = 48°$	
2.5	.146	.0690	.389	.7
2.3	.216	.0875	.575	2.7
2.1	.257	.0920	.698	5.0
1.9	.311	.1035	.892	7.5
1.7	.357	.1185	1.110	10.0
1.5	.362	.1230	1.231	12.9
1.3	.342	.1170	1.256	16.2
	$\beta_{0.75R} = 60°$		$\beta = 60°$	
3.7	.220	.1655	.501	1.8
3.5	.265	.1720	.635	3.1
3.3	.308	.1830	.688	4.5
3.1	.347	.1915	.799	6.0
2.9	.380	.1955	.906	7.7
2.7	.405	.1960	1.011	9.5
2.5	.414	.2030	1.133	11.4
2.3	.335	.1940	1.107	13.8

TABLE III – Cont'd

SECTION LIFT COEFFICIENTS

Model U-24 $x = 0.928$ $b/D = 0.0552$

(Data from Figures 28,29)

V/nD	dC_T/dx	dC_Q/dx	C_L	α
	$\beta_{0.75R} = 12°$		$\beta = 7.7°$	
0.6	−0.043	−0.0004	−0.116	− 3.4
.5	− .005	+ .0024	− .011	− 1.9
.4	+ .027	.0043	+ .079	− .5
.3	.052	.0058	.150	+ .9
	$\beta_{0.75R} = 24°$		$\beta = 19.7°$	
1.1	.023	.0063	.066	− 1.1
1.0	.066	.0123	.181	+ .4
.9	.110	.0196	.306	1.8
.8	.147	.0248	.413	3.2
.6	.210	.0284	.599	6.1
.4	.246	.0315	.717	8.9
	$\beta_{0.75R} = 36°$		$\beta = 31.7°$	
1.8	.038	.0135	.098	− .1
1.6	.108	.0355	.287	+ 2.5
1.4	.187	.0525	.505	5.2
1.2	.262	.0620	.716	7.9
1.0	.280	.0760	.824	11.0
.8	.242	.0825	..770	14.4
.6	.218	.0925	.743	17.7
	$\beta_{0.75R} = 48°$		$\beta = 43.7°$	
2.5	.126	.0660	.309	2.8
2.3	.200	.0875	.481	4.9
2.1	.247	.0990	.585	7.2
1.9	.307	.1125	.780	9.5
1.7	.350	.1210	.927	12.1
1.5	.240	.1125	.744	15.3
1.3	.171	.1080	.615	18.6
	$\beta_{0.75R} = 60°$		$\beta = 55.7°$	
3.7	.184	.1500	.401	3.6
3.5	.240	.1630	.494	5.0
3.3	.295	.1735	.593	6.6
3.1	.340	.1815	.665	8.3
2.9	.375	.1920	.798	10.0
2.7	.422	.2075	.941	11.9
2.5	.415	.2050	.993	13.9
2.3	.262	.1635	.752	16.5

TABLE III - Cont'd

SECTION LIFT COEFFICIENTS

Model 0.4E $x = 0.253$ $b/D = 0.0623$

(Data from Figures 32,33)

V/nD	dC_T/dx	dC_Q/dx	C_L	α
	$\beta_{0.75R} = 12°$		$\beta = 23.2°$	
0.53	-0.019	-0.0009	-0.451	-10.2
.45	- .008	- .0004	- .210	- 7.2
.35	+ .008	+ .0005	+ .254	- 2.5
	$\beta_{0.75R} = 24°$		$\beta = 35.2°$	
1.0	- .0463	- .0055	- .843	-12.5
.9	- .0330	- .0035	- .648	-10.3
.8	- .0190	- .0017	- .392	- 8.0
.65	+ .0043	+ .0006	+ .125	- 4.5
.5	.0239	.0020	.690	- .9
.35	.0368	.0025	1.179	+ 3.8
	$\beta_{0.75} = 36°$		$\beta = 47.2°$	
1.6	- .071	- .0120	- .802	-13.3
1.4	- .049	- .0080	- .665	-10.5
1.2	- .024	- .0035	- .379	- 7.7
1.0	0	+ .0010	+ .080	- 4.0
.8	+ .020	.0035	.578	- 0.6
.6	.038	.0045	1.136	+ 4.6
	$\beta_{0.75R} = 48°$		$\beta = 59.2°$	
2.35	- .070	- .0210	- .629	- 9.8
2.1	- .047	- .0130	- .481	- 8.3
1.9	- .033	- .0060	- .288	- 7.0
1.7	- .017	- .0005	- .066	- 5.5
1.5	+ .004	+ .0040	+ .225	- 3.7
1.3	.024	.0065	.522	- 1.3
1.1	.039	.0080	.867	+ 1.6
	$\beta_{0.75R} = 60°$		$\beta = 71.2°$	
3.65	- .064	- .0200	- .260	- 5.6
3.5	- .050	- .0150	- .212	- 5.3
3.3	- .036	- .0080	- .131	- 4.8
3.1	- .025	- .0020	- .045	- 4.3
2.9	- .016	+ .0040	+ .063	- 3.7
2.7	- .005	.0090	.183	- 3.0
2.5	+ .020	.0135	.337	- 2.3
2.3	.040	.0160	.480	- 1.4
2.1	.050	.0175	.624	- .3

TABLE III - Cont'd

SECTION LIFT COEFFICIENTS

Model 0.4E   x = 0.520   b/D = 0.0699

(Data from Figures 32,33)

V/nD	dC_T/dx	dC_Q/dx	C_L	α
	$\beta_{0.75R} = 12°$		$\beta = 15.2°$	
0.53	+0.019	+0.0022	+0.134	− 3.6
.45	.044	.0039	.309	− 2.2
.35	.074	.0054	.527	− .5
	$\beta_{0.75R} = 24°$		$\beta = 27.2°$	
1.0	.015	.0026	.094	− 4.8
.9	.045	.0070	.279	− 3.3
.8	.077	.0104	.500	− .9
.65	.115	.0140	.787	+ 2.1
.5	.143	.0160	1.029	5.1
.35	.166	.0174	1.254	8.1
	$\beta_{0.75R} = 36°$		$\beta = 39.2°$	
1.6	0	.0028	.028	− 5.3
1.4	.058	.0145	.332	− 2.4
1.2	.107	.0230	.646	+ .9
1.0	.153	.0285	.983	4.5
.8	.190	.0310	1.306	8.4
.6	.223	.0330	1.656	12.3
	$\beta_{0.75R} = 48°$		$\beta = 51.2°$	
2.35	.027	.0130	.132	− 4.3
2.1	.093	.0295	.392	− 1.6
1.9	.127	.0385	.592	+ .4
1.7	.155	.0460	.808	3.0
1.5	.184	.0510	1.047	5.9
1.3	.215	.0550	1.332	9.0
1.1	.251	.0580	1.676	12.3
	$\beta_{0.75R} = 60°$		$\beta = 63.2°$	
3.65	.028	.0430	.195	− 3.1
3.5	.075	.0540	.282	− 2.4
3.3	.110	.0655	.387	− 1.3
3.1	.138	.0745	.494	− .1
2.9	.162	.0830	.617	+ 1.3
2.7	.184	.0905	.755	2.7
2.5	.206	.0950	.899	4.4
2.3	.234	.0950	1.041	6.2
2.1	.260	.0990	1.247	8.2

TABLE III - Cont'd

SECTION LIFT COEFFICIENTS

Model 0.4E $x = 0.752$ **b/D = 0.0678**

(Data from Figures 32,33

V/nD	dC_T/dx	dC_Q/dx	C_L	α
	$\beta_{0.75R} = 12°$		$\beta = 12°$	
0.53	+0.039	+0.0048	+0.137	- 1.4
.45	.075	.0073	.264	- .3
.35	.123	.0100	.425	+ .8
	$\beta_{0.75R} = 24°$		$\beta = 24°$	
1.0	.100	.0178	.331	.0
.9	.143	.0230	.479	1.6
.8	.178	.0268	.608	3.2
.65	.221	.0308	.776	5.6
.5	.263	.0339	.948	7.8
.35	.315	.0408	1.176	9.7
	$\beta_{0.75R} = 36°$		$\beta = 36°$	
1.6	.134	.0350	.394	1.0
1.4	.202	.0495	.629	3.9
1.2	.257	.0580	.820	6.9
1.0	.330	.0670	1.127	9.9
.8	.390	.0845	1.448	12.8
.6	.381	.0870	1.517	16.3
	$\beta_{0.75R} = 48°$		$\beta = 48°$	
2.35	.192	.075	.490	2.3
2.1	.259	.092	.702	5.1
1.9	.309	.102	.881	7.5
1.7	.355	.114	1.088	10.1
1.5	.409	.128	1.346	12.7
1.3	.399	.122	1.405	15.9
1.1	.348	.114	1.344	19.6
	$\beta_{0.75R} = 60°$		$\beta = 60°$	
3.65	.167	.1480	.440	2.2
3.5	.224	.1575	.523	3.2
3.3	.295	.1680	.639	4.6
3.1	.339	.1765	.750	6.1
2.9	.361	.1860	.862	7.8
2.7	.372	.1925	.969	9.6
2.5	.384	.2010	1.095	11.5
2.3	.414	.2055	1.243	13.6
2.1	.362	.1905	1.223	16.2

TABLE III - Cont'd

SECTION LIFT COEFFICIENTS

Model 0.4E   x = 0.928   b/D = 0.0552

(Data from Figures 32,33)

V/nD	dC_T/dx	dC_Q/dx	C_L	α
	$\beta_{0.75R} = 12°$		$\beta = 9.5°$	
0.53	+0.012	+0.0029	+0.036	− 0.9
.45	.040	.0030	.112	+ .2
.35	.077	.0029	.216	1.5
	$\beta_{0.75R} = 24°$		$\beta = 21.5°$	
1.0	.101	.0182	.275	1.9
.9	.141	.0253	.392	3.4
.8	.173	.0300	.489	4.8
.65	.207	.0332	.595	7.1
.5	.240	.0355	.701	9.2
.35	.230	.0509	.713	11.4
	$\beta_{0.75R} = 36°$		$\beta = 33.5°$	
1.6	.172	.0495	.442	4.0
1.4	.221	.0595	.590	6.8
1.2	.281	.0680	.769	9.6
1.0	.265	.0840	.806	12.8
.8	.163	.0775	.557	16.6
.6	.092	.0840	.375	20.6
	$\beta_{0.75R} = 48°$		$\beta = 45.5°$	
2.35	.233	.0945	.533	6.0
2.1	.296	.1110	.712	8.8
1.9	.334	.1240	.854	11.2
1.7	.301	.1355	.878	13.9
1.5	.214	.1140	.696	17.1
1.3	.151	.1110	.579	20.4
1.1	.097	.1290	.502	23.8
	$\beta_{0.75R} = 60°$		$\beta = 57.5°$	
3.65	.196	.1855	.484	5.7
3.5	.258	.1850	.551	6.8
3.3	.341	.1880	.659	8.3
3.1	.366	.1980	.751	10.0
2.9	.385	.2190	.869	11.7
2.7	.402	.2280	.969	13.6
2.5	.284	.1965	.815	15.9
2.3	.212	.1720	.706	18.4
2.1	.084	.1730	.554	21.0

TABLE III - Cont'd

SECTION LIFT COEFFICIENTS

| Model P_{C2} | | $x = 0.253$ | | $b/D = 0.0623$ |

(Data from Figures 26,27)

V/nD	dC_T/dx	dC_Q/dx	C_L	α
	$\beta_{0.75R} = 20°$		$\beta = 44.8°$	
0.90	−0.009	−0.0008	−0.120	− 3.1
.75	+ .020	+ .0013	+ .282	− .4
.60	.039	.0030	.735	+ 3.8
.45	.049	.0039	1.101	7.1
.35	.052	.0040	1.313	10.5
	$\beta_{C.75R} = 30°$		$\beta = 54.8°$	
1.4	− .024	− .0035	− .225	− 4.5
1.2	+ .008	+ .0025	+ .163	− 2.6
1.0	.035	.0060	.580	+ .0
.8	.051	.0075	.991	3.9
.6	.057	.0080	1.427	8.9
.4	.064	.0080	1.994	14.6
	$\beta_{0.75R} = 40°$		$\beta = 64.8°$	
2.0	− .0120	− .0035	− .104	− 3.1
1.8	+ .0090	+ .0035	+ .120	− 2.0
1.6	.0275	.0085	.365	− .7
1.4	.0440	.0120	.650	+ 1.2
1.2	.0565	.0130	.915	3.6
1.0	.0625	.0120	1.126	7.3
.8	.0675	.0115	1.458	11.5
	$\beta_{0.75R} = 50°$		$\beta = 74.8°$	
2.7	.032	.0175	.288	− .2
2.5	.040	.0230	.436	+ .4
2.3	.048	.0260	.575	1.1
2.1	.055	.0260	.682	2.3
1.9	.061	.0260	.819	3.6
1.7	.066	.0260	.995	5.1
1.5	.070	.0240	1.143	7.1
1.3	.071	.0222	1.326	9.7
	$\beta_{0.75R} = 60°$		$\beta = 84.8°$	
3.6	.093	.078	.739	3.8
3.4	.096	.074	.784	4.3
3.2	.100	.070	.834	4.9
3.0	.100	.066	.889	5.5
2.8	.102	.061	.931	6.4
2.6	.102	.055	.973	7.3
2.4	.098	.049	1.009	8.4
2.2	.095	.045	1.088	9.6

TABLE III - Cont'd

SECTION LIFT COEFFICIENTS

Model P_{C2} $x = 0.520$ $b/D = 0.0699$

(Data from Figures 26,27)

V/nD	dC_T/dx	dC_Q/dx	C_L	a
	$\beta_{0.75R} = 20°$		$\beta = 29.4°$	
0.90	+0.072	+0.012	+0.353	- 1.2
.75	.126	.018	.639	+ 1.4
.60	.169	.022	.904	4.1
.45	.195	.023	1.092	7.0
.35	.201	.023	1.167	9.2
	$\beta_{0.75R} = 30°$		$\beta = 39.4°$	
1.4	.068	.015	.275	- 2.2
1.2	.130	.027	.580	+ .8
1.0	.180	.035	.878	4.2
.8	.205	.037	1.097	8.1
.6	.251	.036	1.385	11.9
.4	.247	.049	1.716	15.7
	$\beta_{0.75R} = 40°$		$\beta = 49.4°$	
2.0	.085	.026	.280	- 2.3
1.8	.138	.040	.500	+ .0
1.6	.185	.051	.739	2.5
1.4	.223	.057	.966	5.4
1.2	.255	.058	1.189	8.7
1.0	.280	.061	1.452	12.1
.8	.325	.075	1.976	14.9
	$\beta_{0.75R} = 50°$		$\beta = 59.4°$	
2.7	.150	.069	.439	- .7
2.5	.192	.082	.593	+ .9
2.3	.222	.090	.741	2.6
2.1	.245	.094	.886	4.6
1.9	.267	.094	1.029	6.9
1.7	.294	.094	1.207	9.4
1.5	.322	.098	1.460	12.0
1.3	.364	.106	1.836	14.6
	$\beta_{0.75R} = 60°$		$\beta = 69.4°$	
3.6	.255	.176	.664	2.0
3.4	.280	.182	.760	3.0
3.2	.302	.180	.839	4.2
3.0	.318	.176	.921	5.5
2.8	.331	.172	1.011	6.9
2.6	.336	.167	1.105	8.4
2.4	.330	.157	1.173	10.3
2.2	.327	.158	1.329	12.1

TABLE III - Cont'd

SECTION LIFT COEFFICIENTS

Model P_{C2} $x = 0.752$ $b/D = 0.0678$

(Data from Figures 26,27)

V/nD	dC_T/dx	dC_Q/dx	c_L	α
	$\beta_{0.75R} = 20°$		$\beta = 20°$	
0.90	+0.062	+0.0110	+0.158	− 1.6
.75	.160	.0230	.412	+ .3
.60	.232	.0300	.613	2.4
.45	.278	.0325	.751	4.5
.35	.296	.0350	.818	6.0
	$\beta_{0.75R} = 30°$		$\beta = 30°$	
1.4	.091	.021	.209	− 1.4
1.2	.203	.044	.493	+ 1.4
1.0	.280	.055	.711	4.3
.8	.348	.063	.925	7.3
.6	.376	.075	1.083	10.5
.4	.352	.083	1.108	14.0
	$\beta_{0.75R} = 40°$		$\beta = 40°$	
2.0	.112	.037	.230	− .9
1.8	.218	.068	.474	+ 1.4
1.6	.291	.085	.668	4.0
1.4	.359	.096	.866	6.7
1.2	.429	.109	1.098	9.5
1.0	.417	.117	1.185	12.8
.8	.367	.106	1.114	16.7
	$\beta_{0.75R} = 50°$		$\beta = 50°$	
2.7	.217	.093	.377	.3
2.5	.288	.123	.544	2.1
2.3	.333	.135	.665	4.2
2.1	.376	.148	.806	6.4
1.9	.422	.161	.979	8.8
1.7	.464	.175	1.154	11.2
1.5	.384	.165	1.099	14.5
1.3	.340	.150	1.054	17.9
	$\beta_{0.75R} = 60°$		$\beta = 60°$	
3.6	.320	.221	.533	2.2
3.4	.364	.237	.629	3.5
3.2	.405	.244	.714	5.0
3.0	.442	.248	.806	6.6
2.8	.474	.255	.912	8.2
2.6	.485	.261	1.016	10.0
2.4	.415	.256	1.035	12.2
2.2	.330	.230	.967	14.8

TABLE III - Cont'd

SECTION LIFT COEFFICIENTS

Model P_{C2}		$x = 0.928$		$b/D = 0.0552$

(Data from Figures 26,27)

V/nD	dC_T/dx	dC_Q/dx	C_L	α
	$\beta_{0.75R} = 20°$		$\beta = 15.0°$	
0.90	-0.005	+0.0020	-0.007	- 2.1
.75	+ .080	.0115	+ .168	- .1
.60	.150	.0190	.319	+ 1.9
.45	.225	.0245	.484	3.6
.35	.227	.0270	.498	5.1
	$\beta_{0.75R} = 30°$		$\beta = 25.0°$	
1.4	.039	.0110	.081	- .8
1.2	.149	.0320	.300	+ 1.8
1.0	.244	.0475	.505	4.5
.8	.306	.0530	.650	7.4
.6	.308	.0610	.691	10.5
.4	.225	.0990	.590	13.5
	$\beta_{0.75R} = 40°$		$\beta = 35.0°$	
2.0	.089	.026	.152	.3
1.8	.185	.058	.345	2.6
1.6	.275	.080	.532	5.1
1.4	.350	.094	.702	7.7
1.2	.373	.110	.807	10.6
1.0	.313	.112	.741	13.9
.8	.274	.125	.712	17.2
	$\beta_{0.75R} = 50°$		$\beta = 45.0°$	
2.7	.165	.080	.274	1.8
2.5	.259	.115	.440	3.7
2.3	.328	.135	.577	5.8
2.1	.377	.151	.699	8.0
1.9	.406	.165	.808	10.4
1.7	.385	.164	.827	13.1
1.5	.282	.150	.692	16.3
1.3	.220	.157	.634	19.4
	$\beta_{0.75R} = 60°$		$\beta = 55.0°$	
3.6	.270	.195	.416	3.8
3.4	.316	.216	.500	5.4
3.2	.361	.229	.577	7.2
3.0	.405	.240	.662	9.0
2.8	.442	.251	.755	10.7
2.6	.450	.264	.828	12.9
2.4	.385	.244	.784	15.1
2.2	.285	.218	.680	17.6

TABLE IV

SECTION LIFT CHARACTERISTICS

High Speed Condition (Line I)   Data from Figure 41

$$C_P = 0.05 \qquad V/nD = 0.90$$

$x =$	0.2	0.3	0.4	0.45	0.55	0.65	0.75	0.85	0.95
$b/D =$	.0614	.0631	.0638	.0656	.0709	.0711	.0679	.0622	.0512

Model U-24 $\beta_{0.75R} = 21.8°$

dC_T/dx	+0.0100	0.0280	0.0475	0.0580	0.0800	0.0945	0.0967	0.0815	0.0465
dC_Q/dx	+ .00164	.00440	.00718	.00875	.01200	.01495	.01620	.01467	.00825
C_L	+ .347	.506	.521	.506	.452	.396	.327	.239	.133
α	+2.5	– .3	– .1	– .7	– .8	– .1	– .2	0	+ .1

Model U-60 $\beta_{0.75R} = 22.9°$

dC_T/dx	– .017	– .003	+ .035	.053	.085	.109	.119	.098	.061
dC_Q/dx	– .0018	+ .0005	.0052	.0078	.0130	.0179	.0192	.0173	.0077
C_L	– .448	+ .002	.381	.458	.485	.461	.402	.285	.169
α	–6.2	–4.3	–1.4	–1.0	+ .3	1.0	.9	.3	– .4

Model 0.4E $\beta_{0.75R} = 23.4°$

dC_T/dx	– .0305	– .0310	– .0060	+ .0125	.0505	.0895	.1260	.1440	.1140
dC_Q/dx	– .0031	– .0036	– .0006	+ .0017	.0075	.0144	.0209	.0260	.0200
C_L	– .796	– .490	– .058	+ .106	.285	.376	.426	.423	.326
α	–11.5	–8.9	–5.3	–4.7	–2.4	0	+1.1	2.1	3.1

Model 0.8E $\beta_{0.75R} = 22.2°$

dC_T/dx	– .0086	+ .0070	.0323	.0463	.0754	.0980	.1082	.0827	.0440
dC_Q/dx	– .00068	+ .00151	.00526	.00741	.01180	.01573	.01770	.01521	.00674
C_L	– .193	+ .151	.365	.412	.430	.412	.365	.243	.124
α	– .4	–3.1	–1.2	–1.3	– .7	+ .3	.1	.9	0

TABLE IV - Cont'd

SECTION LIFT CHARACTERISTICS

High Speed Condition (Line I)   Data from Figure 41

$C_P = 0.2$ $V/nD = 1.80$

x =	0.2	0.3	0.4	0.45	0.55	0.65	0.75	0.85	0.95
b/D =	.0614	.0631	.0638	.0656	.0709	.0711	.0679	.0622	.0512

Model U-24 $\beta_{0.75R} = 41.1°$

	0.2	0.3	0.4	0.45	0.55	0.65	0.75	0.85	0.95
dC_T/dx	+0.024	0.051	0.076	0.089	0.123	0.163	0.192	0.188	0.160
dC_Q/dx	+ .0095	.0164	.0237	.0283	.0385	.0496	.0608	.0675	.0518
C_L	+ .588	.619	.611	.595	.562	.565	.561	.508	.415
α	+5.3	.4	0	- .4	+ .2	1.8	2.6	3.7	4.8

Model U-60 $\beta_{0.75R} = 42.8°$

	0.2	0.3	0.4	0.45	0.55	0.65	0.75	0.85	0.95
dC_T/dx	- .0195	+ .0070	.0535	.0780	.1290	.1880	.2235	.2200	.1755
dC_Q/dx	- .0020	+ .0030	.0160	.0241	.0407	.0574	.0704	.0757	.0591
C_L	- .154	+ .108	.418	.515	.593	.653	.652	.585	.461
α	-4.1	-3.4	- .7	- .1	+1.6	3.4	4.1	4.7	4.9

Model 0.4E $\beta_{0.75R} = 43.8°$

	0.2	0.3	0.4	0.45	0.55	0.65	0.75	0.85	0.95
dC_T/dx	- .0425	- .0360	+ .0105	.0385	.1045	.1800	.2450	.2725	.2755
dC_Q/dx	- .0073	- .0087	+ .0025	.0111	.0304	.0520	.0752	.0939	.0873
C_L	- .506	- .350	+ .071	.243	.460	.609	.707	.726	.711
α	-8.8	-8.2	-4.7	-3.9	- .7	+2.7	5.0	7.1	9.0

Model 0.8E $\beta_{0.75R} = 42.3°$

	0.2	0.3	0.4	0.45	0.55	0.65	0.75	0.85	0.95
dC_T/dx	+ .0040	.0255	.0575	.0780	.1265	.1790	.2145	.2130	.1870
dC_Q/dx	+ .0028	.0094	.0187	.0249	.0401	.0541	.0668	.0738	.0603
C_L	+ .167	.347	.477	.526	.584	.619	.623	.568	.485
α	+2.3	-2.2	- .5	- .4	+ .9	2.8	3.7	5.4	5.4

TABLE IV – Cont'd

SECTION LIFT CHARACTERISTICS

High Speed Condition (Line I)   Data from Figure 41

$C_P = 0.5$ $V/nD = 2.85$

$x =$	0.2	0.3	0.4	0.45	0.55	0.65	0.75	0.85	0.95
$b/D =$	.0614	.0631	.0638	.0656	.0709	.0711	.0679	.0622	.0512

Model U-24 $\beta_{0.75R} = 55.5°$

dC_T/dx	+0.041	0.094	0.136	0.158	0.205	0.247	0.277	0.283	0.259
dC_Q/dx	+ .031	.051	.070	.081	.101	.121	.140	.150	.132
C_L	+ .802	.829	.811	.788	.714	.683	.669	.637	.579
α	+12.0	4.9	3.0	1.9	1.9	3.2	4.0	5.3	6.6

Model U-60 $\beta_{0.75R} = 57.0°$

dC_T/dx	+ .019	.070	.125	.155	.211	.260	.296	.284	.262
dC_Q/dx	+ .011	.034	.059	.072	.101	.127	.148	.155	.128
C_L	+ .173	.555	.690	.714	.718	.716	.709	.650	.575
α	+1.9	.1	1.9	2.0	3.2	4.8	5.4	6.1	6.6

Model 0.4E $\beta_{0.75R} = 58.5°$

dC_T/dx	– .034	0	+ .063	.096	.170	.257	.340	.369	.362
dC_Q/dx	– .0060	+ .0030	.0270	.0435	.0820	.1240	.1670	.1990	.1845
C_L	– .170	+ .045	.321	.434	.582	.702	.806	.838	.813
α	–2.4	–4.1	–1.8	–1.3	+1.4	4.5	6.8	9.1	11.2

Model 0.8E $\beta_{0.75R} = 56.5°$

dC_T/dx	+ .033	.079	.125	.149	.200	.251	.294	.274	.265
dC_Q/dx	+ .0209	.0428	.0617	.0734	.0994	.1261	.1475	.1578	.1337
C_L	+ .542	.696	.718	.721	.700	.706	.706	.647	.591
α	+8.1	1.7	2.1	1.8	2.5	4.1	5.0	6.9	7.1

TABLE IV - Cont'd

SECTION LIFT CHARACTERISTICS

Climb Condition (Line II)   Data from Figure 42

$C_p = 0.05$ $V/nD = 0.54$

x =	0.2	0.3	0.4	0.45	0.55	0.65	0.75	0.85	0.95
b/D =	.0614	.0631	.0638	.0656	.0709	.0711	.0679	.0622	.0512

Model U-24 $\beta_{0.75R} = 16.3°$

dC_T/dx	+0.0176	0.0446	0.0693	0.0825	0.1095	0.1320	0.1325	0.1082	0.0320
dC_Q/dx	+ .00175	.00488	.00785	.00937	.01220	.01407	.01420	.01247	.00725
C_L	+ .789	1.000	.899	.828	.682	.586	.464	.324	.097
α	+8.3	5.1	4.4	3.3	2.2	1.9	1.2	.9	.9

Model U-60 $\beta_{0.75R} = 17.4°$

dC_T/dx	+ .006	.029	.061	.081	.120	.142	.144	.120	.051
dC_Q/dx	+ .0005	.0033	.0068	.0088	.0134	.0162	.0166	.0151	.0064
C_L	+ .246	.658	.787	.804	.748	.636	.508	.362	.149
α	- .9	+ .7	3.1	2.9	2.8	3.0	2.1	1.3	.5

Model 0.4E $\beta_{0.75R} = 18.0°$

dC_T/dx	- .0060	+ .0090	.0370	.0545	.0925	.1330	.1590	.1590	.0920
dC_Q/dx	- .0004	+ .0008	.0040	.0059	.0100	.0141	.0171	.0186	.0136
C_L	- .229	+ .184	.472	.541	.573	.590	.557	.477	.273
α	-5.3	-3.7	- .9	- .8	+ .5	2.0	3.3	3.1	4.0

Model 0.8E $\beta_{0.75R} = 16.8°$

dC_T/dx	+ .0125	.0385	.0685	.0850	.1180	.1385	.1400	.1175	.0570
dC_Q/dx	+ .00135	.00380	.00660	.00835	.01240	.01570	.01635	.01440	.00730
C_L	+ .587	.829	.850	.824	.729	.620	.495	.354	.167
α	+4.1	1.8	3.0	2.5	2.1	2.3	1.6	1.9	.8

TABLE IV - Cont'd

SECTION LIFT CHARACTERISTICS

Climb Condition (Line II)   Data from Figure 42

$C_P = 0.2$ $V/nD = 1.08$

x =	0.2	0.3	0.4	0.45	0.55	0.65	0.75	0.85	0.95
b/D =	.0614	.0631	.0638	.0656	.0709	.0711	.0679	.0622	.0512

Model U-24 $\beta_{0.75R} = 35.0°$

dC_T/dx	+0.024	0.066	0.118	0.143	0.195	0.252	0.293	0.300	0.256
dC_Q/dx	+ .0054	.0127	.0211	.0260	.0370	.0491	.0608	.0707	.0585
C_L	+ .829	1.107	1.201	1.180	1.074	1.036	.987	.890	.735
a	+8.8	5.7	6.2	5.8	6.3	7.4	7.7	8.3	9.0

Model U-60 $\beta_{0.75R} = 36.2°$

dC_T/dx	+ .009	.048	.100	.130	.192	.259	.297	.298	.227
dC_Q/dx	+ .0018	.0089	.0183	.0240	.0373	.0511	.0655	.0720	.0581
C_L	+ .281	.782	1.032	1.081	1.068	1.068	1.013	.889	.666
a	-1.3	+ .9	5.0	5.7	7.3	8.7	8.9	8.9	8.9

Model 0.4E $\beta_{0.75R} = 36.2°$

dC_T/dx	- .016	+ .010	.062	.094	.164	.236	.296	.325	.246
dC_Q/dx	- .0016	+ .0018	.0110	.0173	.0318	.0471	.0640	.0814	.0762
C_L	- .311	+ .161	.630	.781	.911	.977	1.004	.978	.753
a	-6.2	-4.1	+ .2	1.2	4.2	7.2	8.9	10.4	12.1

Model 0.8E $\beta_{0.75R} = 35.7°$

dC_T/dx	+ .016	.056	.103	.130	.190	.249	.288	.296	.228
dC_Q/dx	+ .0038	.0113	.0200	.0251	.0373	.0499	.0629	.0728	.0597
C_L	+ .577	.971	1.097	1.104	1.062	1.033	.980	.887	.672
a	+4.7	2.3	5.1	5.5	6.7	8.1	8.4	9.6	9.3

TABLE IV - Cont'd

SECTION LIFT CHARACTERISTICS

Climb Condition (Line II)   Data from Figure 42

$C_P = 0.5$ $V/nD = 1.71$

x =	0.2	0.3	0.4	0.45	0.55	0.65	0.75	0.85	0.95
b/D =	.0614	.0631	.0638	.0656	.0709	.0711	.0679	.0622	.0512

Model U-24 $\beta_{0.75R} = 55.8°$

dC_T/dx	-0.005	+0.029	0.093	0.135	0.254	0.331	0.316	0.203	0.061
dC_Q/dx	+ .0142	.0280	.0488	.0613	.0964	.1326	.1500	.1601	.1420
C_L	+ .930	1.042	1.216	1.264	1.392	1.400	1.173	.831	.462
a	+19.5	15.0	14.6	14.1	14.4	16.1	17.5	19.2	20.7

Model U-60 $\beta_{0.75R} = 56.0°$

dC_T/dx	+ .030	.093	.171	.215	.314	.320	.266	.201	.096
dC_Q/dx	+ .0108	.0305	.0547	.0706	.1081	.1347	.1483	.1546	.1264
C_L	+ .738	1.245	1.505	1.582	1.617	1.393	1.078	.810	.490
a	+6.6	7.4	11.1	11.9	13.9	16.5	17.9	18.8	19.4

Model 0.4E $\beta_{0.75R} = 56.6°$

dC_T/dx	+ .012	.061	.129	.175	.298	.436	.335	.159	.021
dC_Q/dx	+ .0080	.0200	.0420	.0580	.0990	.1510	.1680	.1785	.1530
C_L	+ .531	.816	1.150	1.296	1.499	1.701	1.285	.811	.411
a	+ .4	2.0	6.6	7.8	11.2	14.7	18.1	21.1	23.5

Model 0.8E $\beta_{0.75R} = 55.4°$

dC_T/dx	+ .026	.089	.160	.198	.272	.301	.255	.200	.075
dC_Q/dx	+ .0120	.0310	.0555	.0710	.1050	.1335	.1475	.1570	.1375
C_L	+ .812	1.256	1.500	1.555	1.509	1.353	1.055	.816	.477
a	+13.5	9.3	11.3	11.7	13.3	15.8	17.3	19.4	19.8
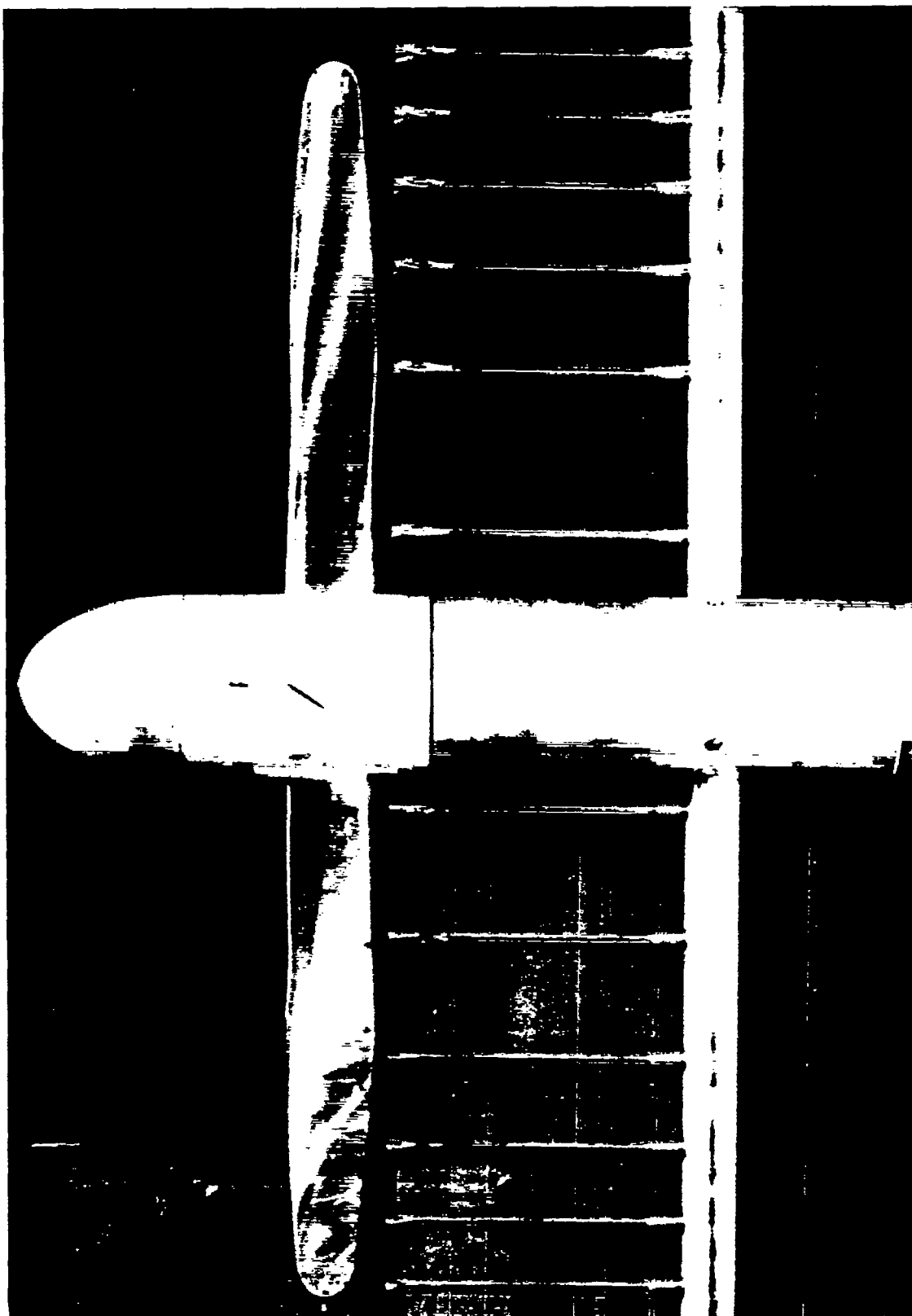
Figure A.
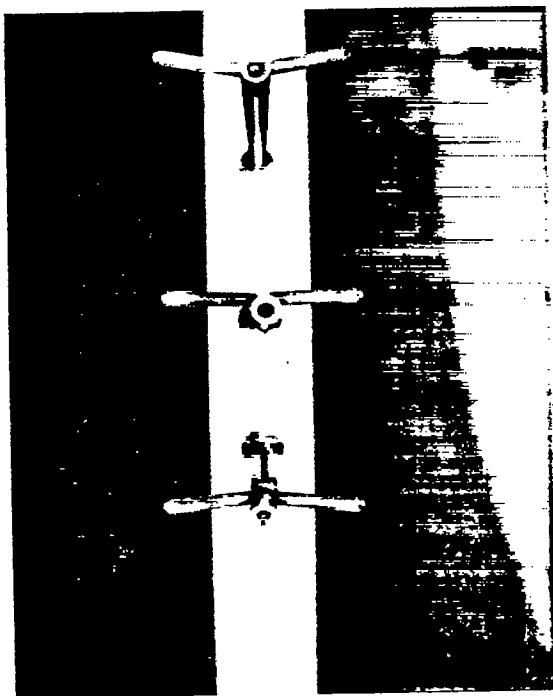
Figure B.
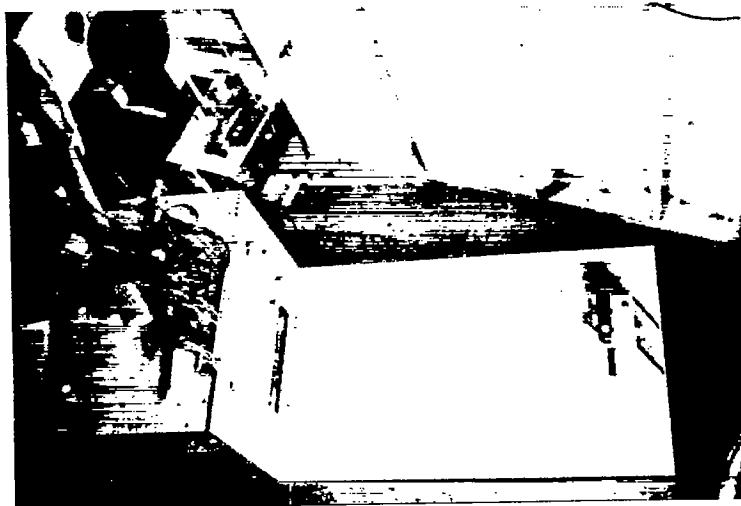
Figure C.
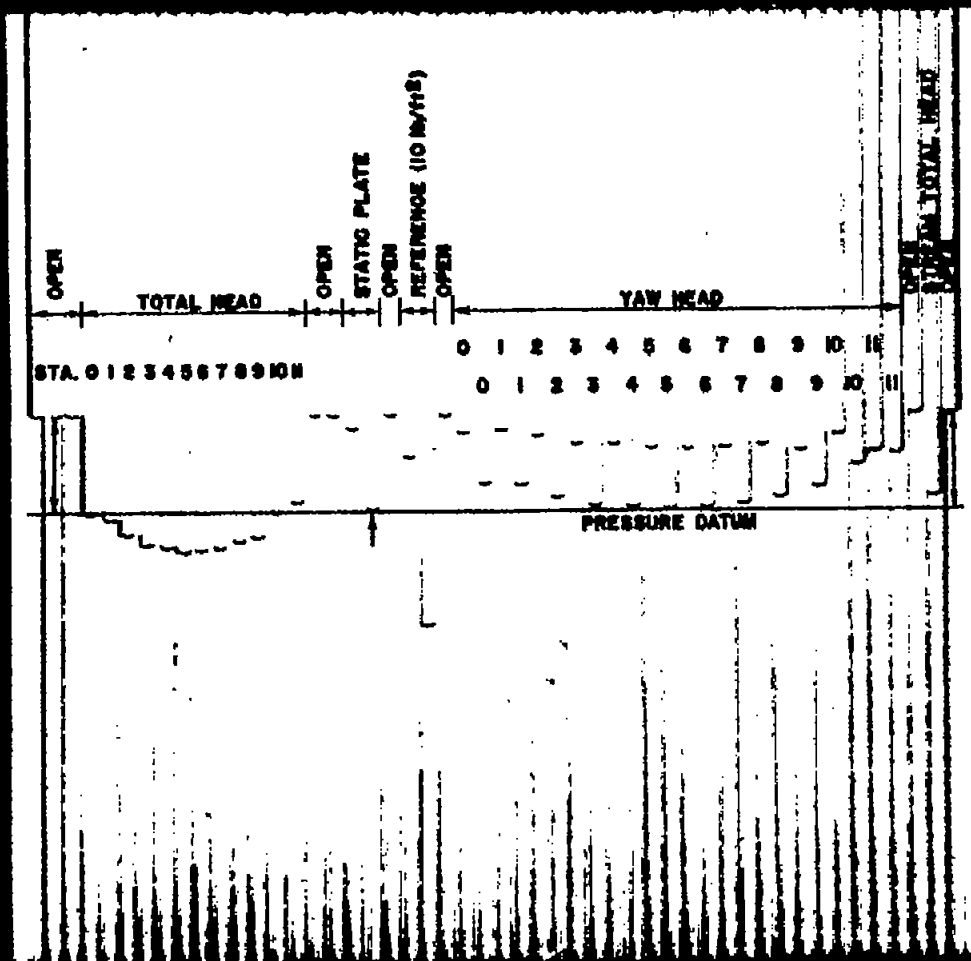
Figure D.— Sample manometer record.
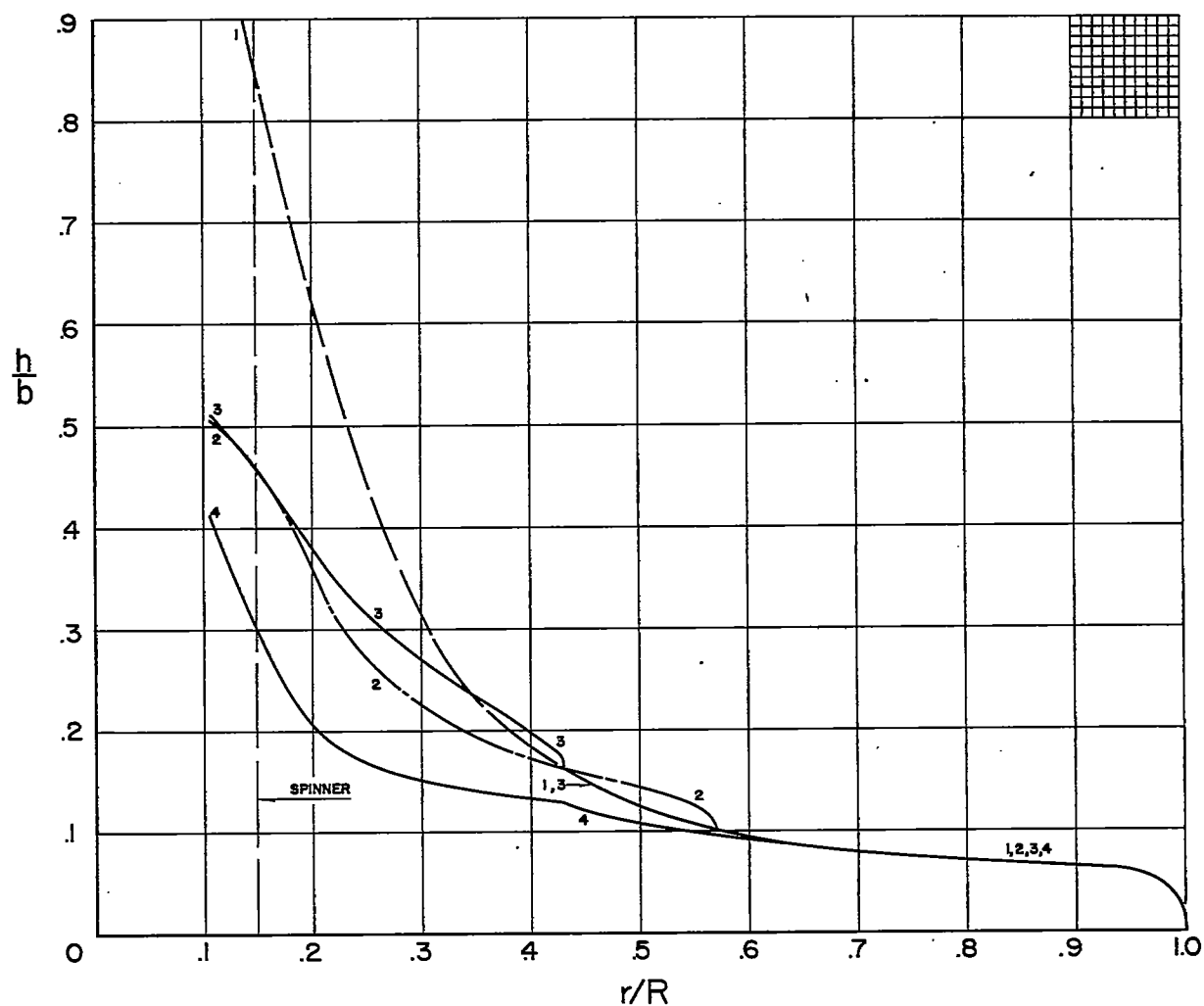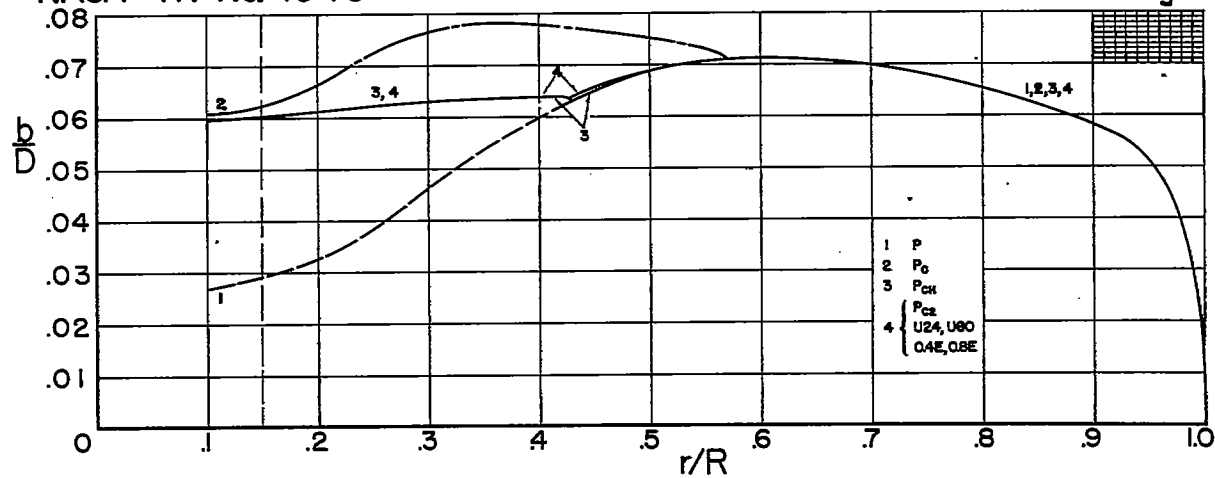
Fig. 1

FIG. 1   BLADE FORM CURVES
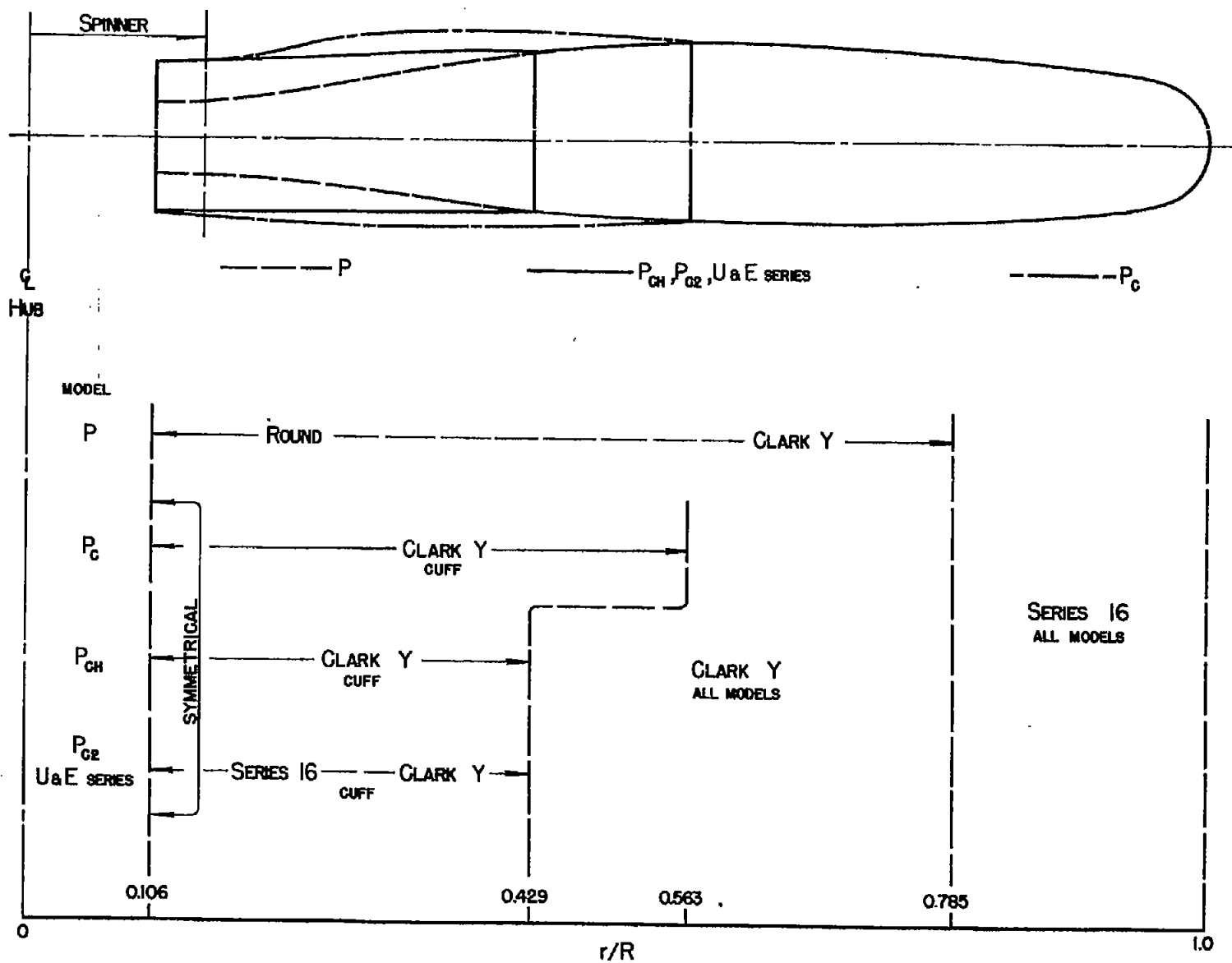
FIG. 2   CHARACTER OF BLADE PROFILES
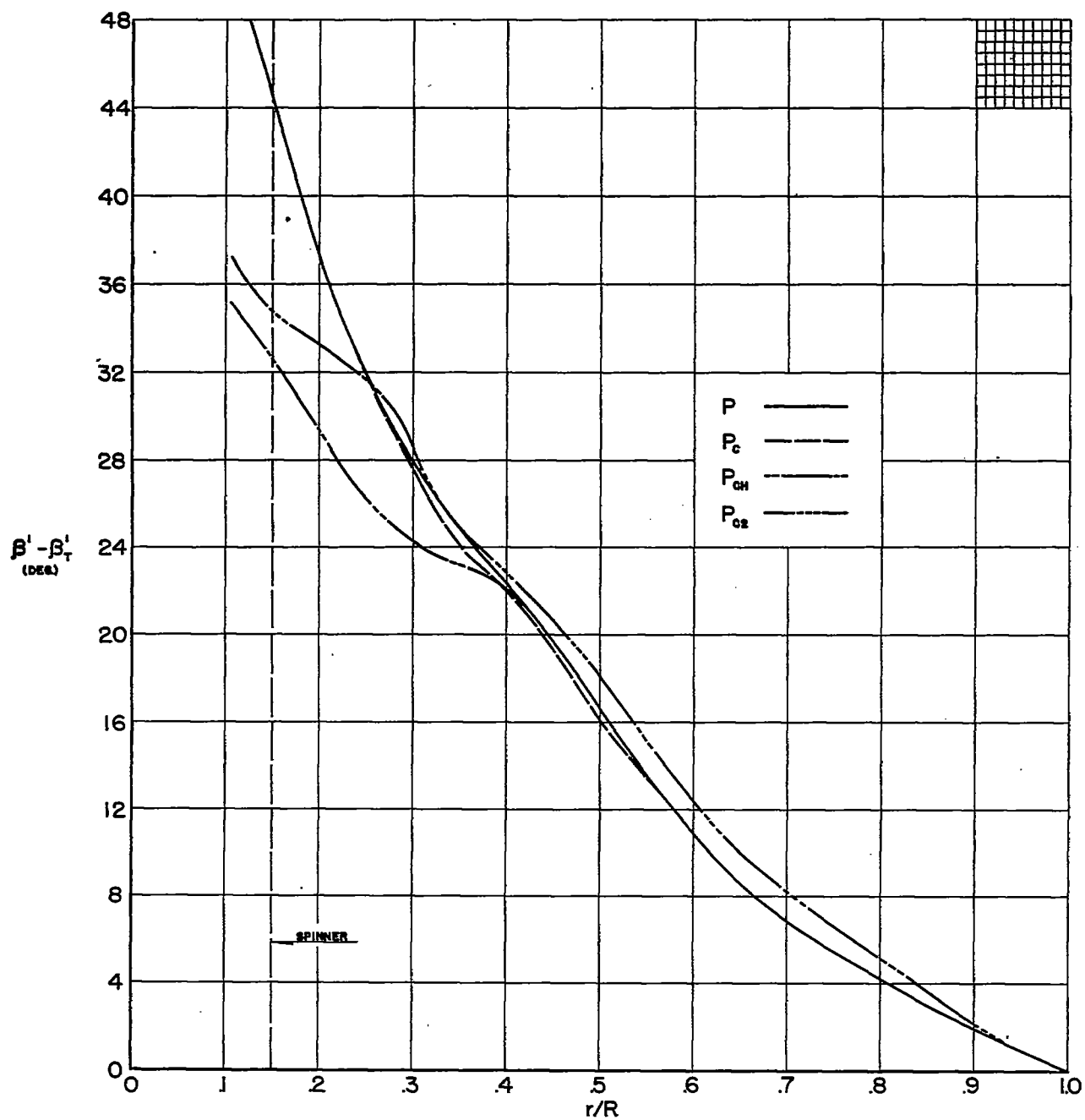
FIG. 3   BLADE TWIST CURVES , FOUR-BLADE MODELS

Fig. 4　　　　　　　　　　　　　　　　　　　　　　NACA TN No. 1040
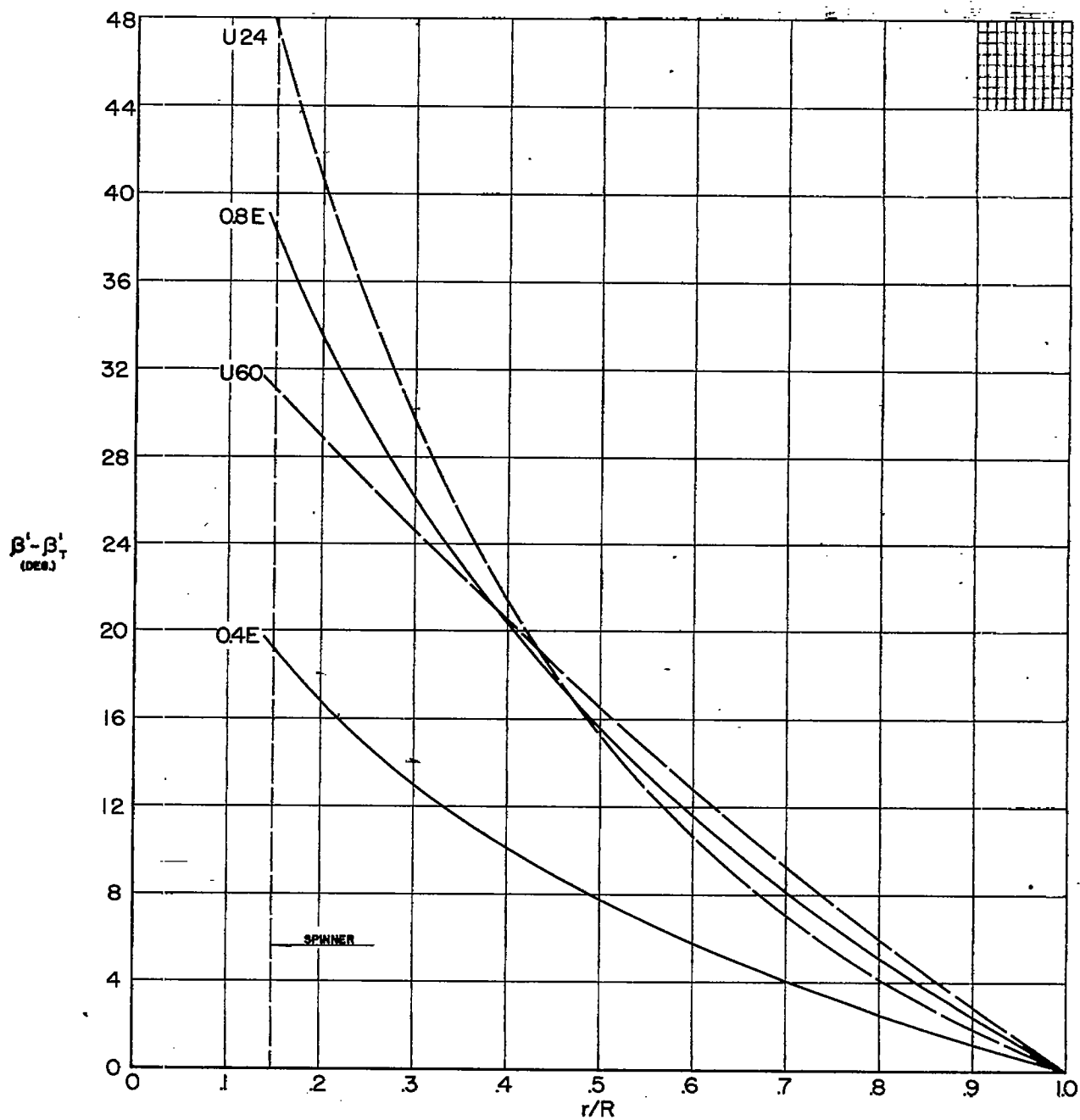
FIG. 4　　BLADE TWIST CURVES , THREE-BLADE MODELS

Assembly

THREE 1/8" O.D. STEEL TUBES SOLDERED TOGETHER

Details

GENERAL
ARRANGEMENT

YAW AND TOTAL
HEAD TUBES

STA. NO.	r/R
11	1.028
9	.928
7	.814
5	.683
3	.520
	0.06 D
1	.253
0	.201
	0.0075 D (Min.)
2	.409
4	.606
6	.752
8	.873
10	.979

BLADE AXIS

MODEL P_0

DIAM. 33.6"
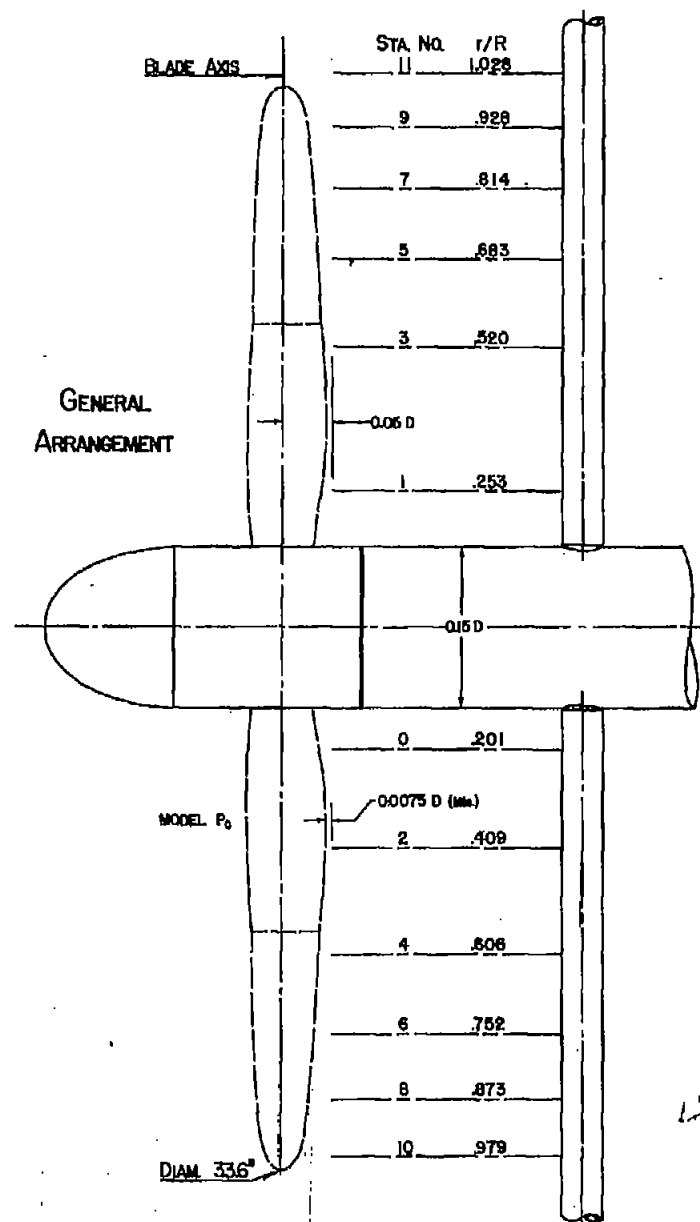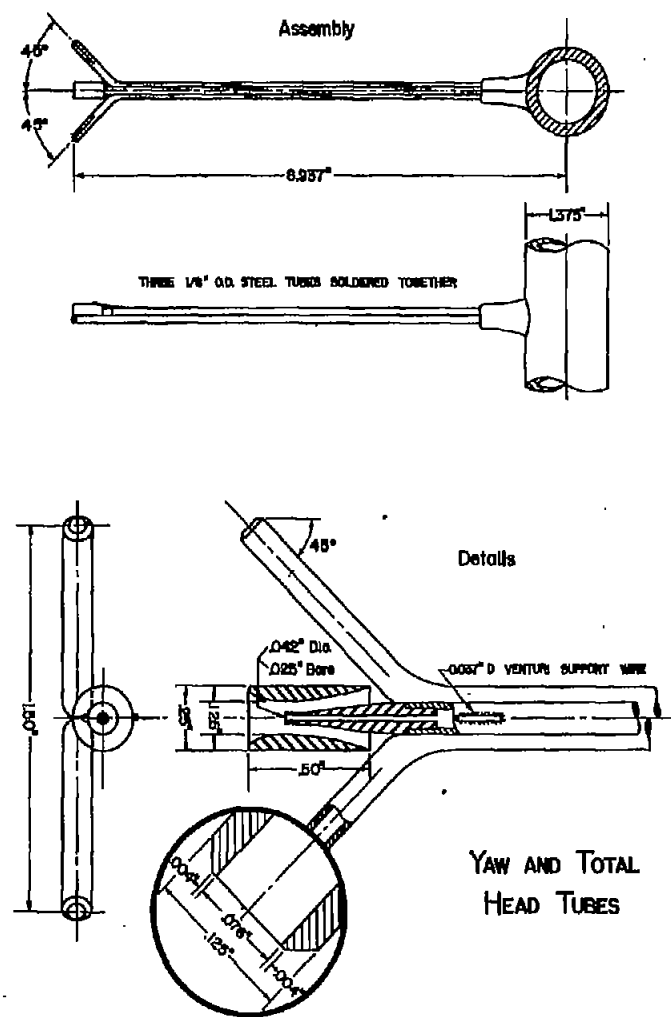
FIG. 5   WAKE SURVEY APPARATUS

Fig. 5

FIG. 6   CALIBRATION DATA

Fig. 7
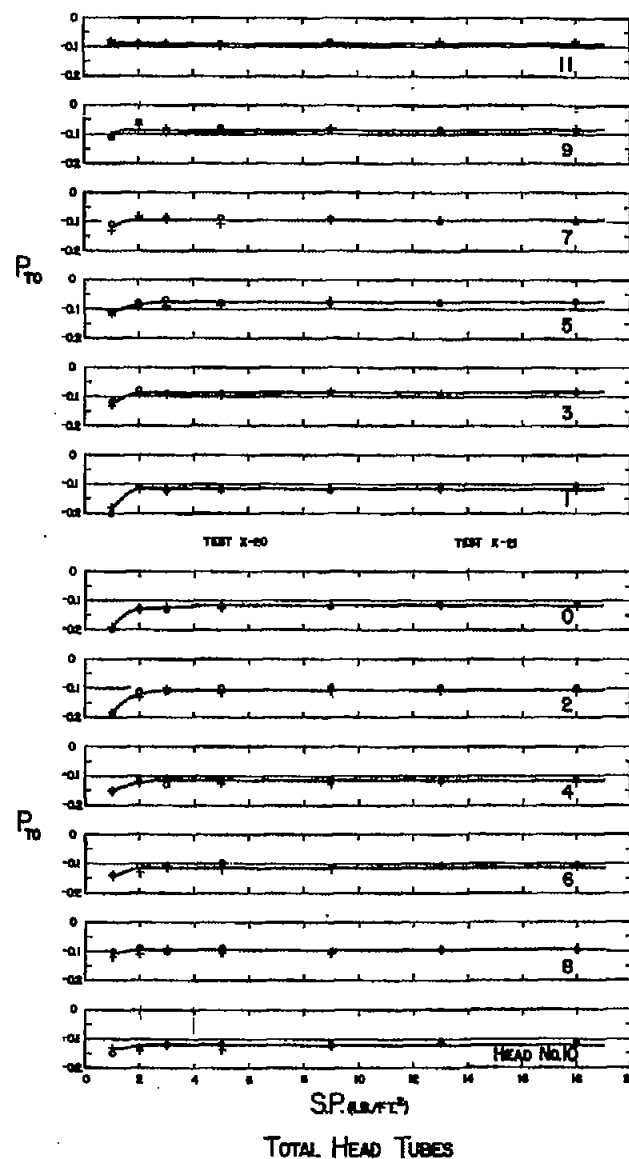
HEAD NO.	0	1	2	3	4	5	6	7	8	9	10	11
P_{TI}	+0.05	+0.11	+0.29	+0.40	+0.44	+0.49	+0.47	+0.44	+0.36	+0.33	+0.03	−0.09
P_{TO}	−0.120	−0.115	−0.105	−0.085	−0.115	−0.075	−0.110	−0.095	−0.095	−0.085	−0.120	−0.090
ΔP_T	+0.170	+0.225	+0.395	+0.485	+0.555	+0.565	+0.585	+0.535	+0.455	+0.415	+0.150	0
P_U	−0.30	−0.29	−0.13	−0.04	−0.02	0	0	−0.05	−0.13	−0.25	−0.51	−0.64
P_D	−0.90	−0.93	−0.87	−0.75	−0.75	−0.71	−0.70	−0.71	−0.75	−0.68	−0.86	−0.66
P_Y	+0.60	+0.64	+0.74	+0.71	+0.73	+0.71	+0.70	+0.66	+0.62	+0.43	+0.35	+0.02
$1/K$	0.478	0.452	0.463	0.467	0.465	0.455	0.472	0.459	0.472	0.472	0.476	0.465
$(P_Y/K)^2$	0.082	0.084	0.117	0.110	0.115	0.104	0.109	0.092	0.086	0.041	0.028	0
E	0.017	0.018	0.024	0.023	0.024	0.022	0.023	0.019	0.018	0.009	0.006	0
$\Delta P_T - E$	0.153	0.207	0.371	0.462	0.531	0.543	0.562	0.516	0.437	0.406	0.144	0
x	0.201	0.253	0.409	0.520	0.606	0.683	0.752	0.814	0.873	0.928	0.979	1.028
$C_1 x$	0.153	0.193	0.312	0.396	0.462	0.521	0.573	0.621	0.665	0.707	0.746	0.783
dC_T/dx	0.023	0.040	0.116	0.183	0.245	0.283	0.322	0.320	0.291	0.287	0.107	0
x^2	0.0404	0.0640	0.167	0.270	0.367	0.467	0.566	0.663	0.762	0.861	0.958	1.057
x^2/K	0.0193	0.0290	0.0775	0.126	0.171	0.212	0.267	0.304	0.359	0.406	0.456	0.492
$P_Y x^2/K$	0.012	0.019	0.057	0.089	0.125	0.151	0.187	0.201	0.223	0.175	0.160	0.010
dC_Q/dx	0.005	0.007	0.022	0.034	0.048	0.058	0.071	0.077	0.085	0.067	0.061	0.004

RECORD NO. _H-2-8_

MODEL _0.8E_

$\beta_{0.75R}$ _36_ DEG.

S.P. _4.82_ PSF

σ _0.927_

V _67.7_ FPS

n _24.54_ RPS

DIAMETER _2.80_ FT.

V/nD _0.985_

$\Delta P_T = P_{TI} - P_{TO}$ $P_Y = P_U - P_D$

$$E = (1/4r^2)(P_Y/K)^2$$

$r =$ _1.094_ $1/4r^2 =$ _0.209_

$C_1 = \dfrac{\pi}{4}\left(\dfrac{V}{nD}\right)^2 = 0.7854(0.985)^2 =$ _0.762_

$C_2 = \dfrac{\pi}{8}\left(\dfrac{V}{nD}\right)^2 = 0.3927(0.985)^2 =$ _0.381_

$dC_T/dx = (\Delta P_T - E)C_1 x$ $dC_Q/dx = (P_Y x^2/K)C_2$

$C_T = C_{TO} - \Delta C_T$ $C_P = 2\pi C_Q$

$C_{TO} =$ _0.1570_

$\Delta C_T =$ _0.0009_

$C_T =$ _0.1561_

$C_Q =$ _0.0368_

$C_P =$ _0.2312_

TESTED	_9-1-43_
RECORDED	_10-30-43_
COMPUTED	_11-20-43_

FIG. 7   SAMPLE COMPUTATION FORM

Fig. 8

$\beta_{0.75R} = 12°$

V/nD=0.310

0.426

0.510

0.595

THRUST

TORQUE

TUBES 1,3,5,7,9,11 - ABOVE ₵
TUBES 02,4,6,8,10 - BELOW ₵
MEAN CURVE

FIG. 8   SAMPLE GRADING CURVES   MODEL 0.8E

Fig. 9.

$\beta_{0.75R} = 36°$

V/nD = 0.587

0.985

1.294

1.628

$\frac{dC_T}{dx}$

$\frac{dC_Q}{dx}$

X

X

THRUST

TORQUE

TUBES 1,3,A,7,9H - ABOVE ¢.
TUBES O,2,4,6,8,0 - BELOW ¢.
MEAN CURVE

FIG. 9   SAMPLE GRADING CURVES   MODEL 0.8E

Fig. 10
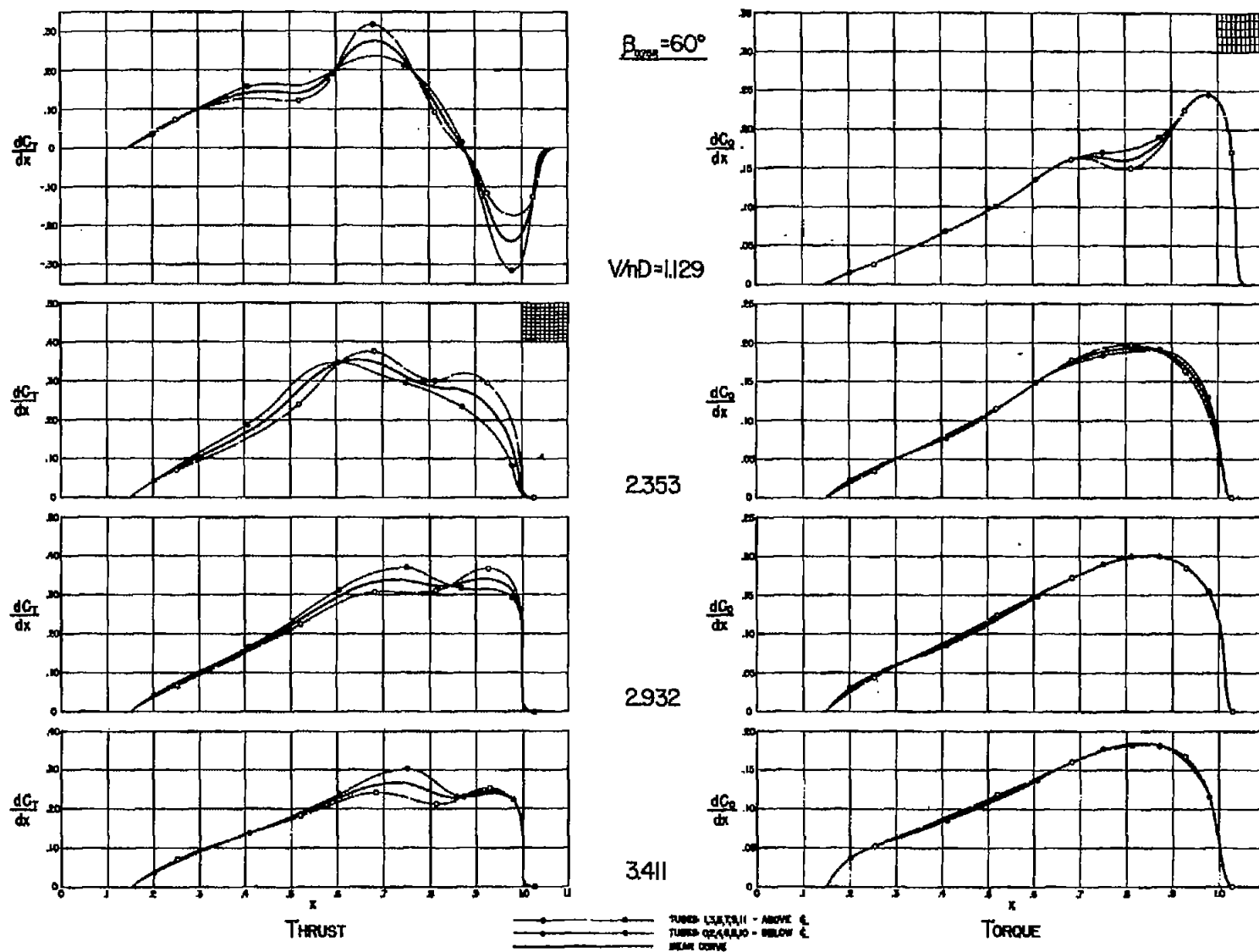
FIG. 10   SAMPLE GRADING CURVES   MODEL O.8E
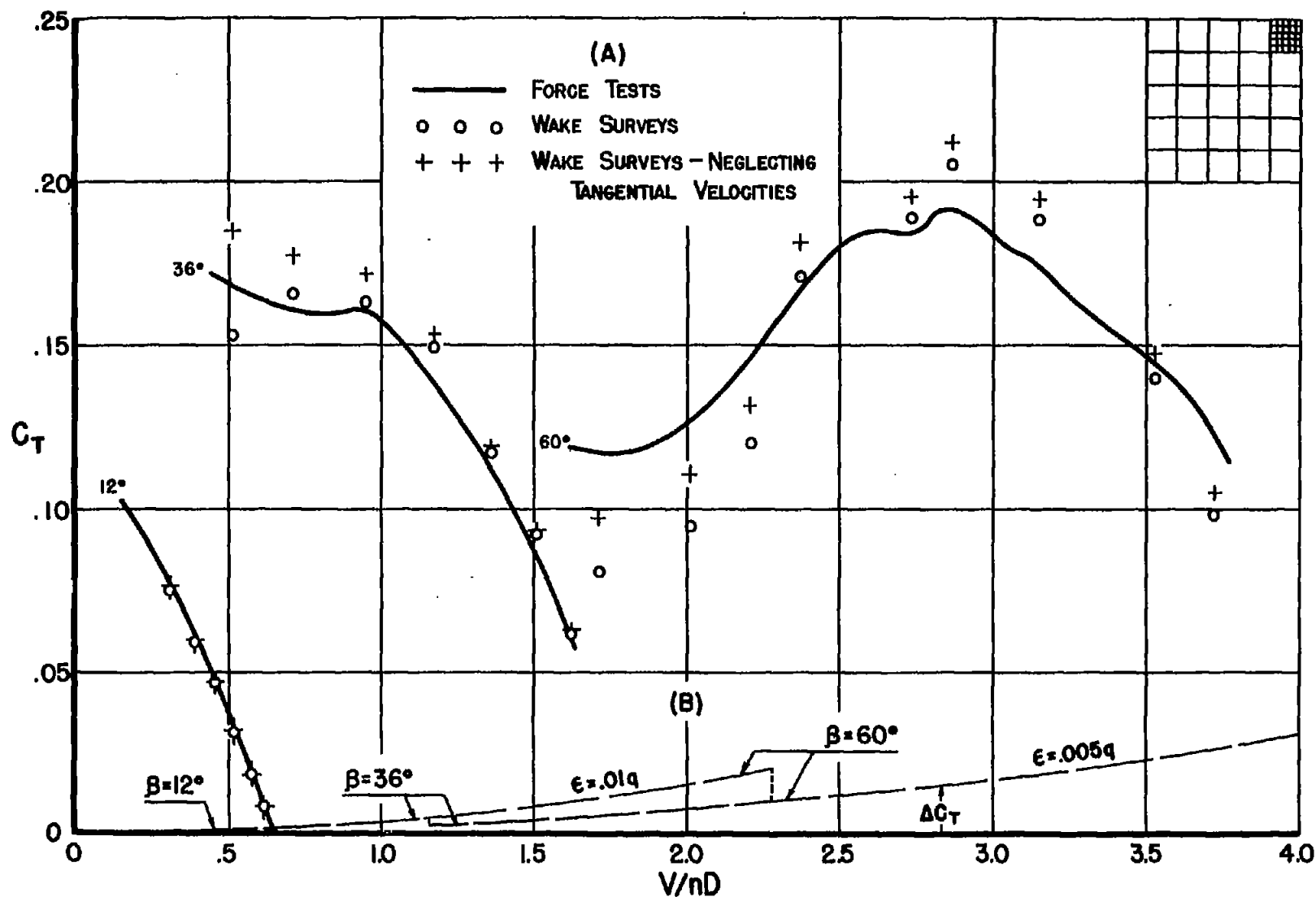
FIG. 11   EFFECTS OF: (A) NEGLECTING TANGENTIAL VELOCITIES AND
(B) LEAST COUNT ERROR IN READING RECORDS

Fig. 11

Fig. 12

—— Force Test   MODEL P   • ○ Wake Survey
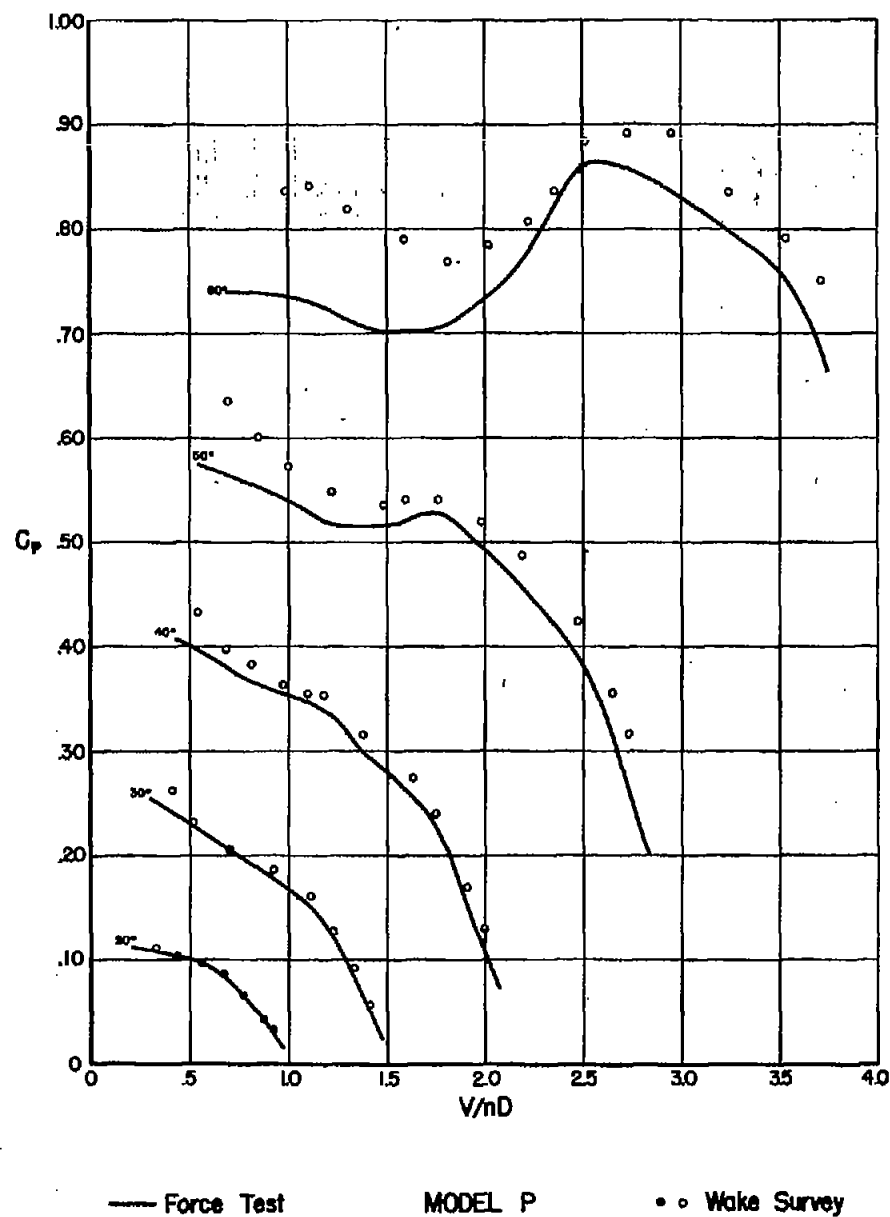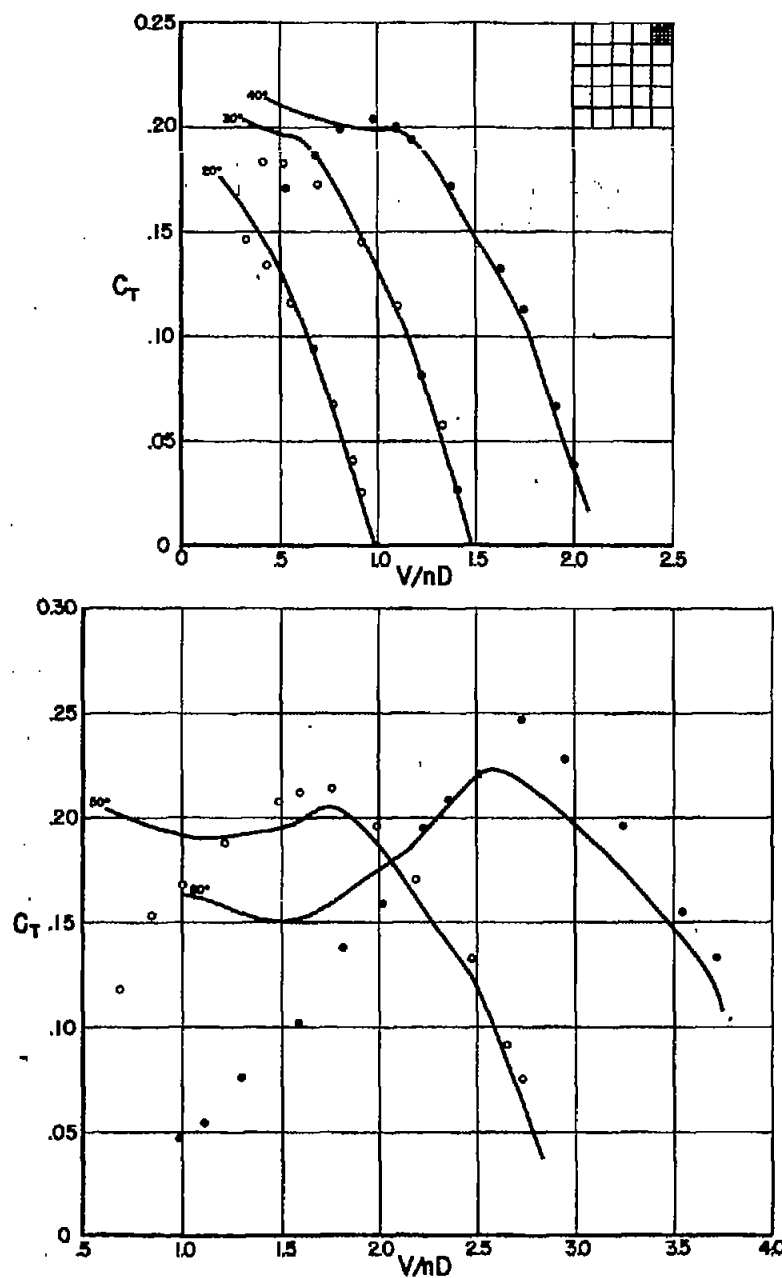
FIG. 12   RESULTS OF WAKE SURVEYS AND FORCE TESTS

Fig. 13

—— Force Test   MODEL P$_G$ • ○ Wake Survey
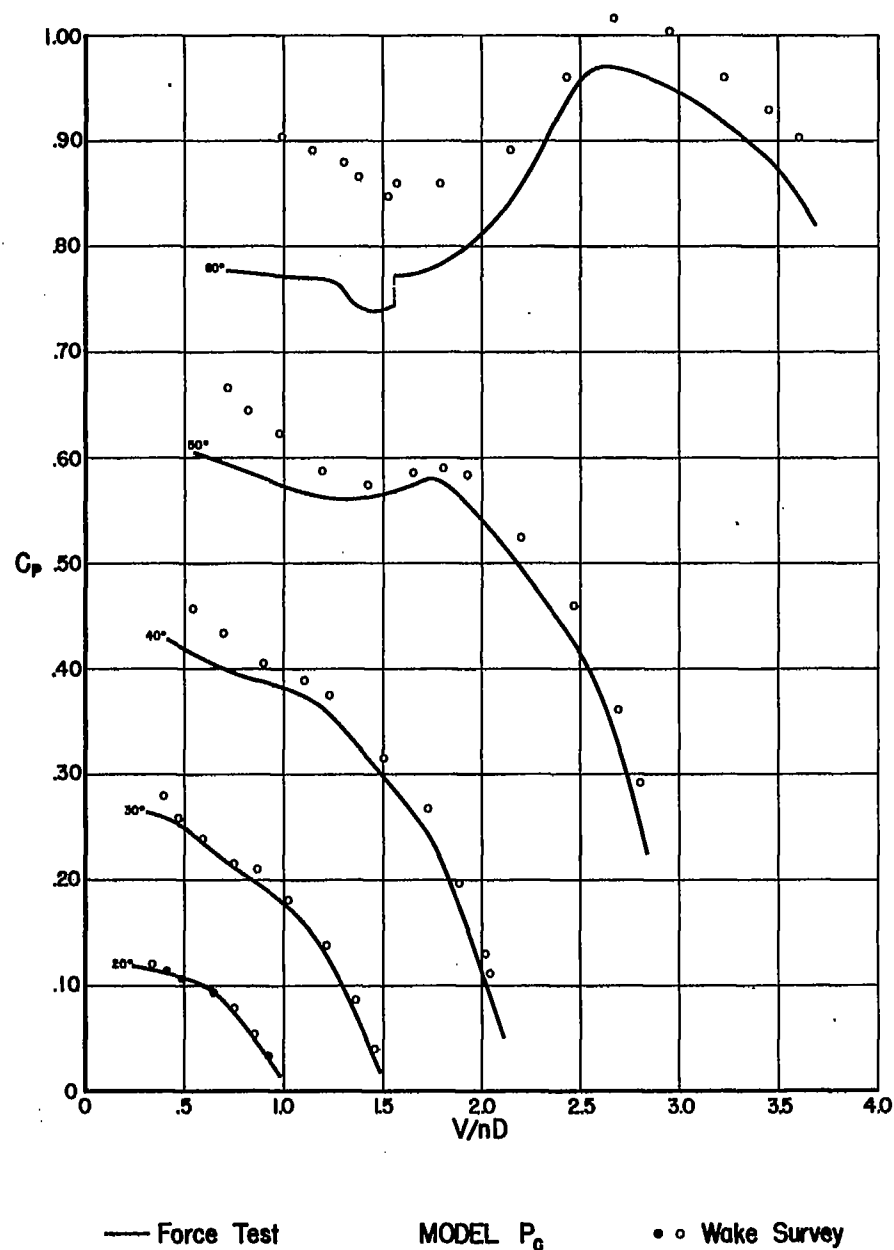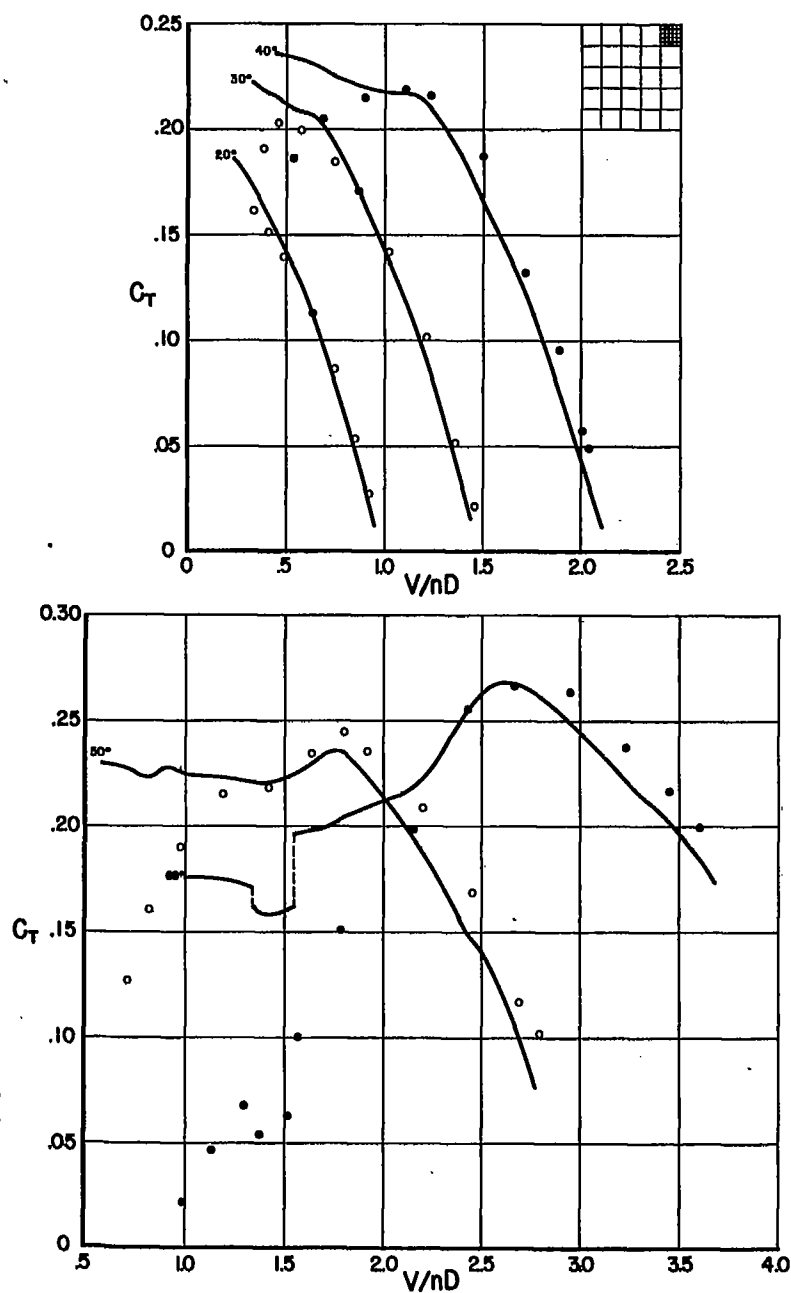
FIG. 13   RESULTS OF WAKE SURVEYS AND FORCE TESTS

Fig. 14
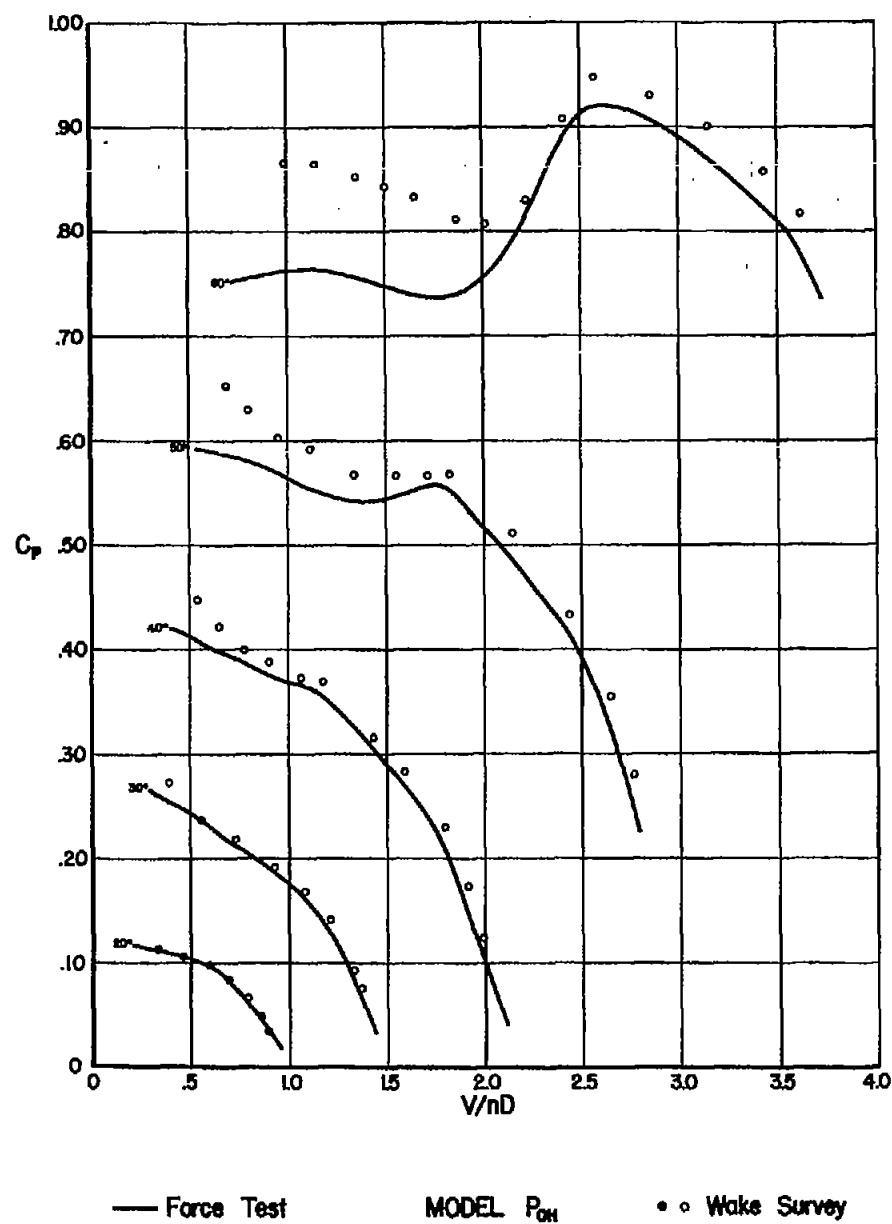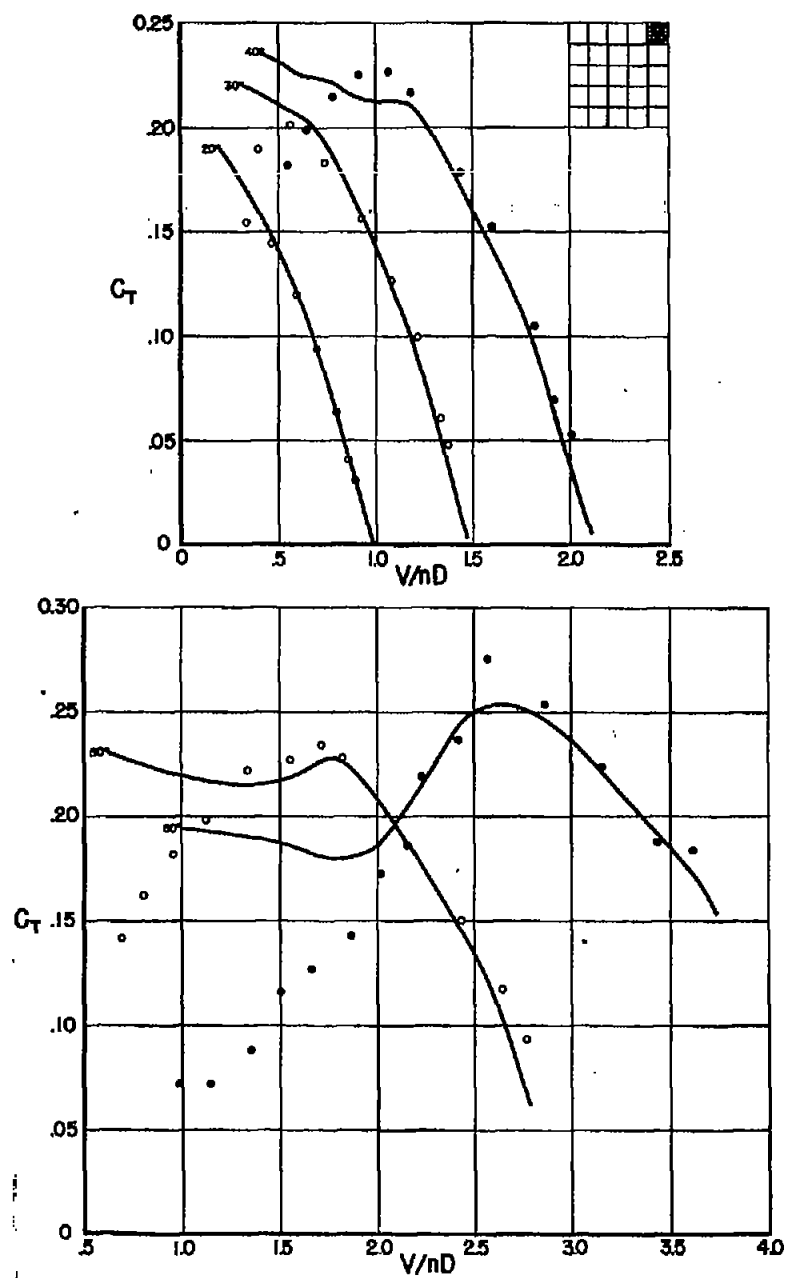
FIG. 14   RESULTS OF WAKE SURVEYS AND FORCE TESTS
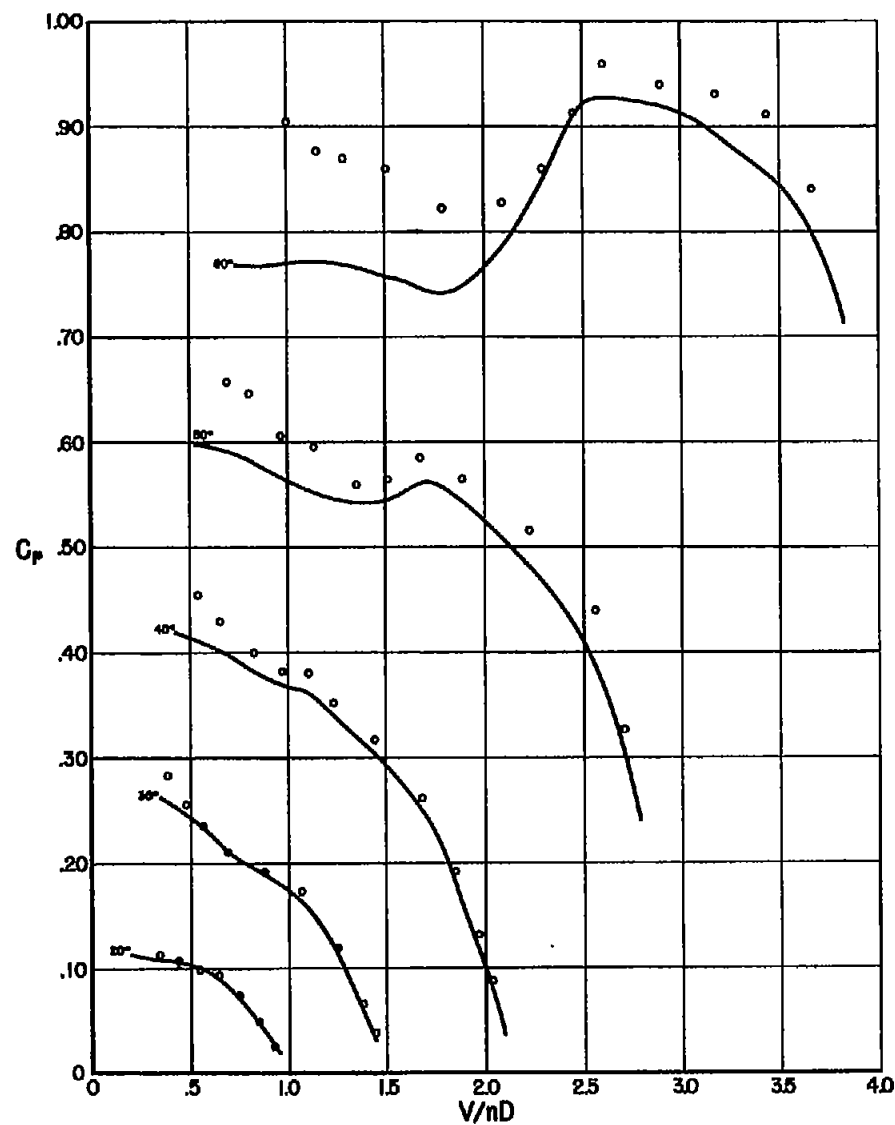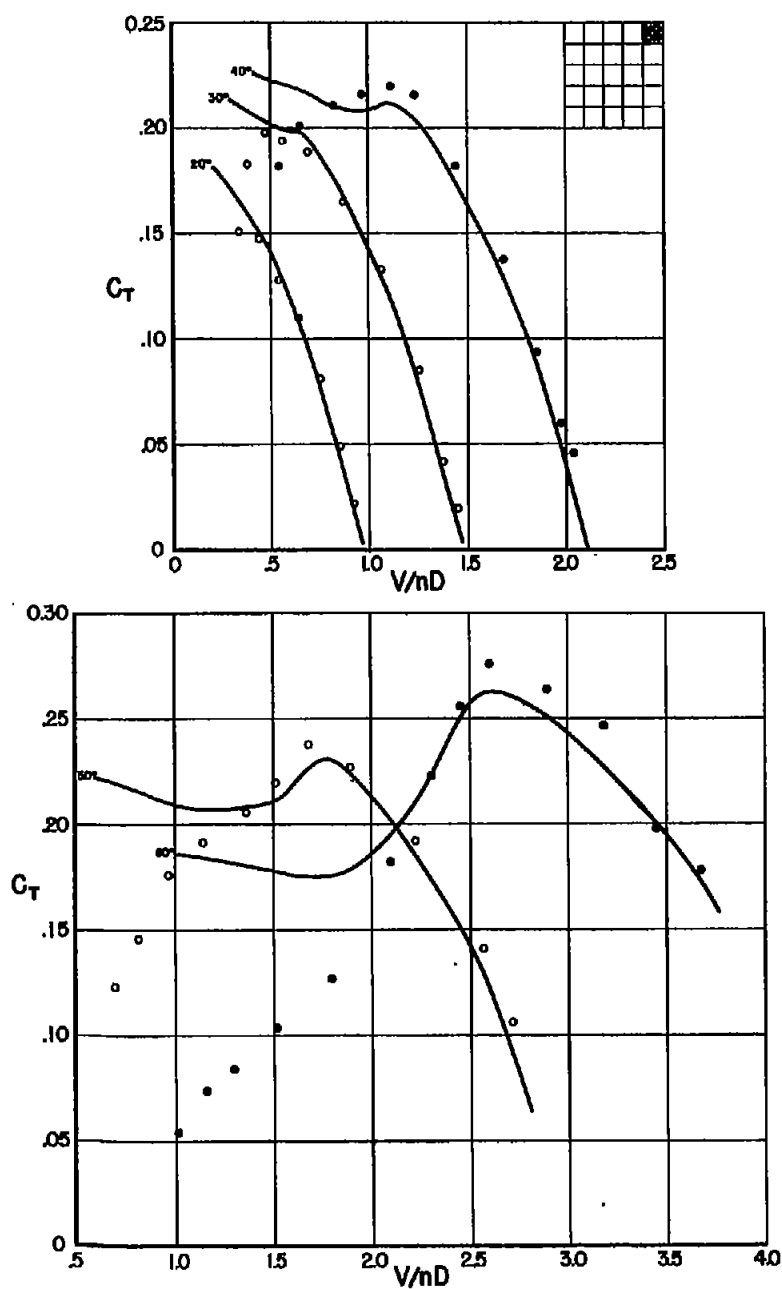
Fig. 15

— Force Test   MODEL P₀₂   • ○ Wake Survey

FIG. 15   RESULTS OF WAKE SURVEYS AND FORCE TESTS

Fig. 16

NACA TN No. 1040

—— Force Test   MODEL U24   •○ Wake Survey
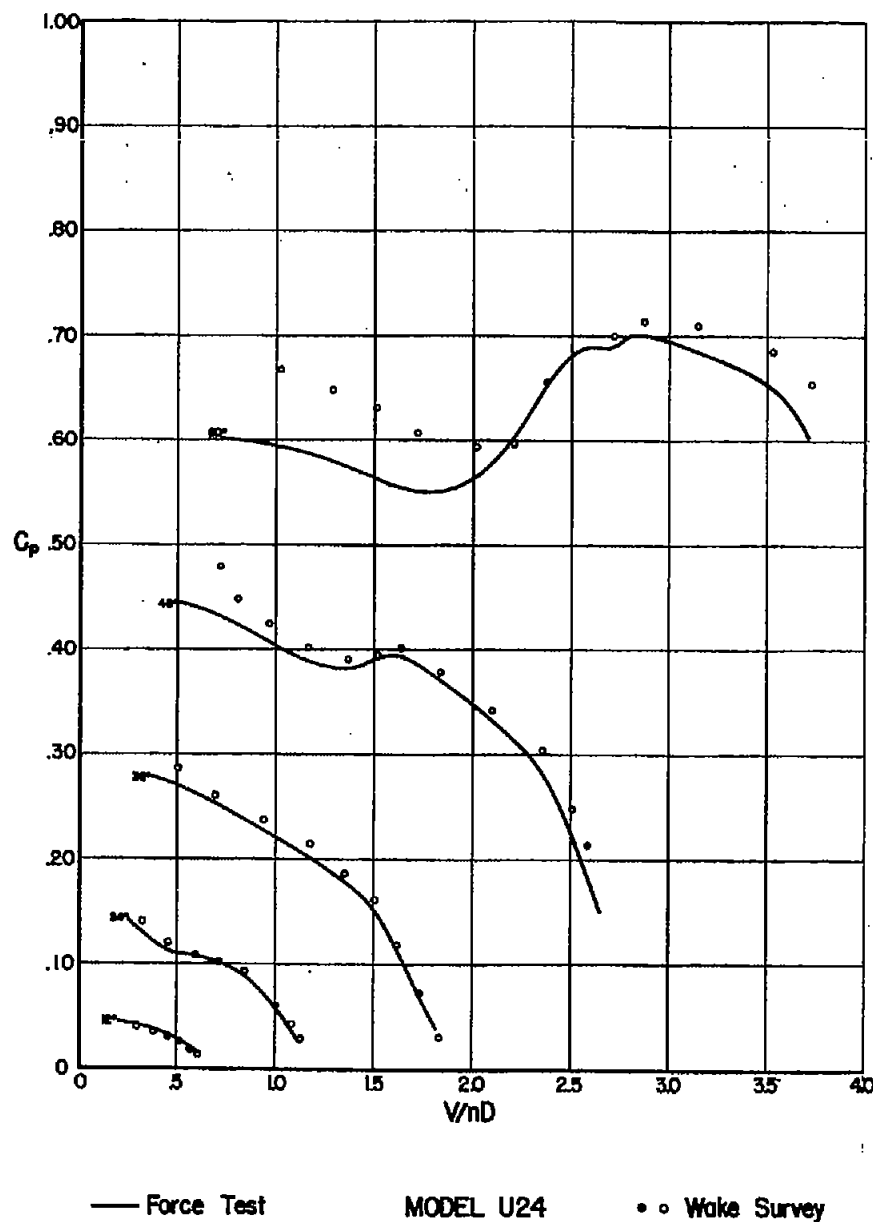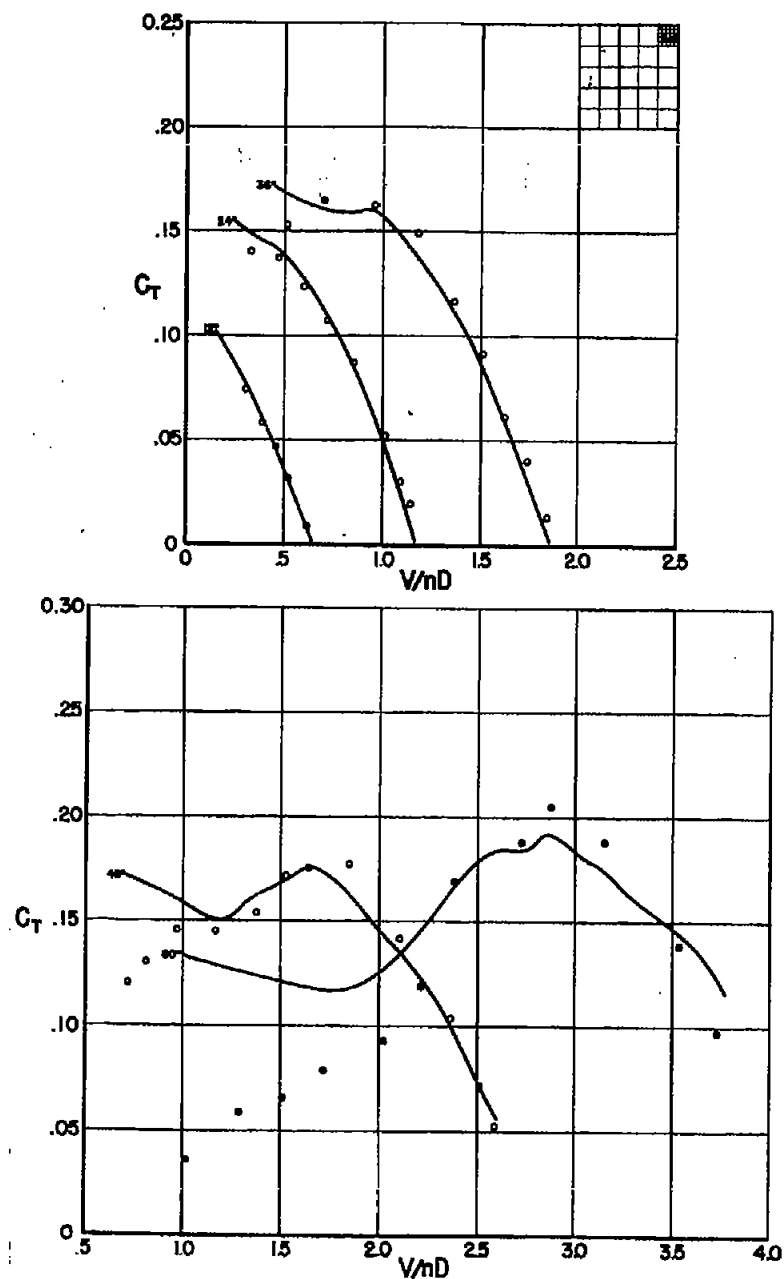
FIG. 16   RESULTS OF WAKE SURVEYS AND FORCE TESTS

Fig. 17

—— Force Test   MODEL U60   • ○ Wake Survey
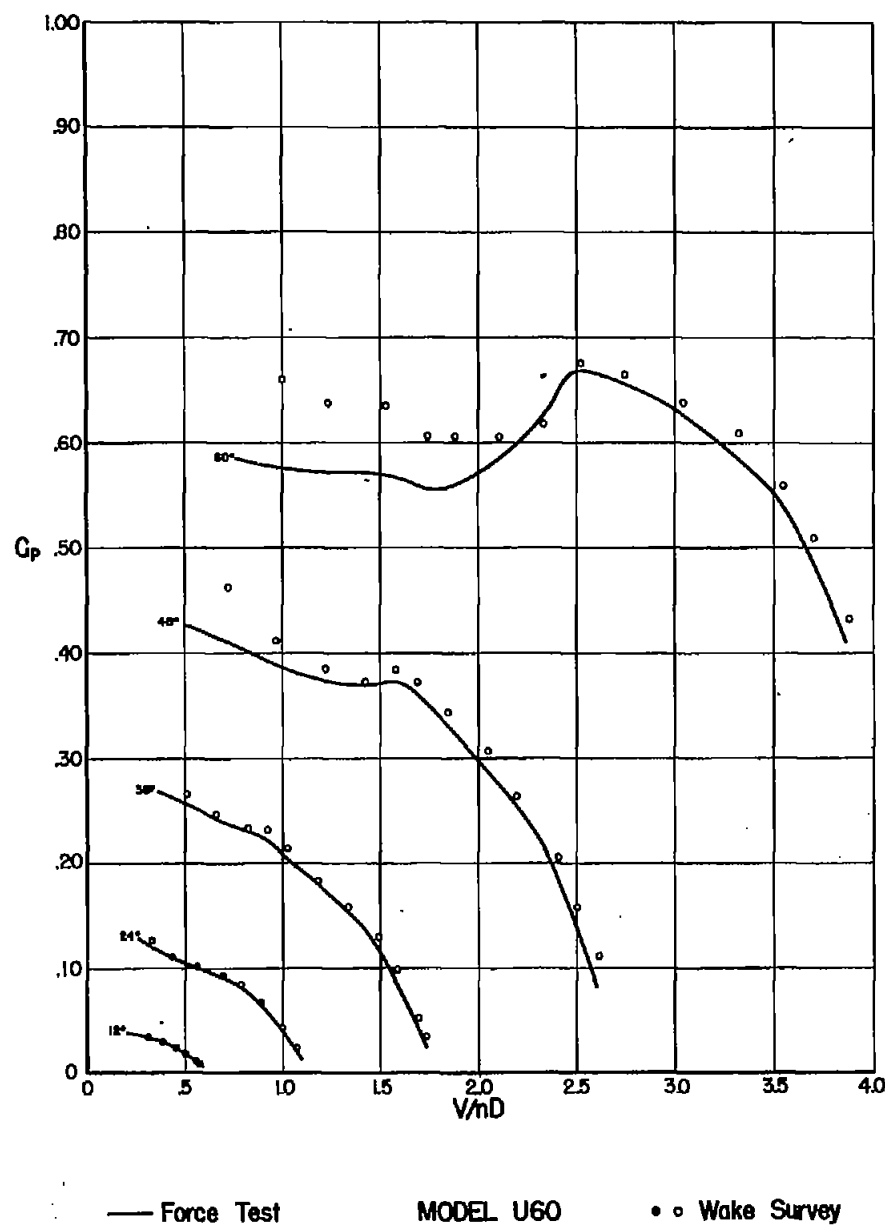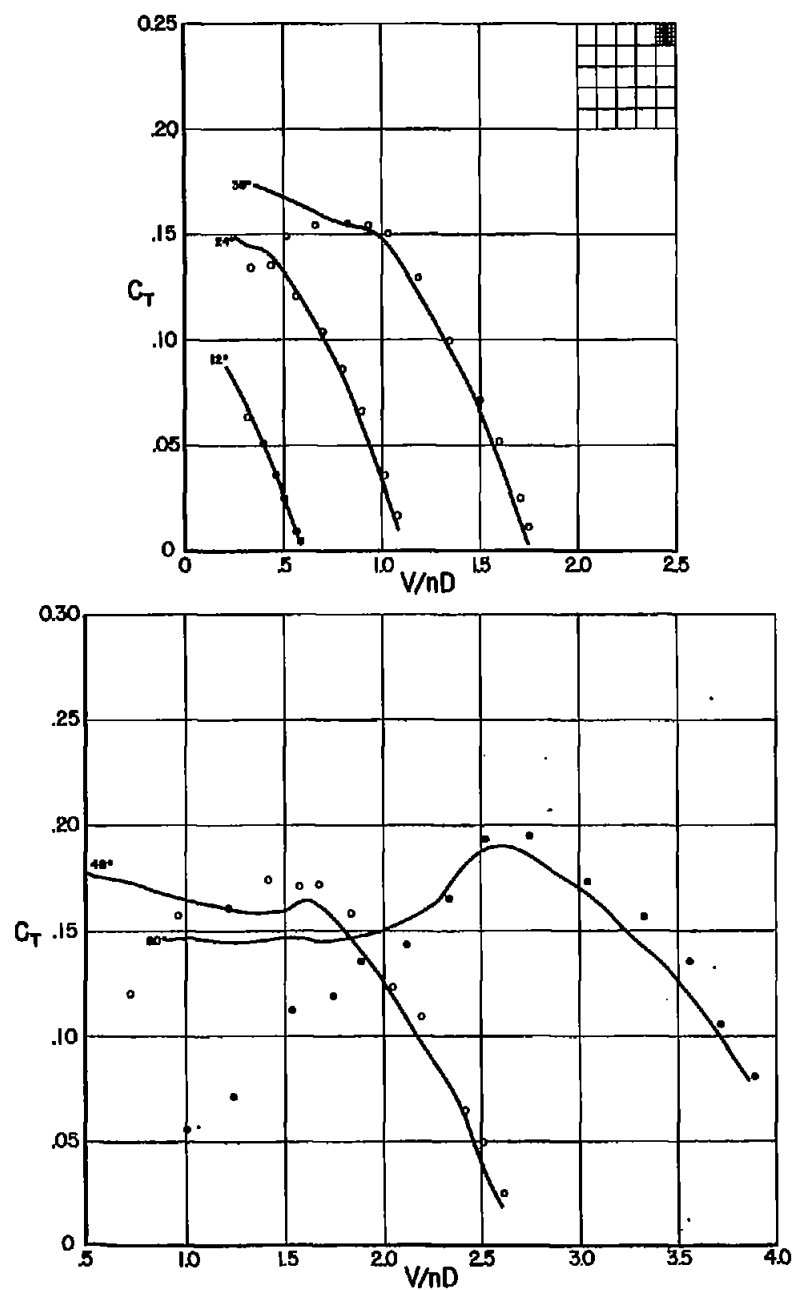
FIG. 17   RESULTS OF WAKE SURVEYS AND FORCE TESTS

Fig. 18

—— Force Test   MODEL 0.4E   • ○ Wake Survey
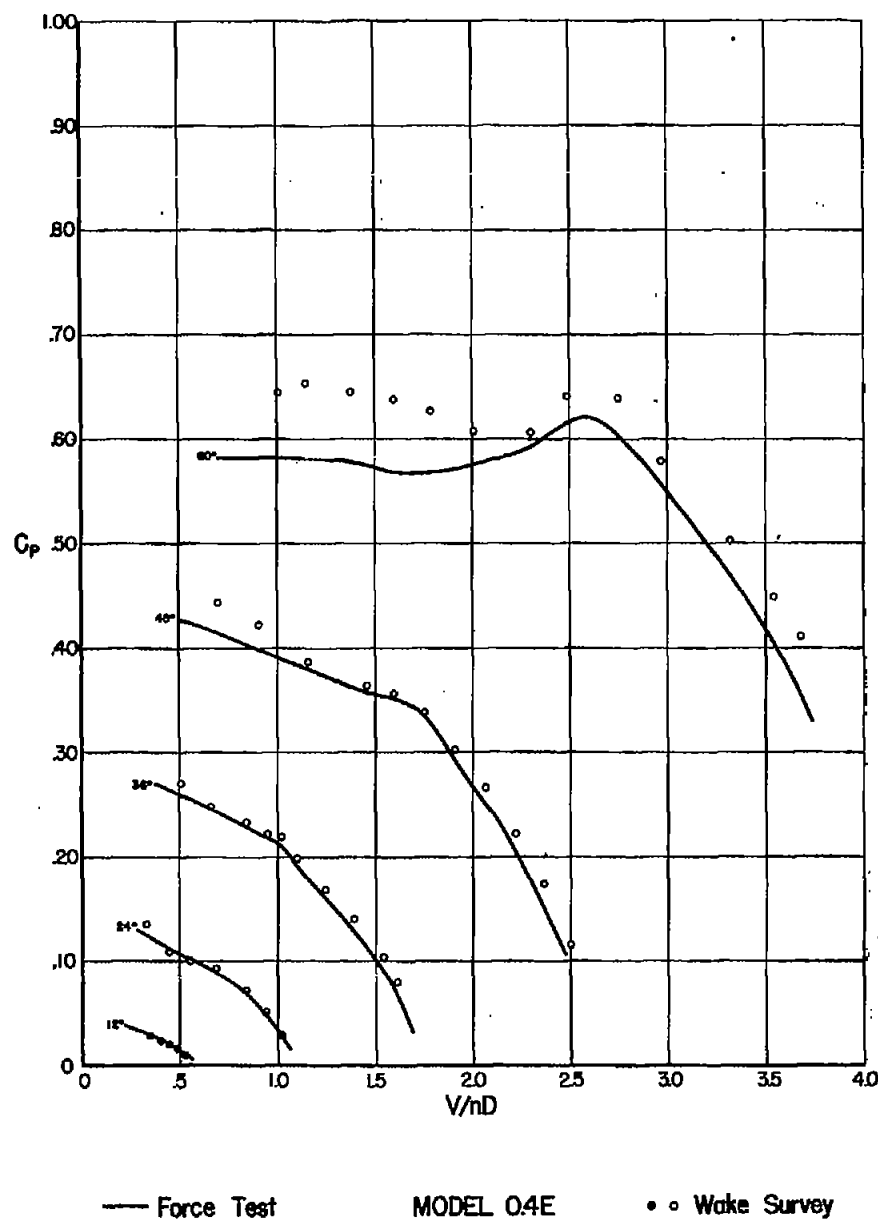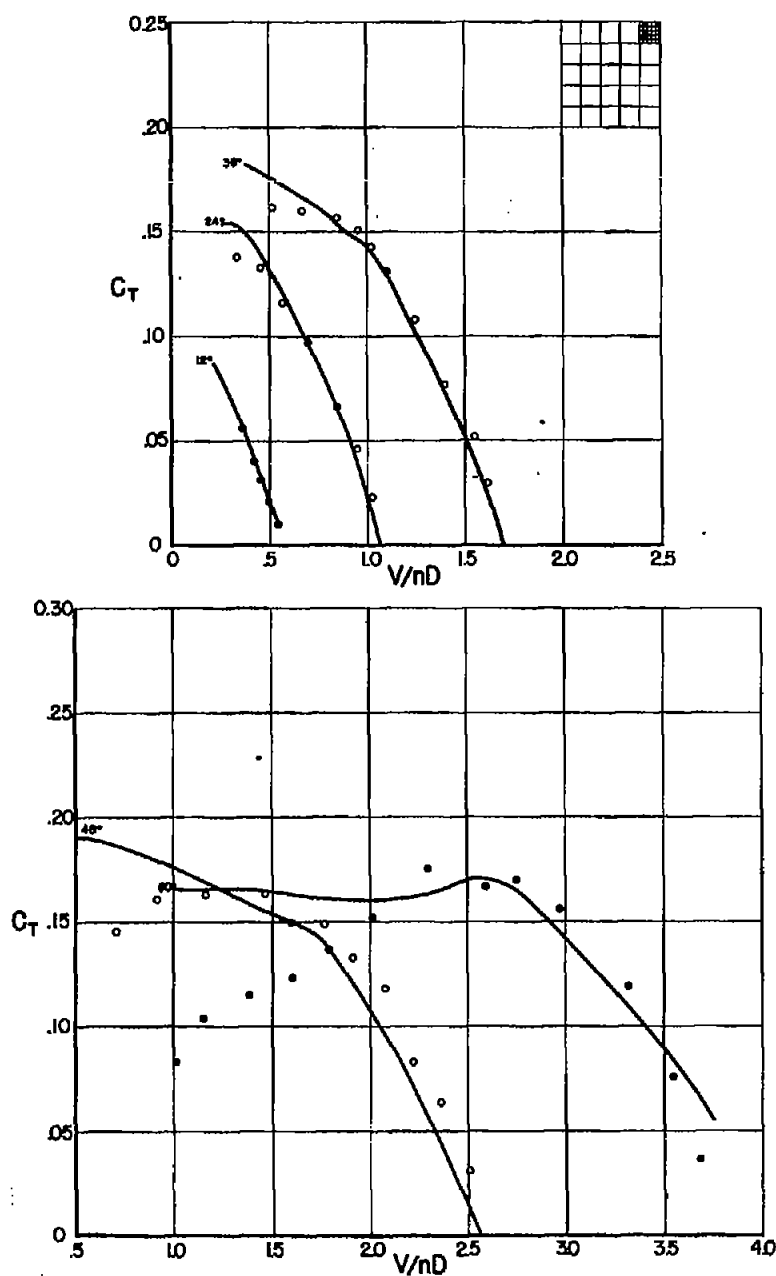
FIG. 18   RESULTS OF WAKE SURVEYS AND FORCE TESTS

FIG. 19   RESULTS OF WAKE SURVEYS AND FORCE TESTS
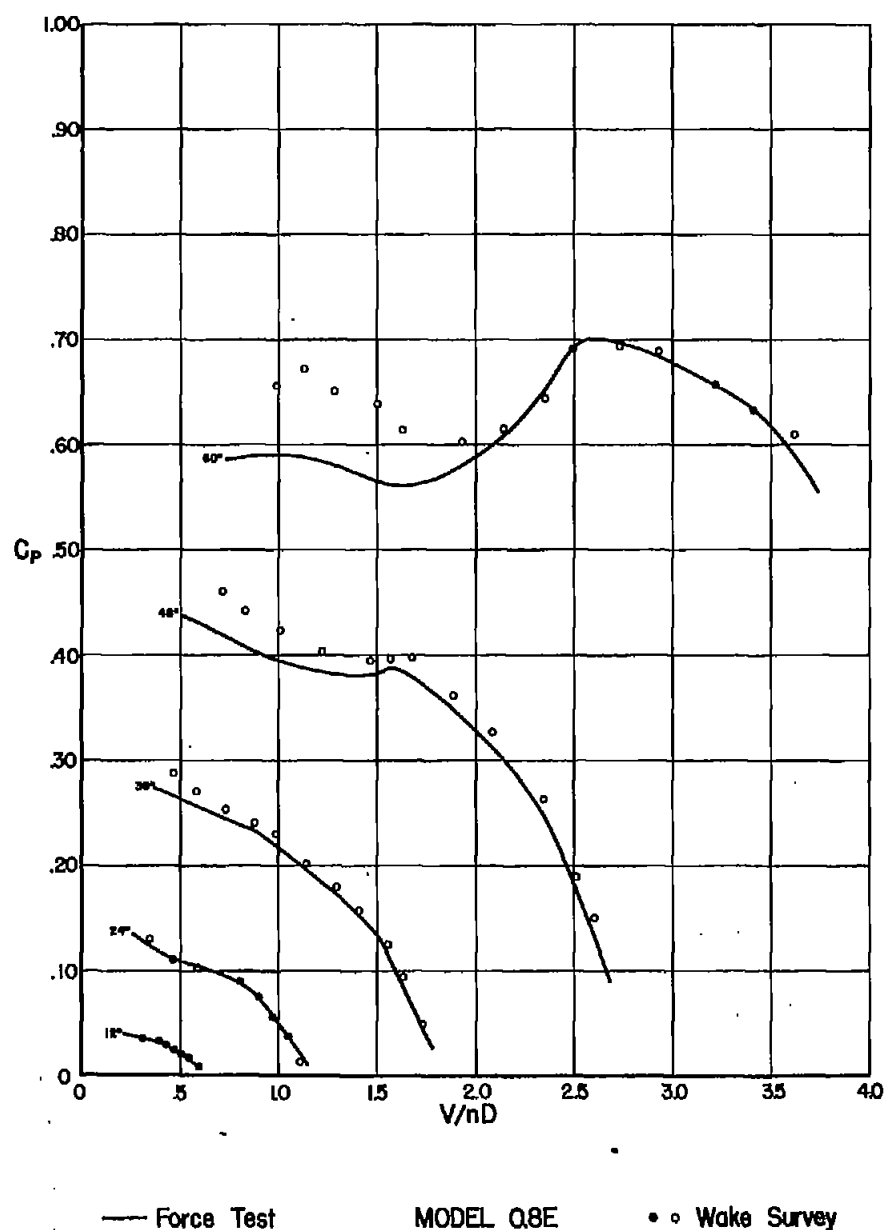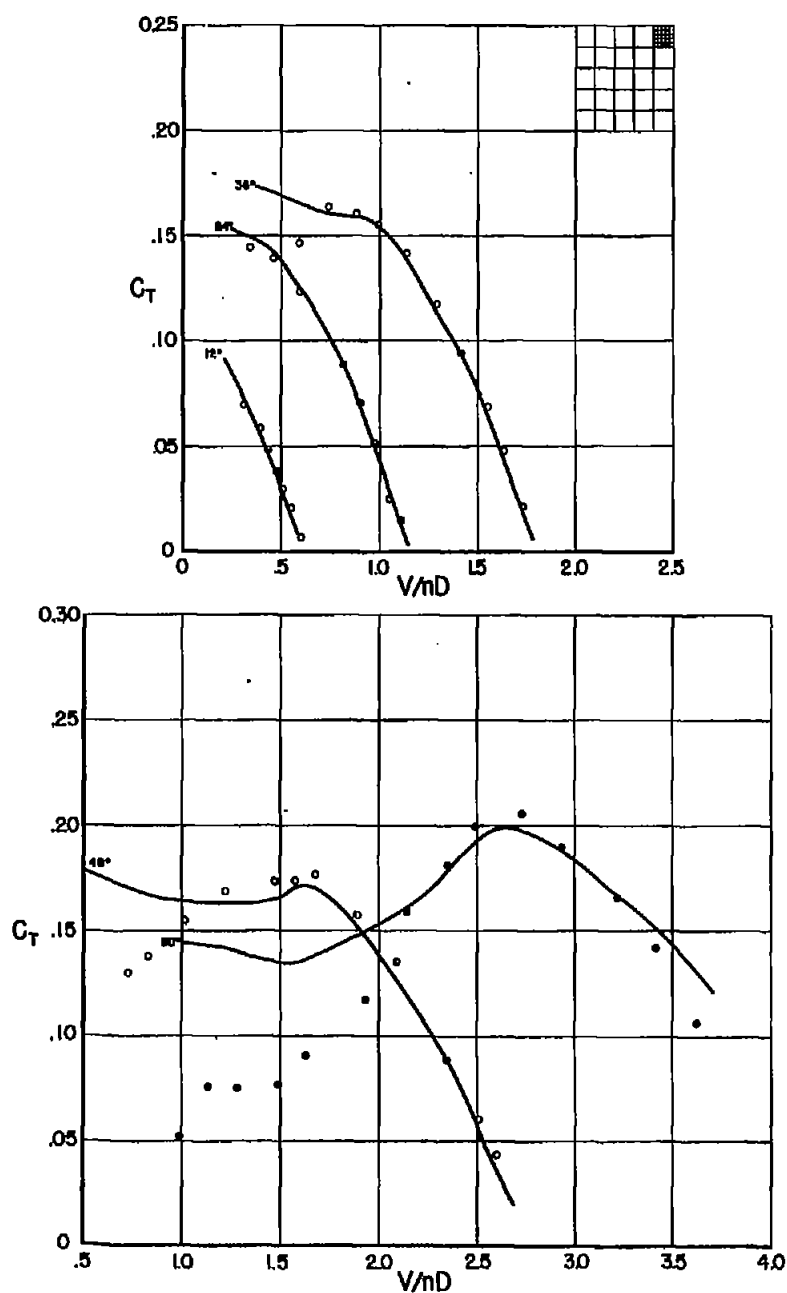
—— Force Test   MODEL 0.8E   • ○ Wake Survey

Fig. 19
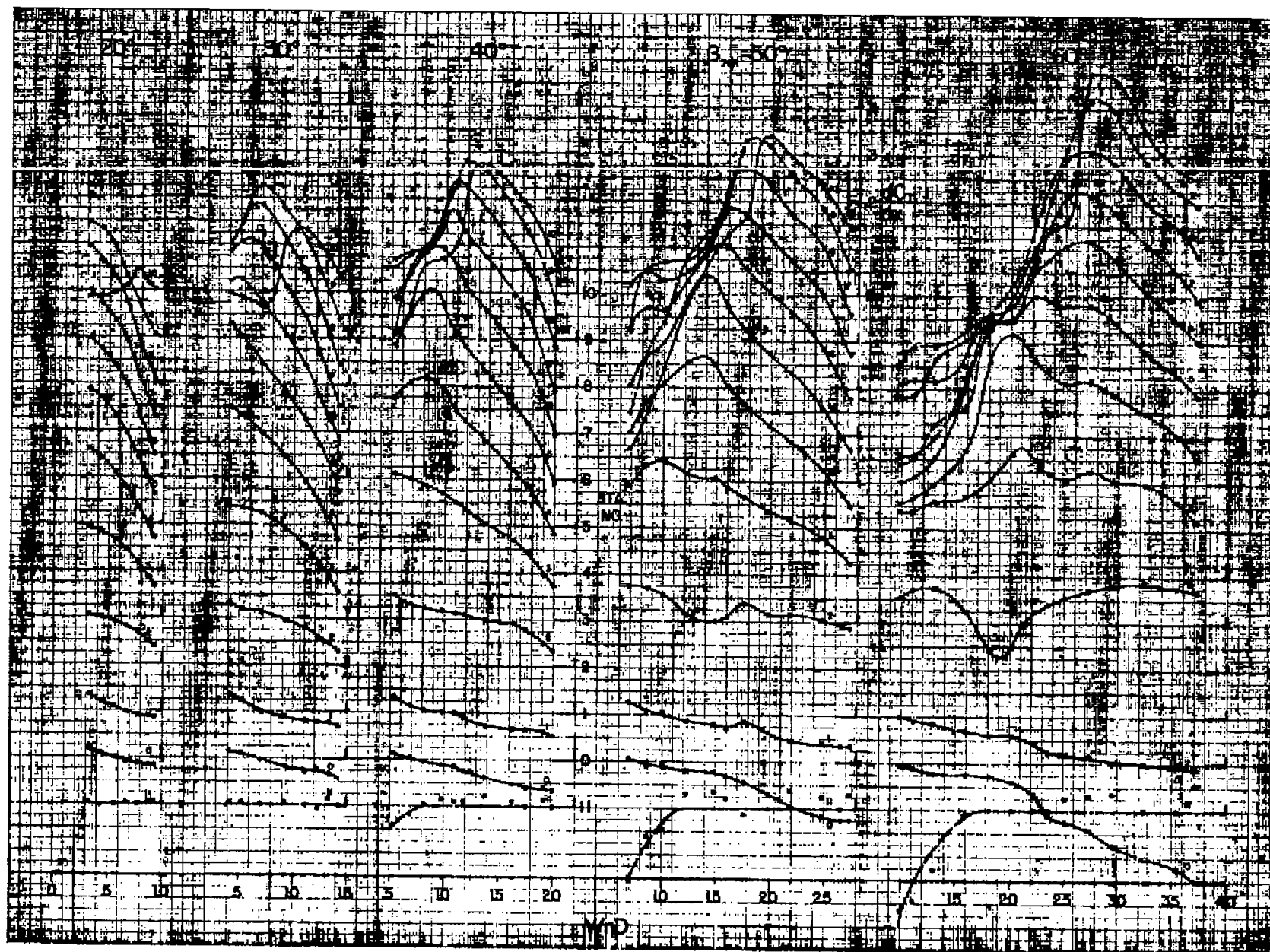
Fig. 20

FIG. 20   SECTION THRUST COEFFICIENTS   MODEL P

Fig. 21

FIG. 21   SECTION TORQUE COEFFICIENTS   MODEL P
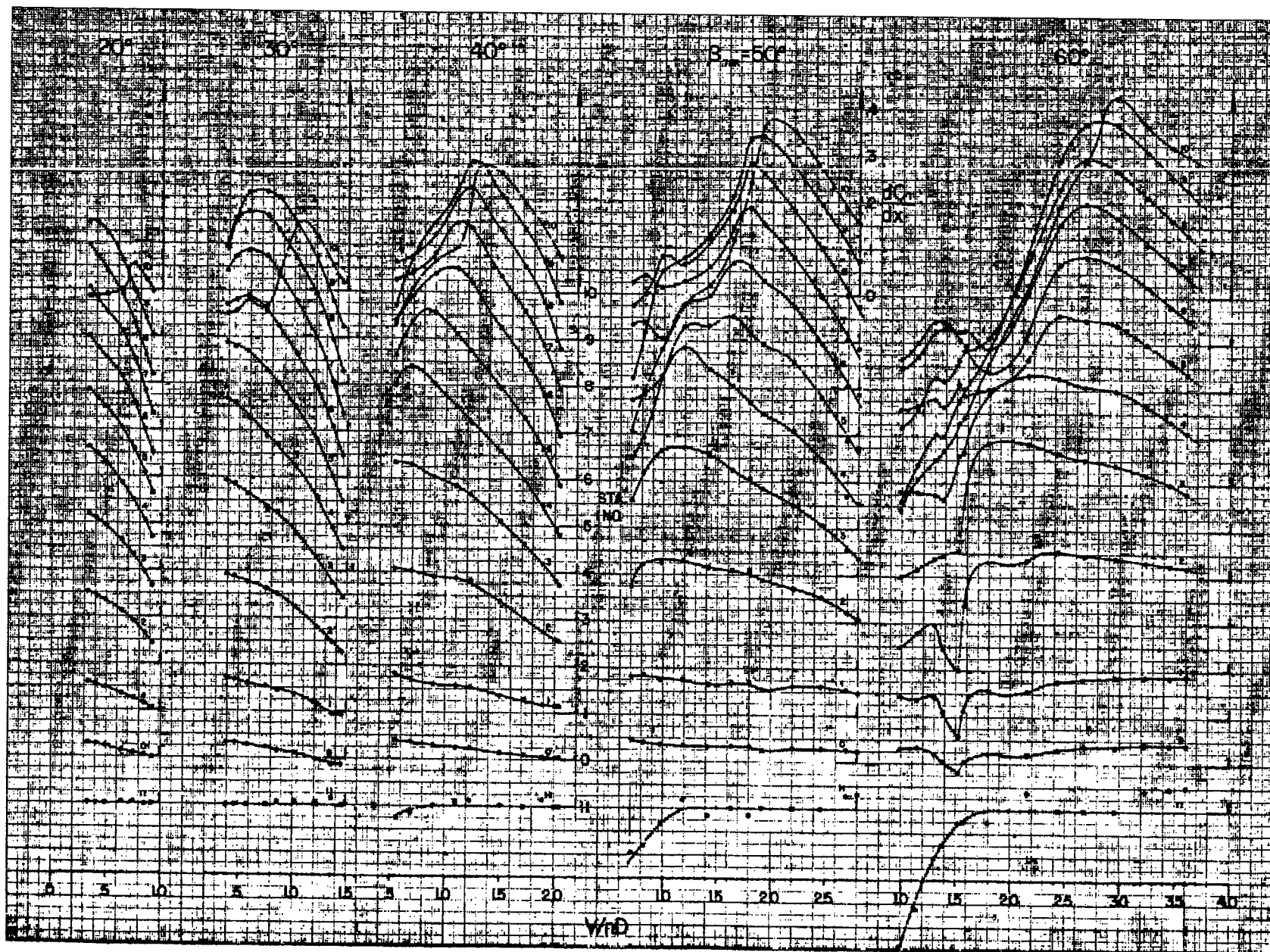
Fig. 22

FIG. 22   SECTION THRUST COEFFICIENTS   MODEL P_c
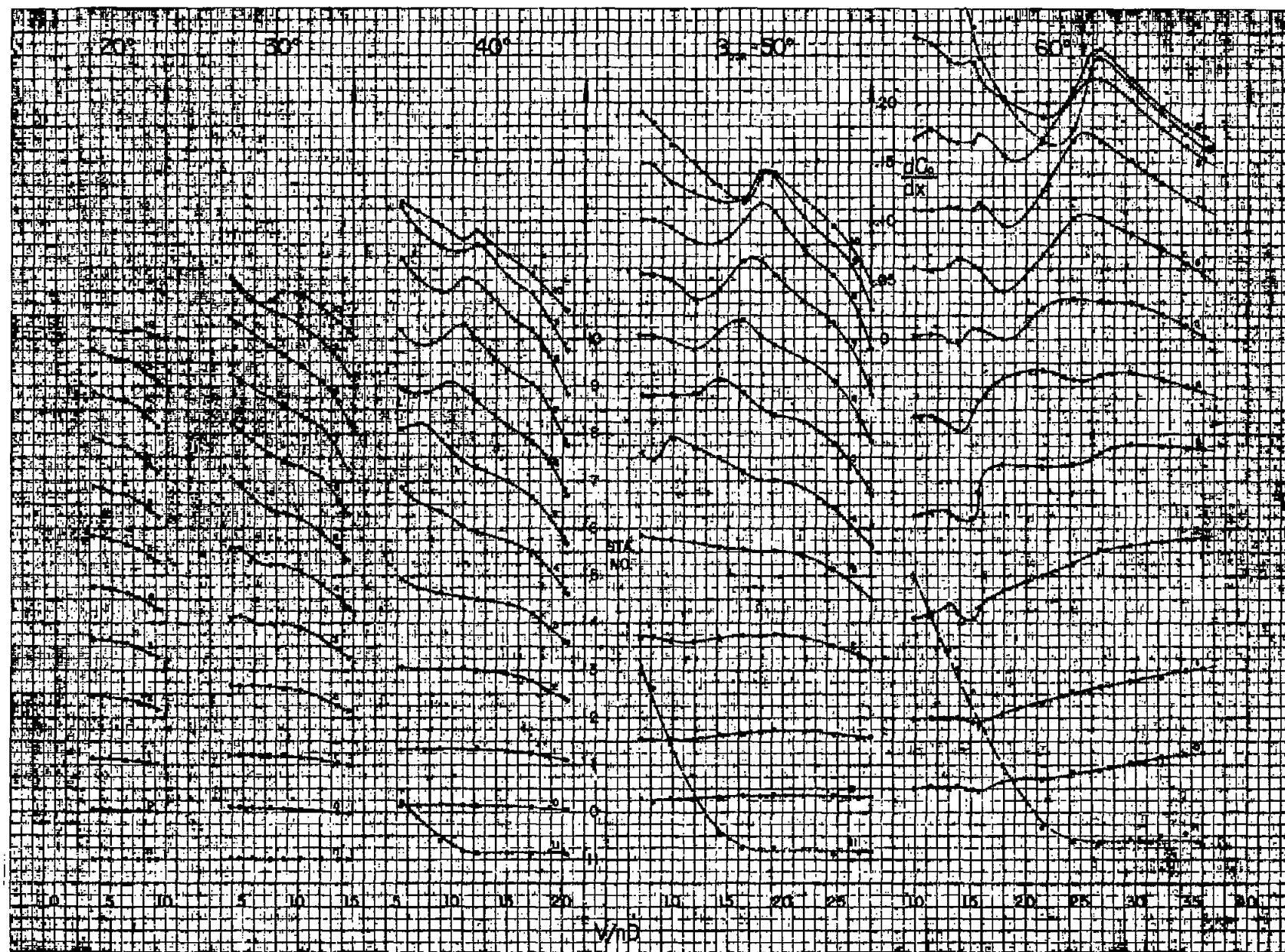
Fig. 23

FIG. 23   SECTION TORQUE COEFFICIENTS   MODEL P₀
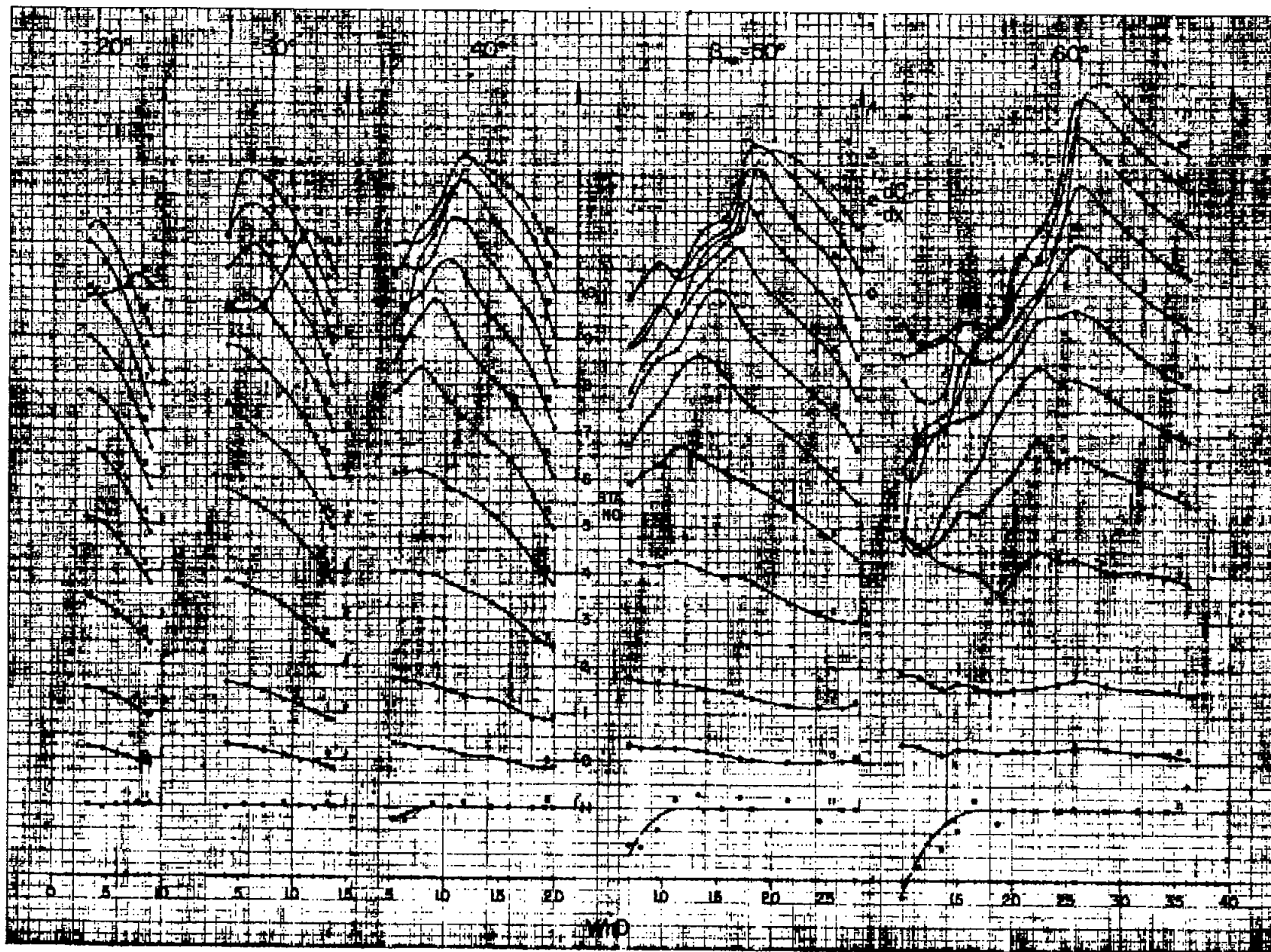
Fig. 24

FIG. 24   Section Thrust Coefficients   Model P_{OH}
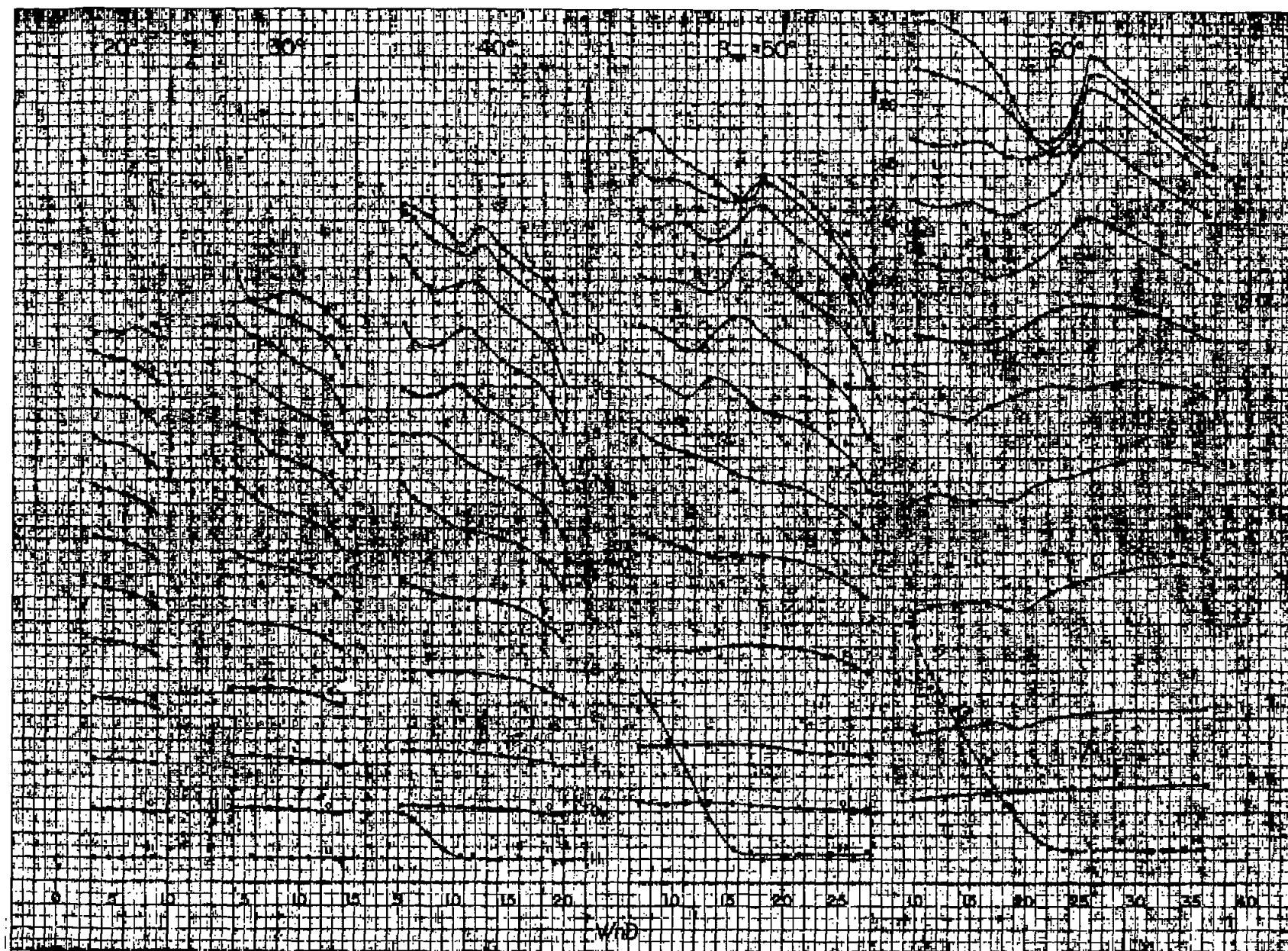
FIG. 25   SECTION TORQUE COEFFICIENTS   MODEL P_{OH}

Fig. 25
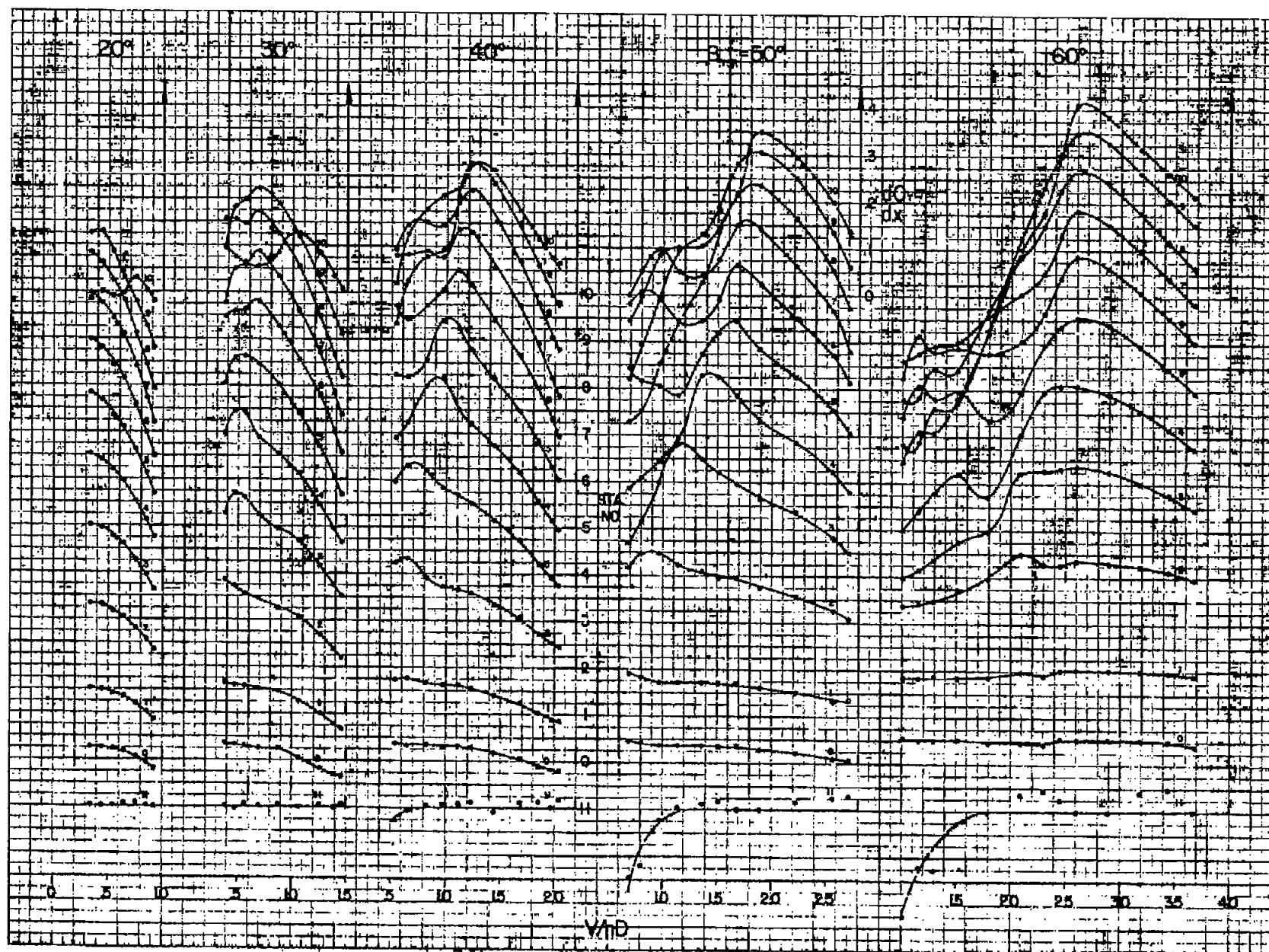
Fig. 26

FIG. 26   SECTION THRUST COEFFICIENTS   MODEL P_{02}
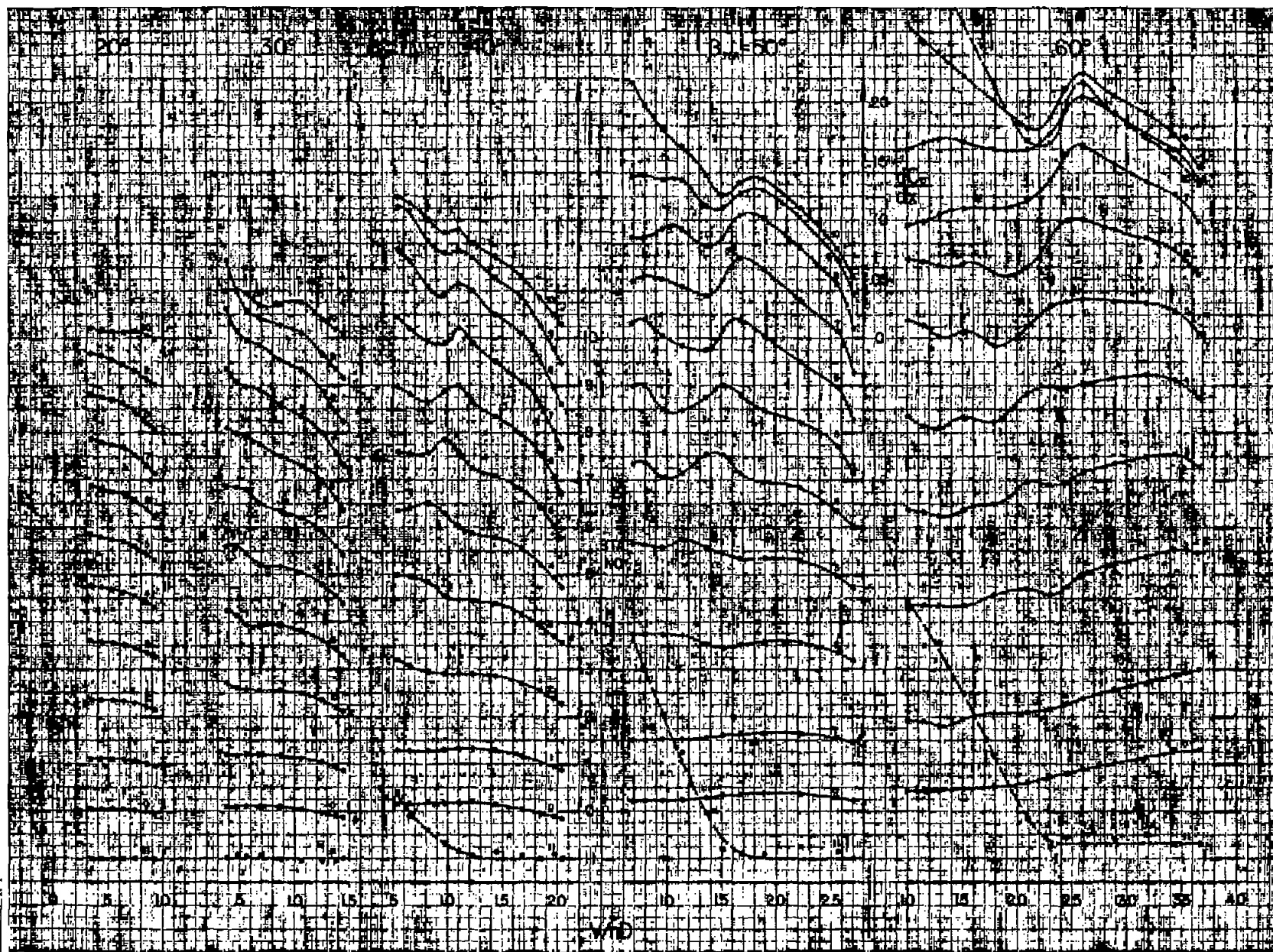
FIG. 27   SECTION TORQUE COEFFICIENTS   MODEL P_{02}

Fig. 27
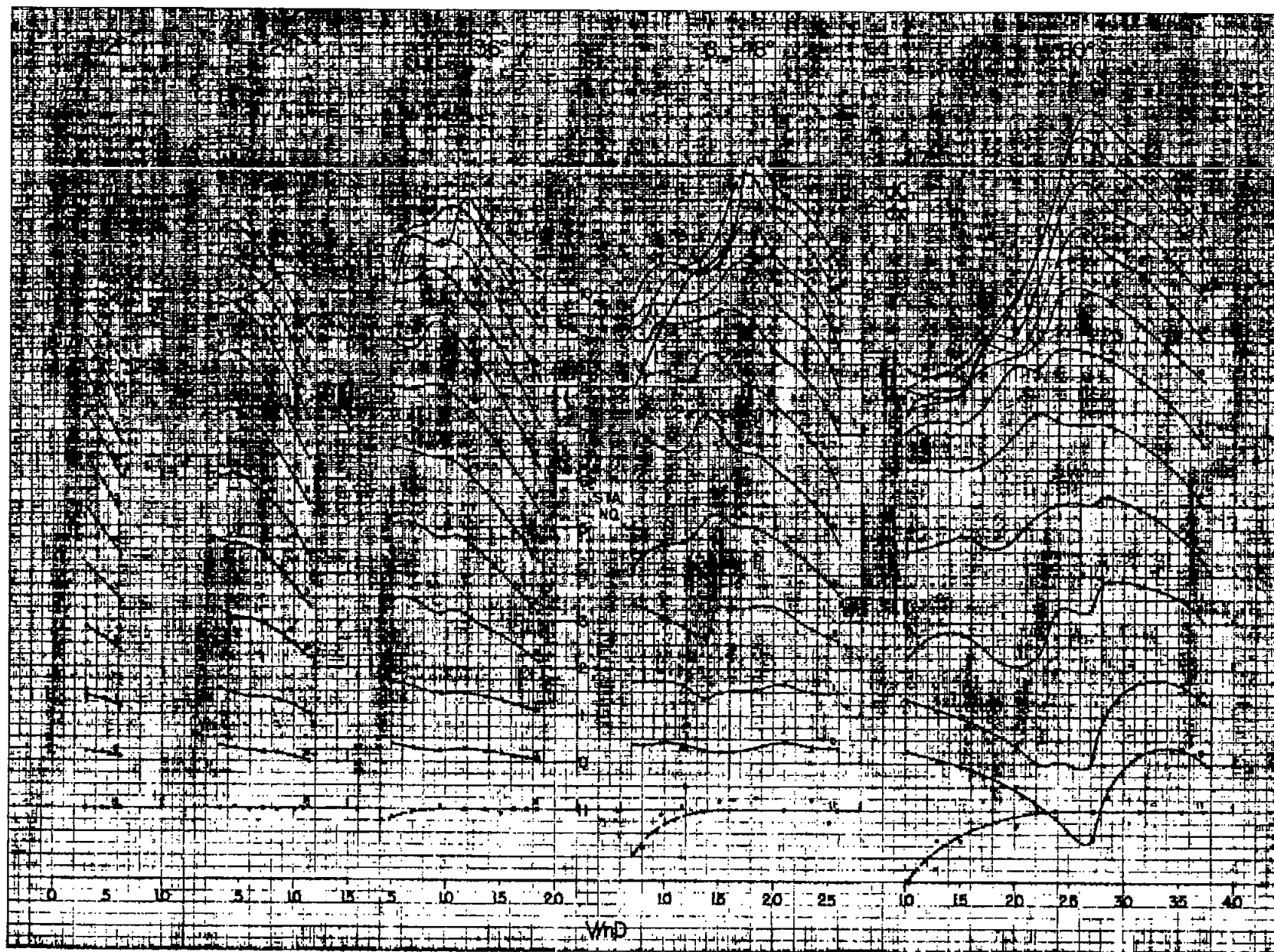
Fig. 28

FIG. 28   SECTION THRUST COEFFICIENTS   MODEL U24
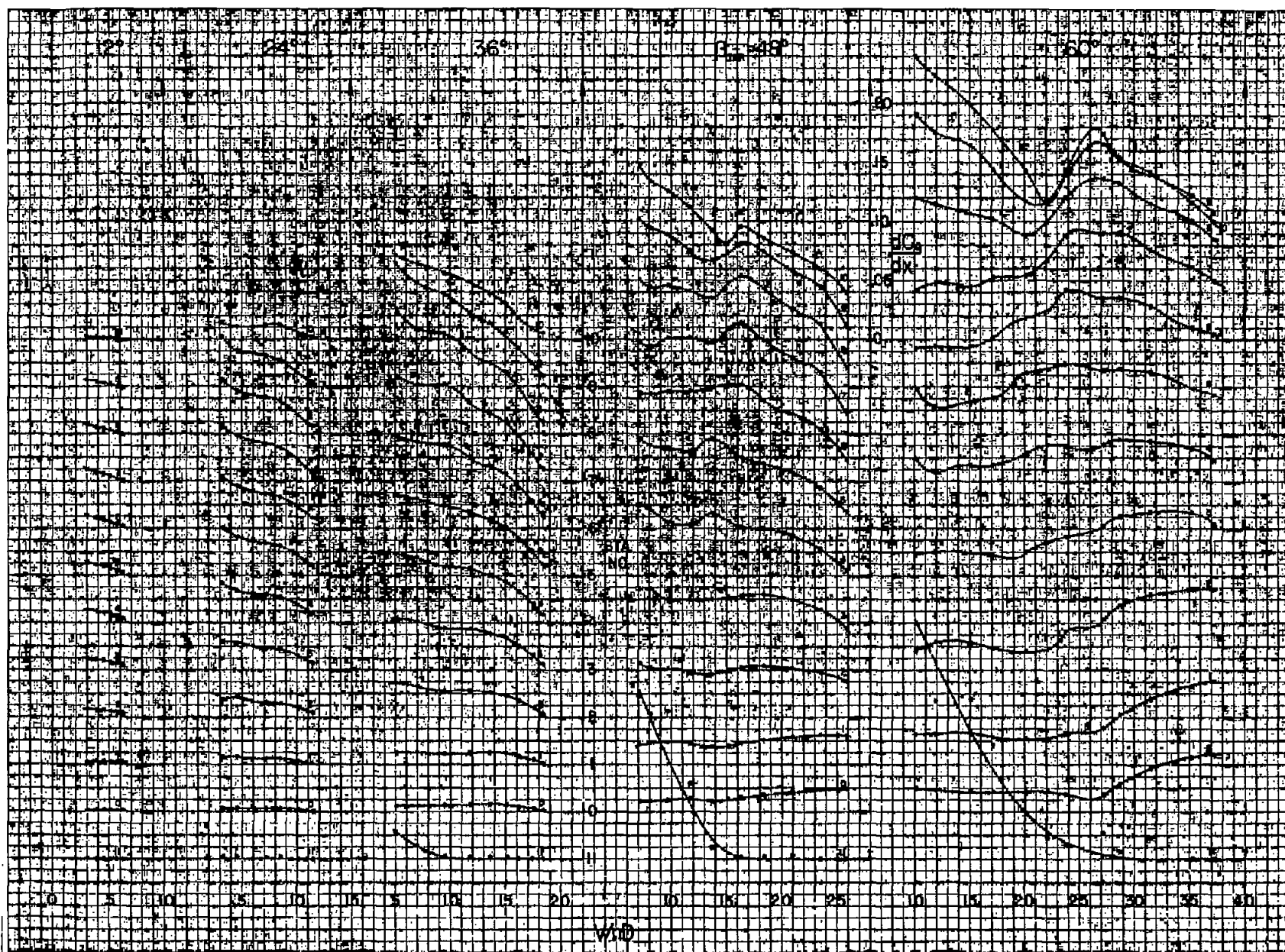
Fig. 29

FIG. 29   SECTION TORQUE COEFFICIENTS   MODEL U24
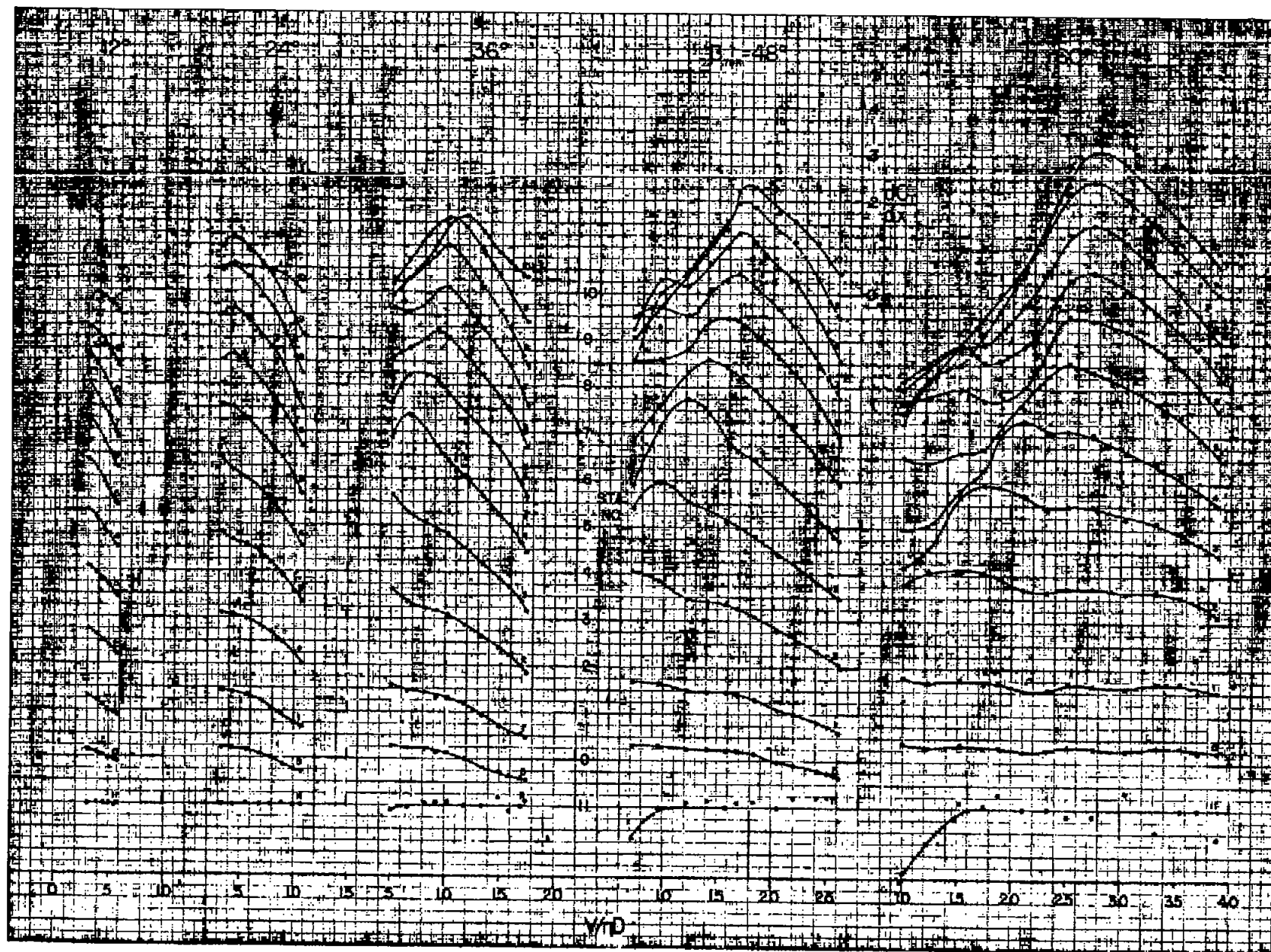
Fig 30

FIG. 30   Section Thrust Coefficients   Model U60
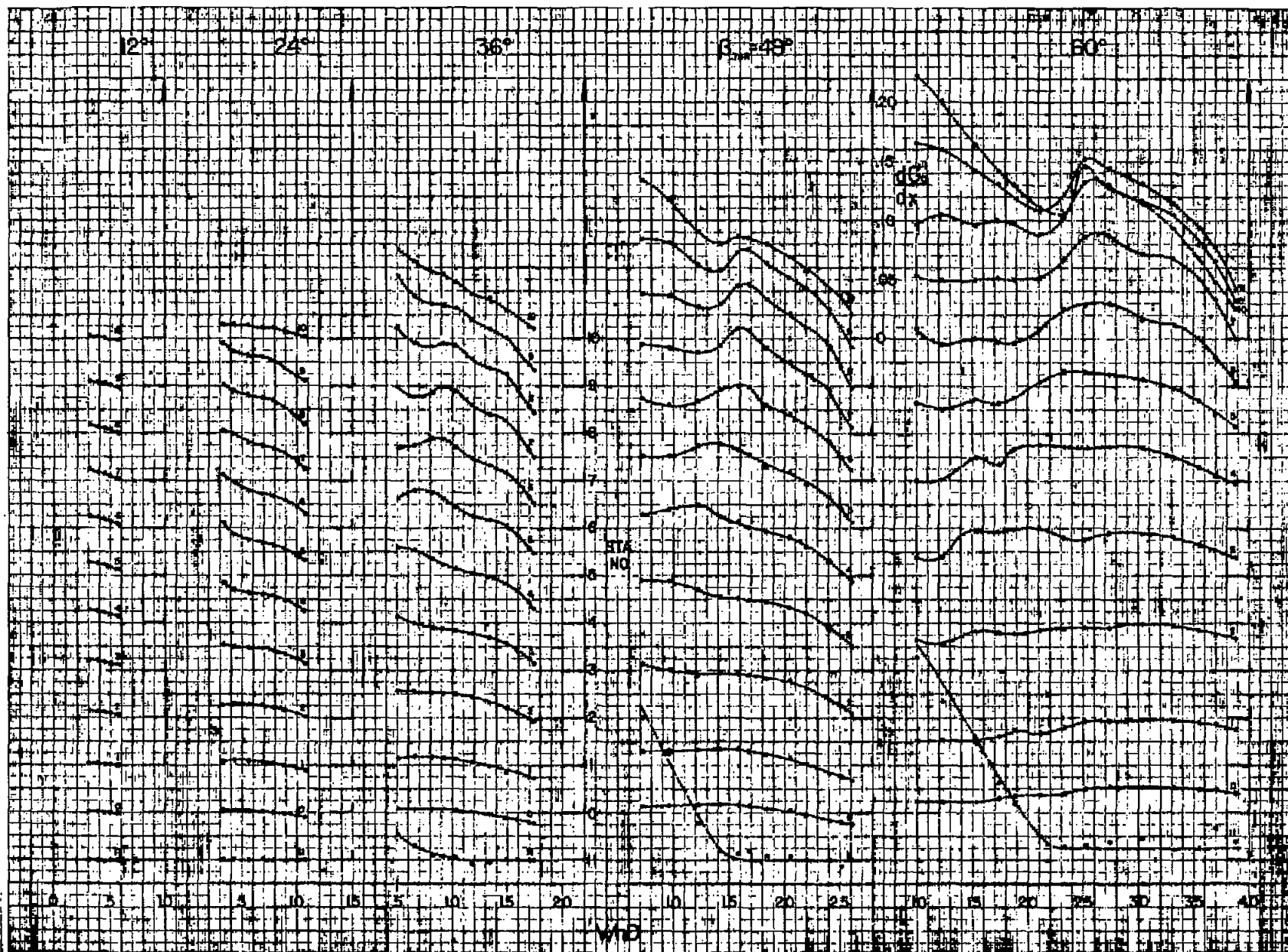
FIG. 31   SECTION TORQUE COEFFICIENTS   MODEL U 60

Fig. 31
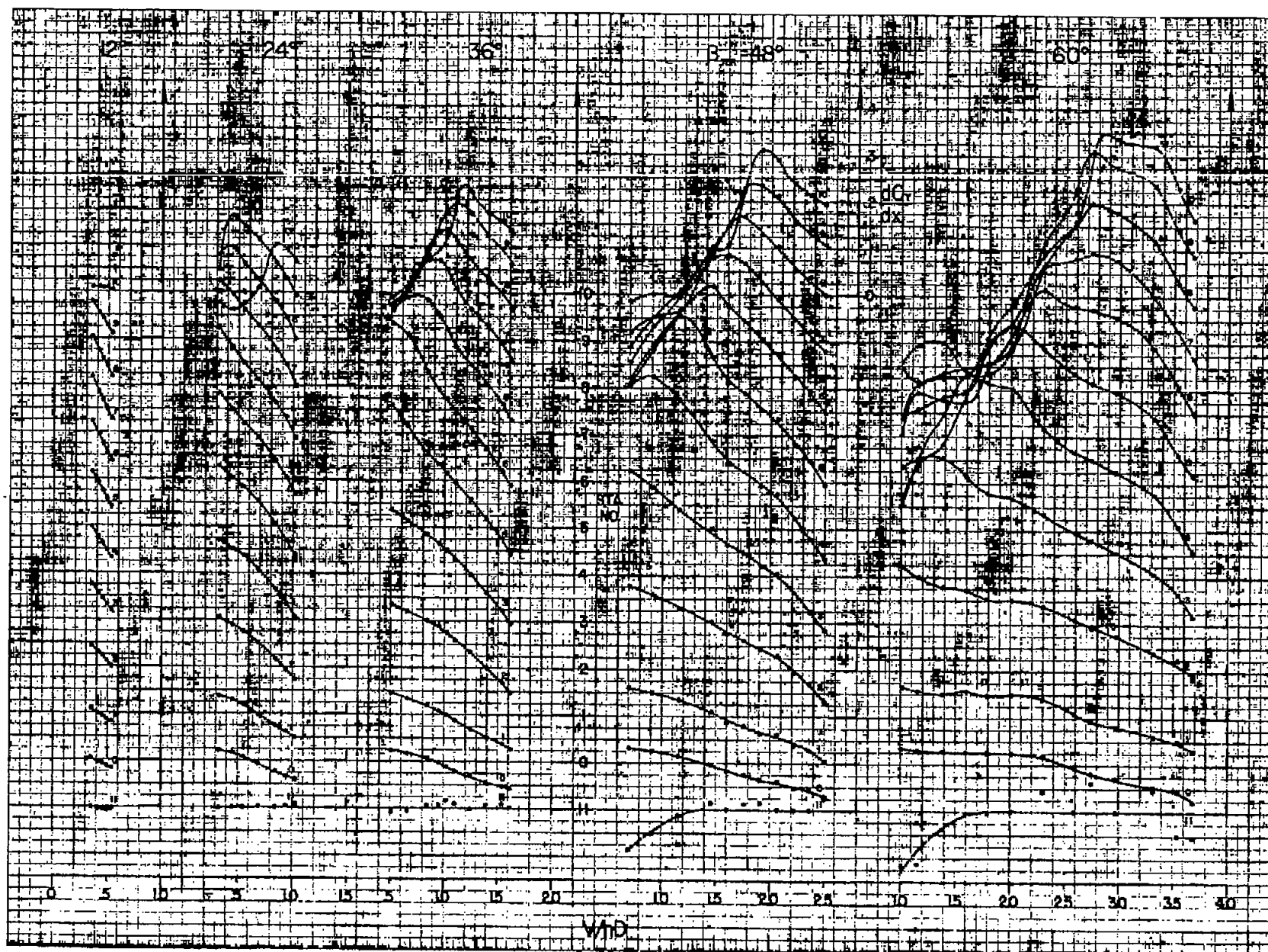
Fig. 32

FIG. 32   SECTION THRUST COEFFICIENTS   MODEL O4E
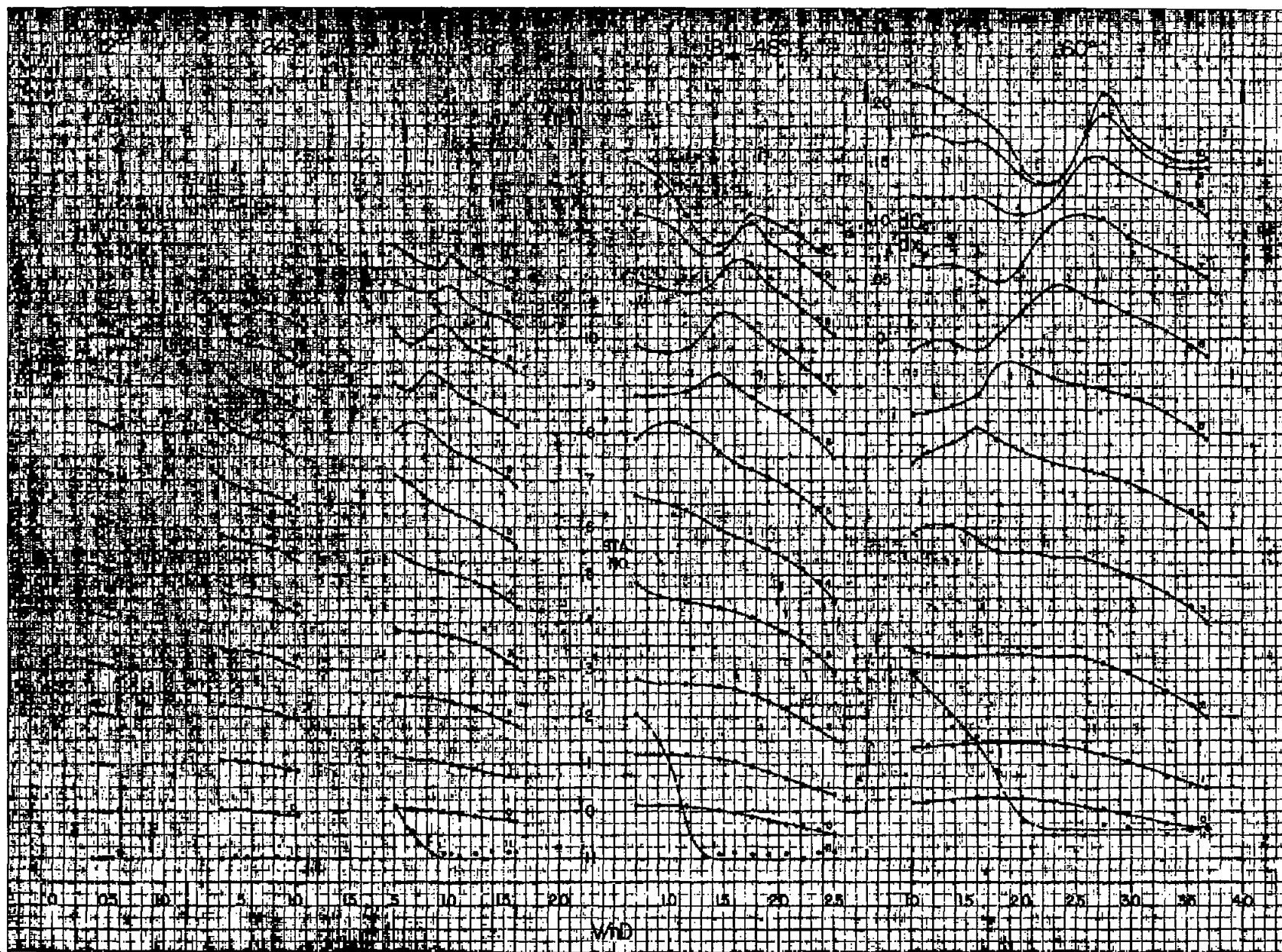
Fig. 33

FIG. 33   SECTION TORQUE COEFFICIENTS   MODEL 04E
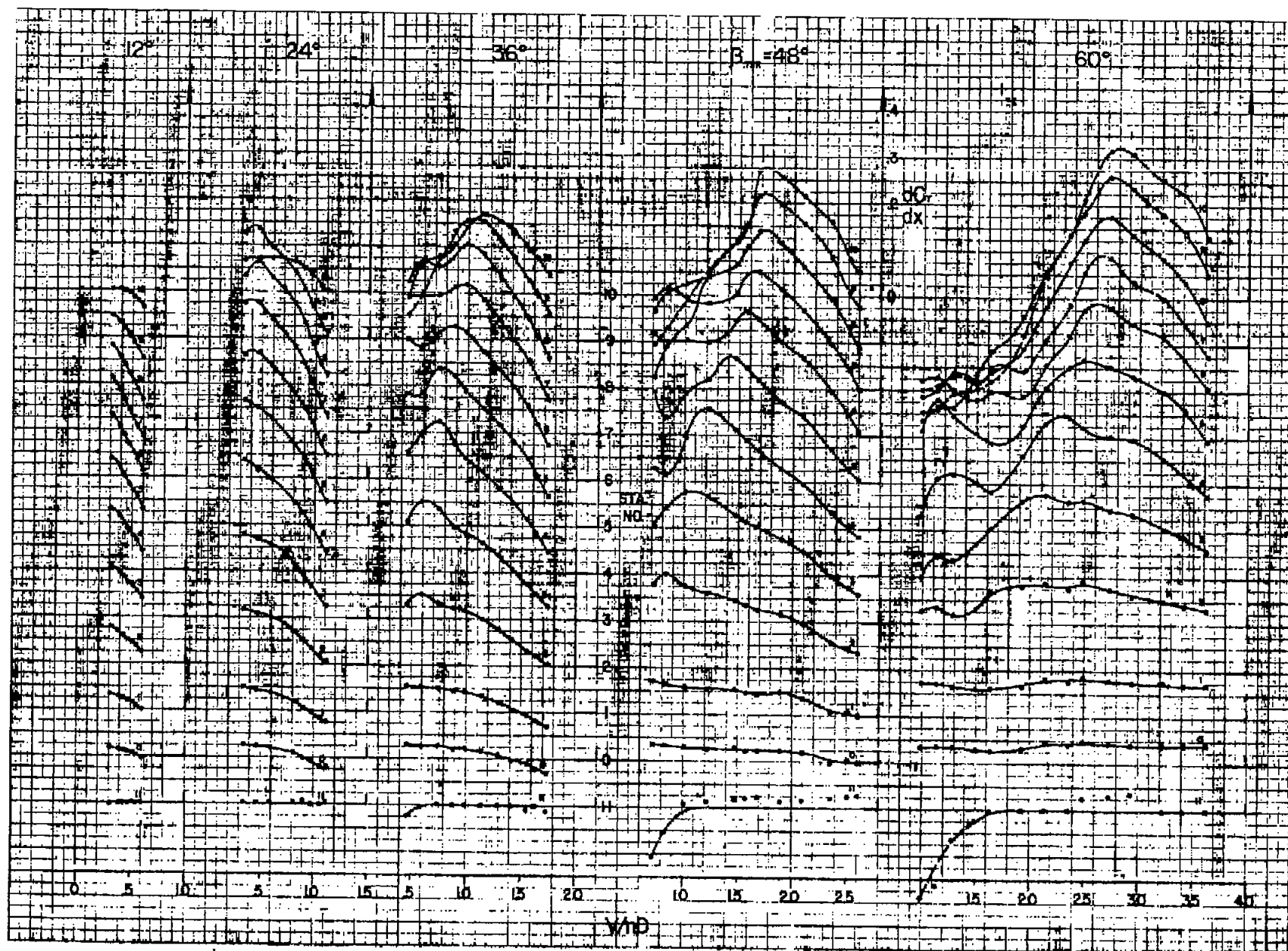
Fig. 34

FIG. 34   Section Thrust Coefficients   Model 0.8E
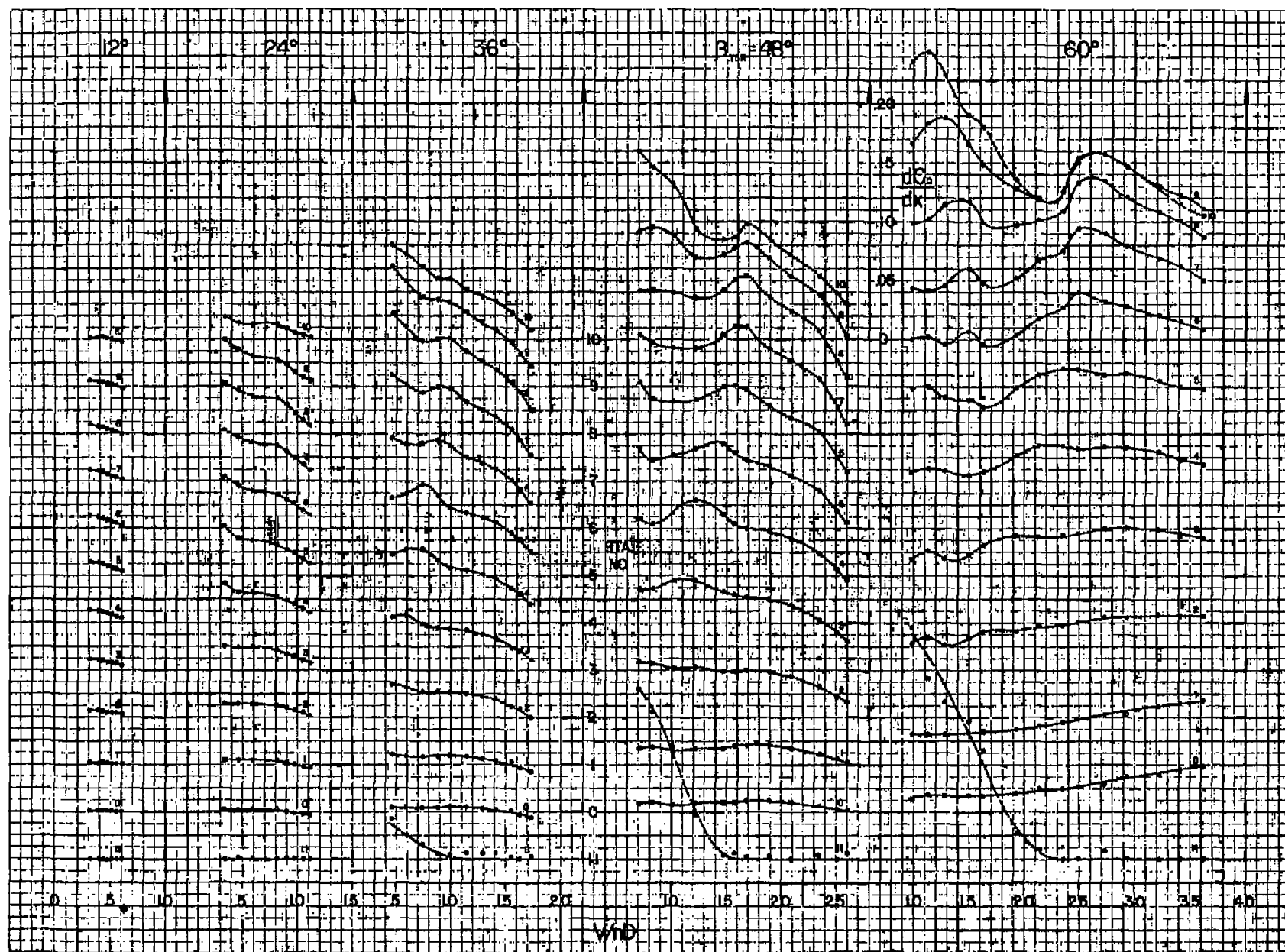
Fig. 35

FIG. 35   SECTION TORQUE COEFFICIENTS   MODEL 0.8E

Fig. 36   NACA TN No. 1040
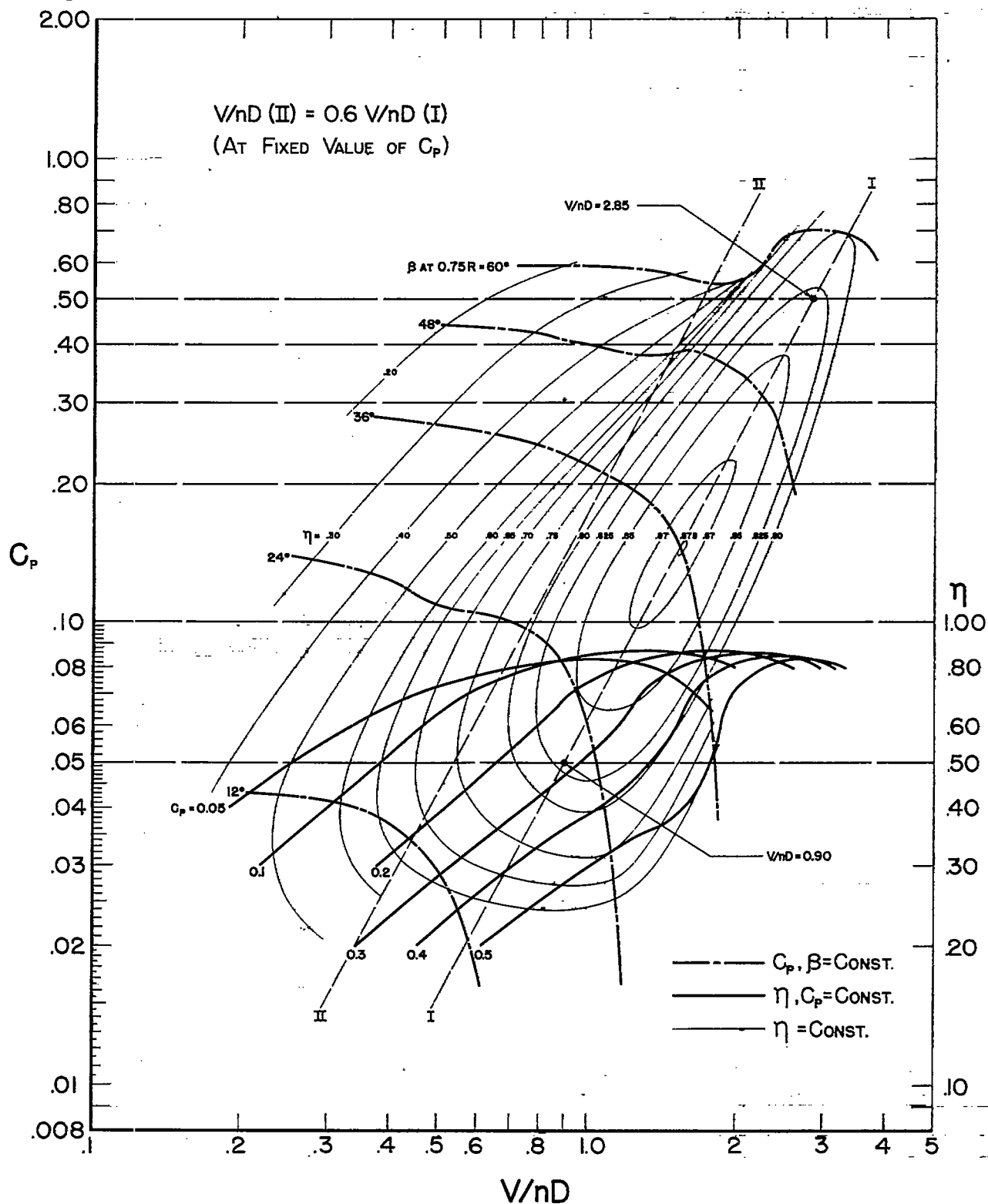
FIG. 36   DEFINITION OF LINES USED IN ANALYSIS OF RESULTS
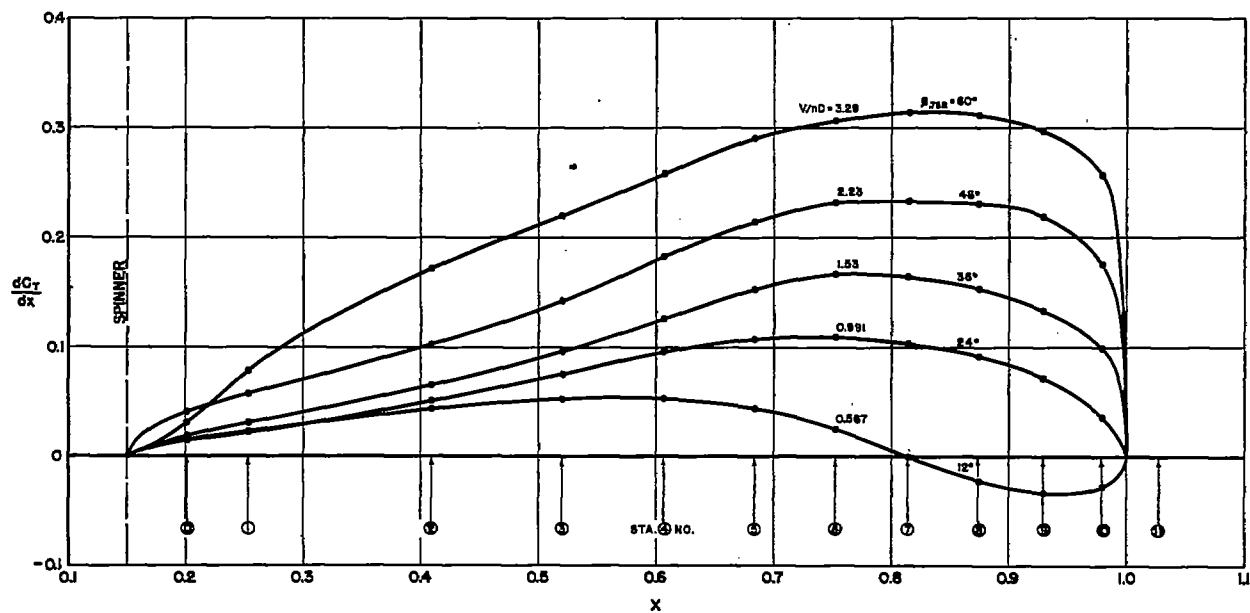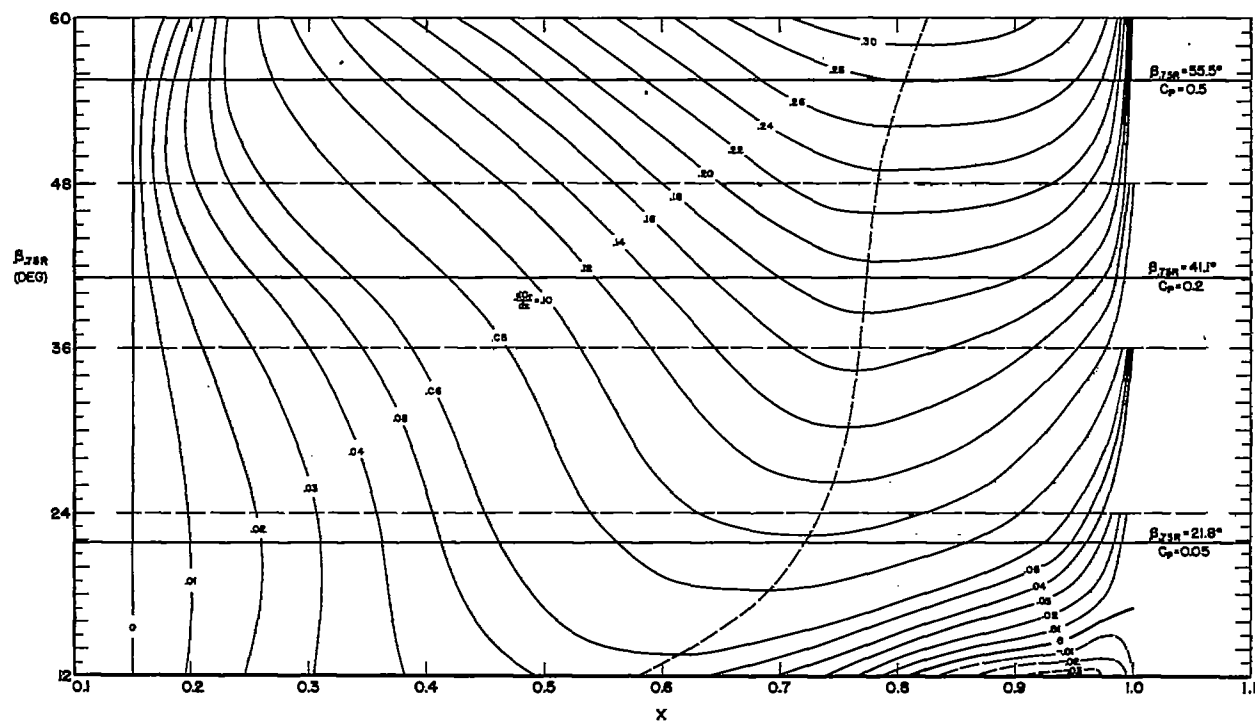
FIG. 36 (a)   THRUST CONTOUR CHART – MODEL U-24, LINE I

FIG. 37   EFFECTS OF ADDING CUFFS – HIGH SPEED (LINE I)

Fig. 37
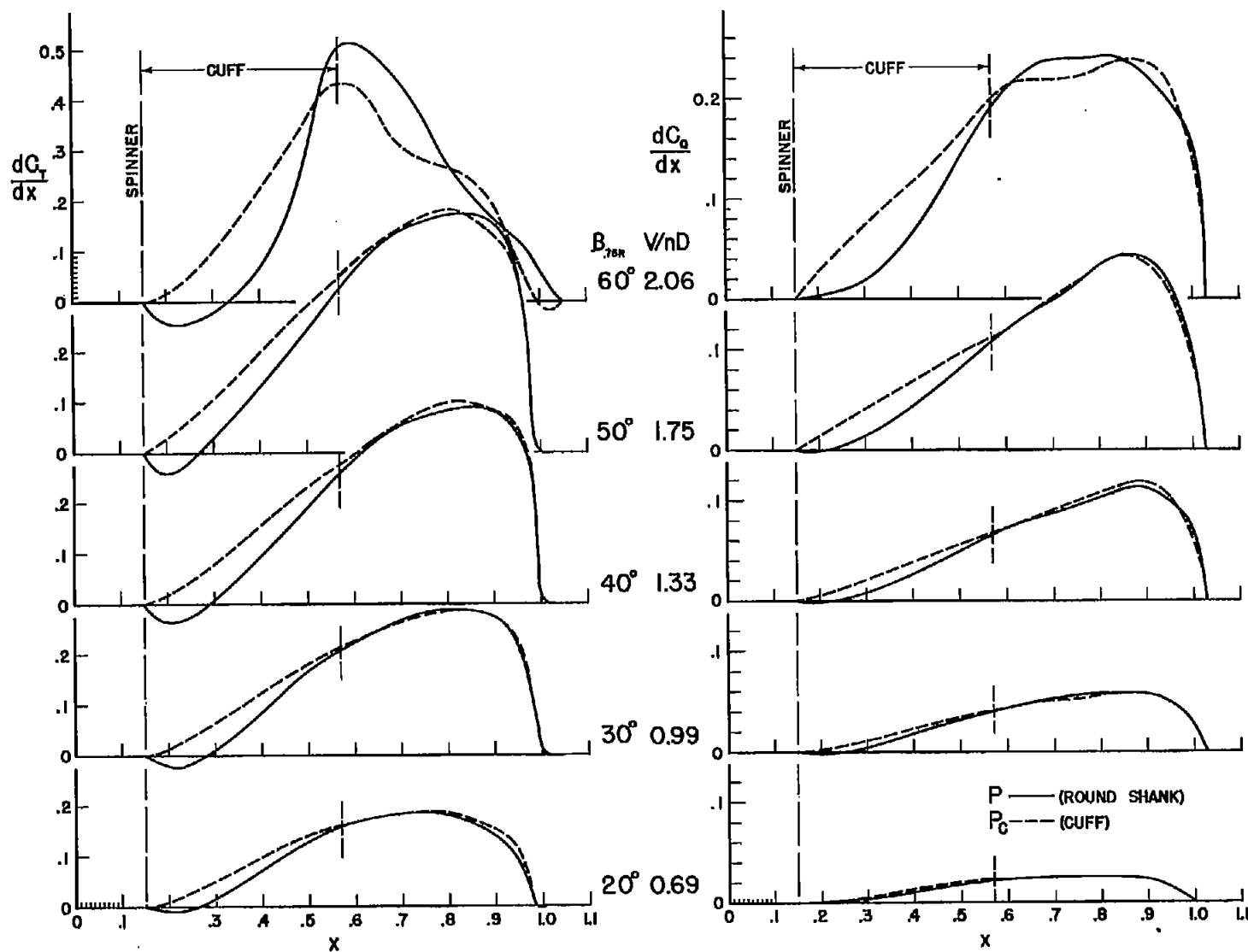
NACA TN No. 1040

FIG. 38   EFFECTS OF ADDING CUFFS – CLIMB (LINE II)

Fig. 38

Fig. 39
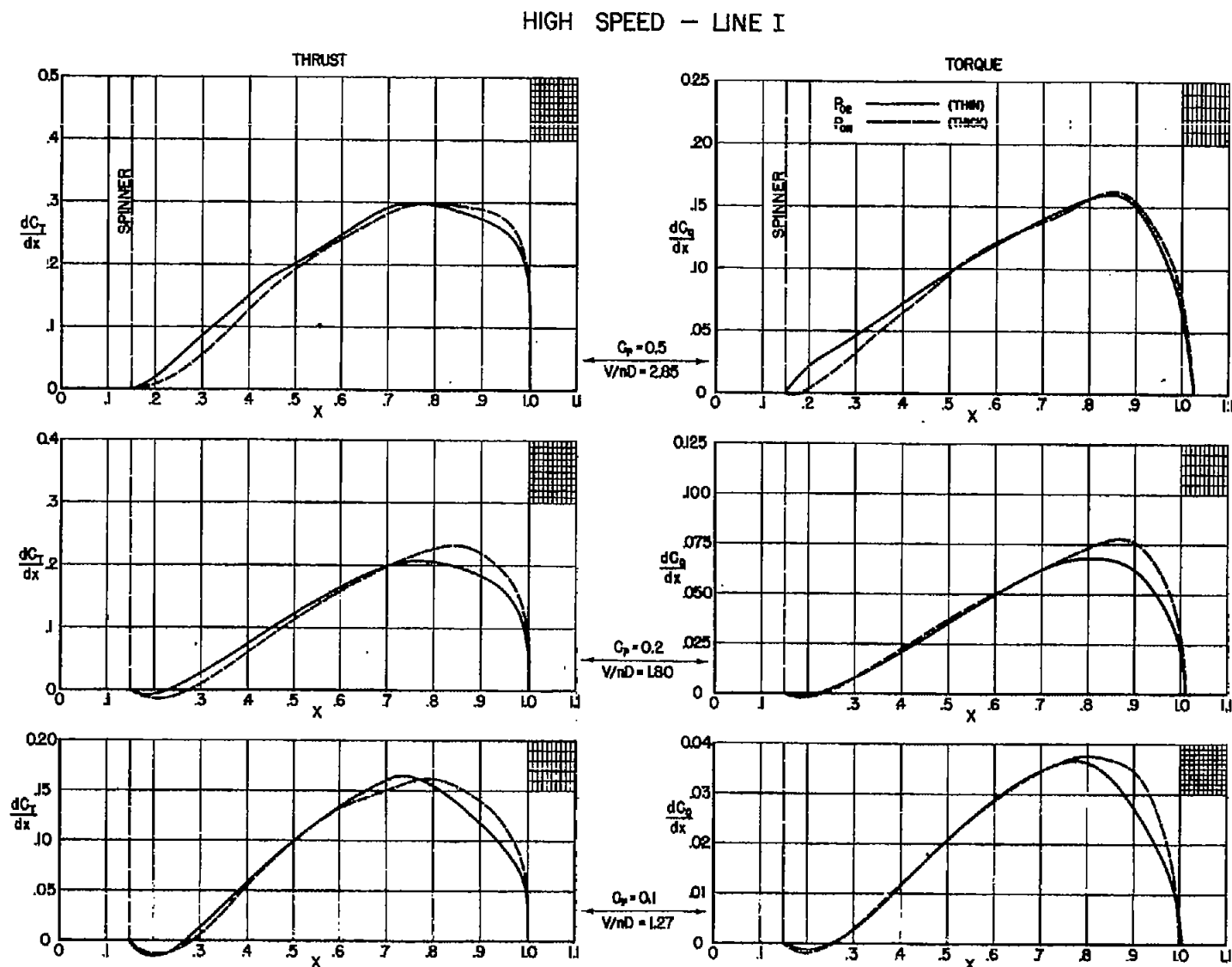
HIGH SPEED — LINE I

FIG. 39   MODELS WITH THIN AND THICK SHANKS — HIGH SPEED (LINE I)

CLIMB — LINE II
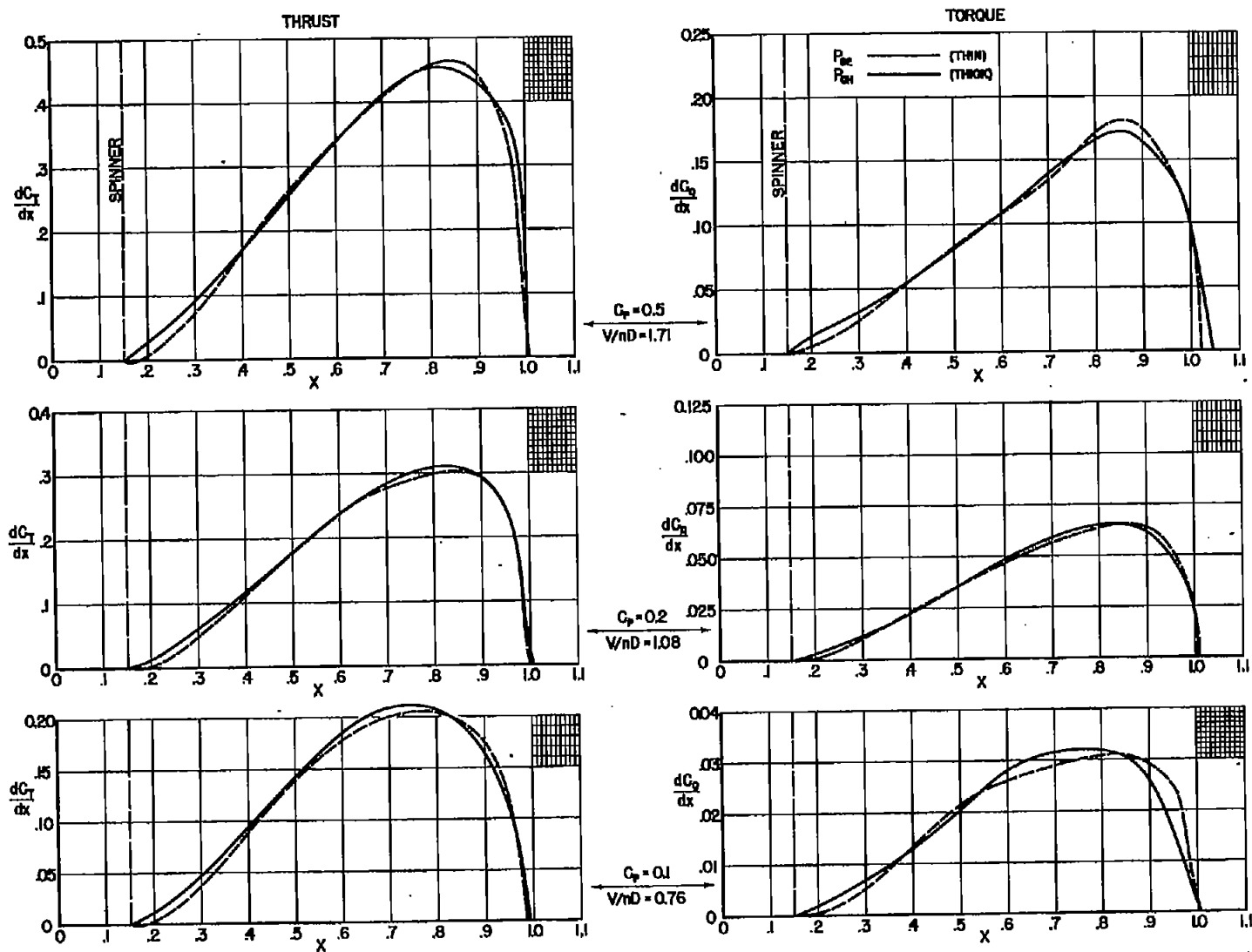
FIG. 40   MODELS   WITH   THIN   AND   THICK   SHANKS — CLIMB   (LINE II)

Fig. 40

Fig. 41

HIGH SPEED — LINE I
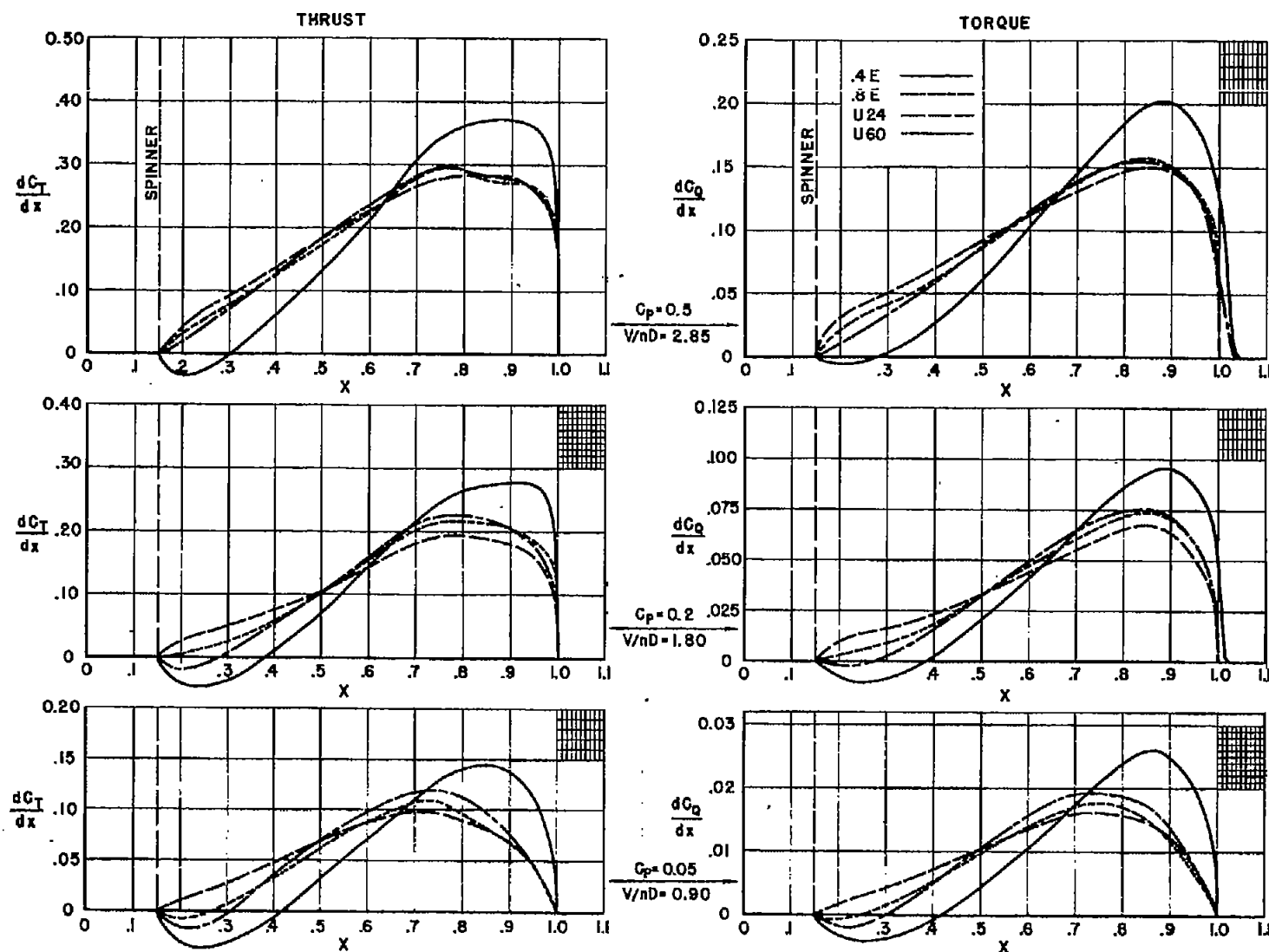
THRUST

TORQUE

FIG. 41   EFFECTS OF PITCH DISTRIBUTION — HIGH SPEED (LINE I)

FIG. 42   EFFECTS OF PITCH DISTRIBUTION — CLIMB (LINE II)

NACA TN No. 1040

Fig. 42
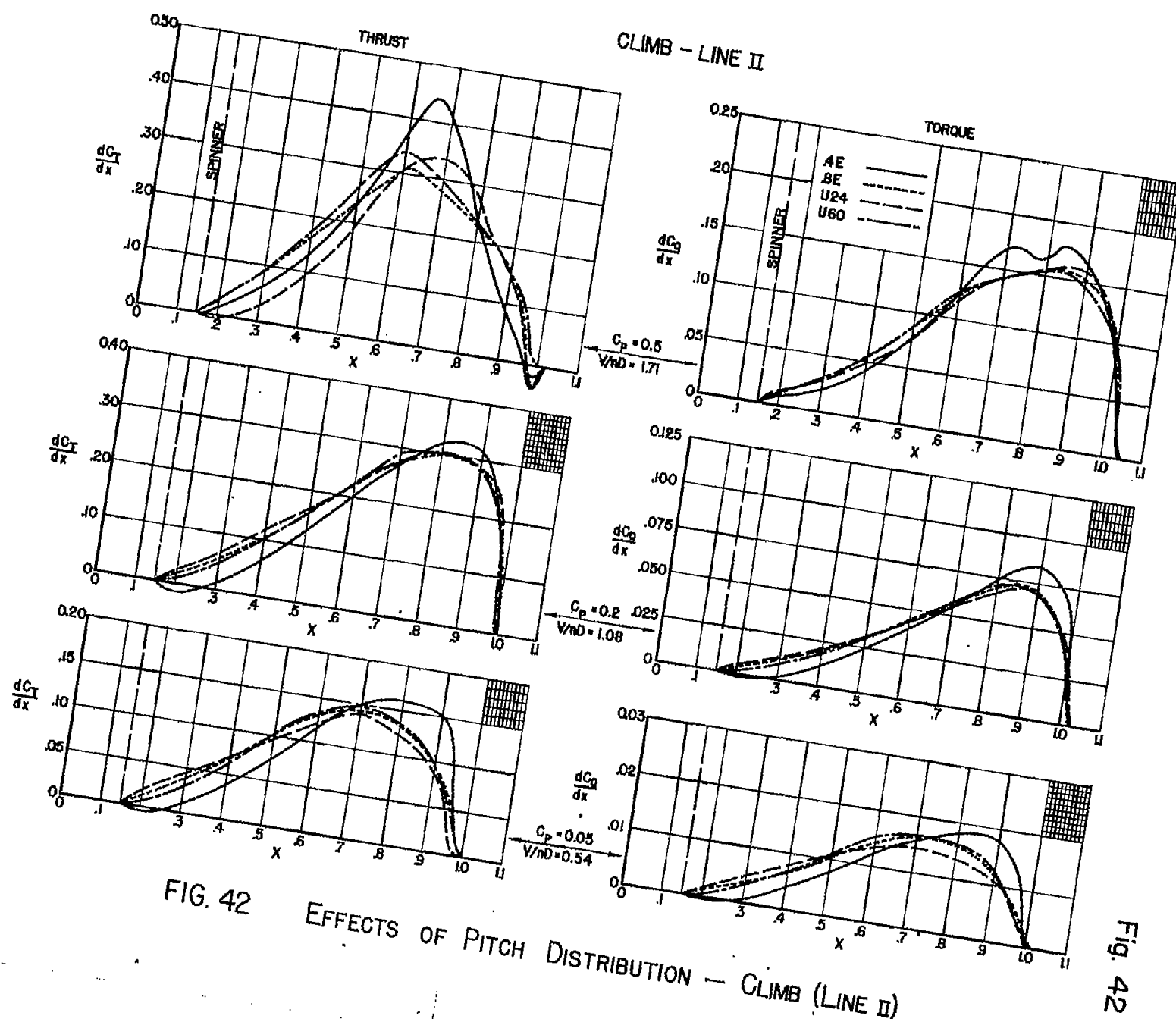
Fig. 43　　　　　　　　　　　NACA TN No. 1040
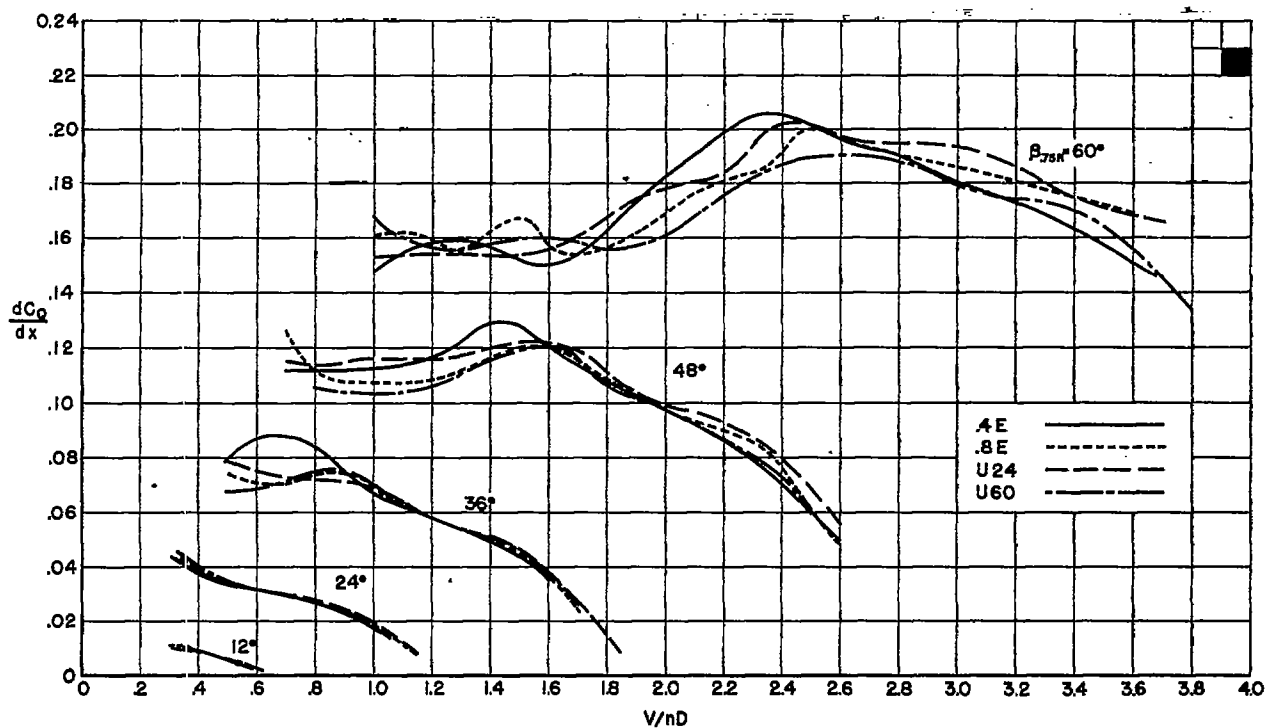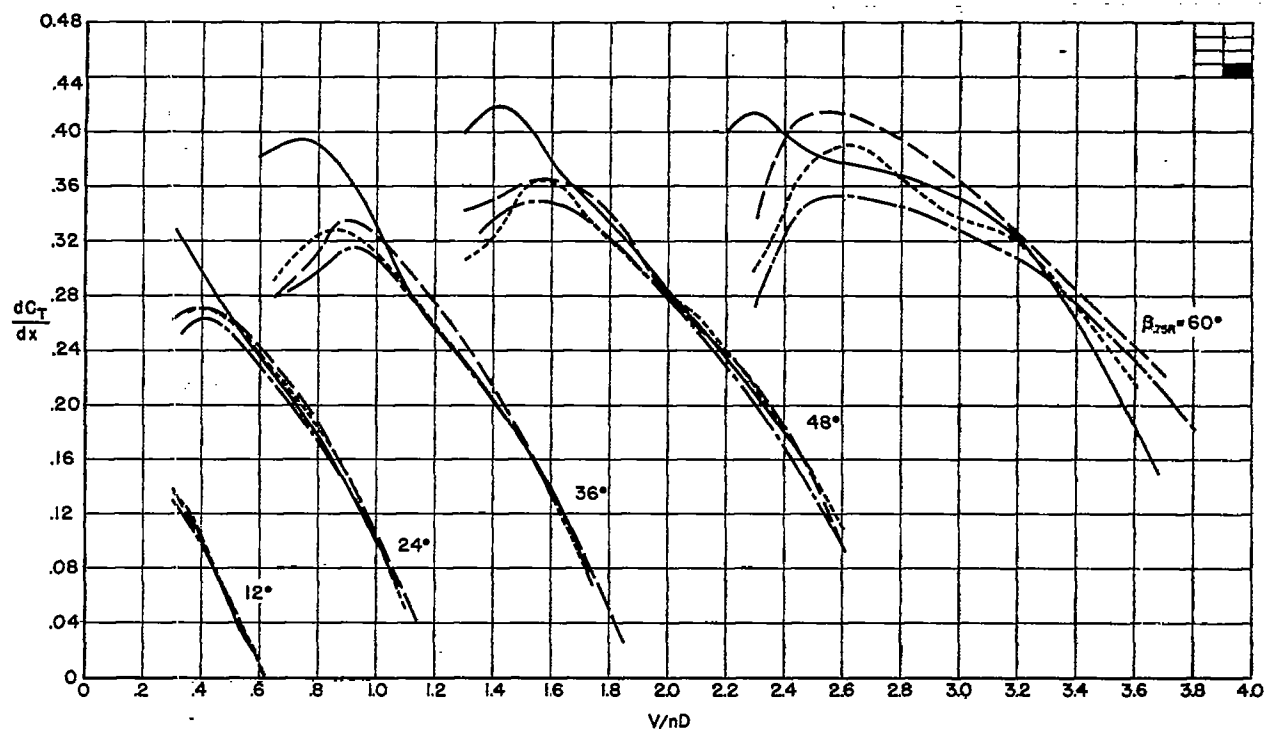
FIG. 43　　ELEMENTARY THRUST AND TORQUE COEFFICIENTS – SECTION No. 6

V/nD vs. Pitch Angle of Element - dC$_T$/dx = Const.

Corresponding Values of dC$_q$/dx
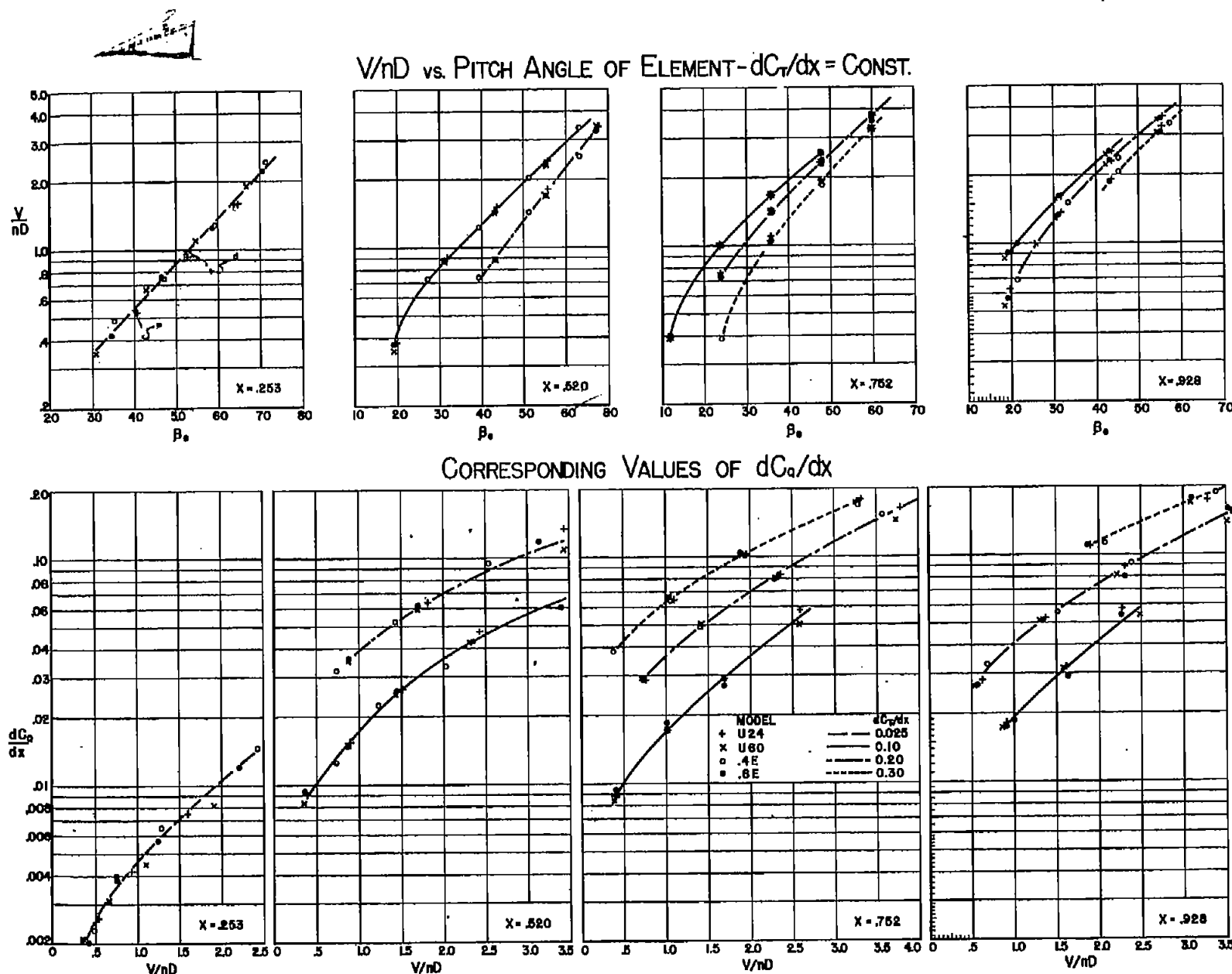
FIG. 44   Evidence of Independent Action of Blade Elements

Fig. 44
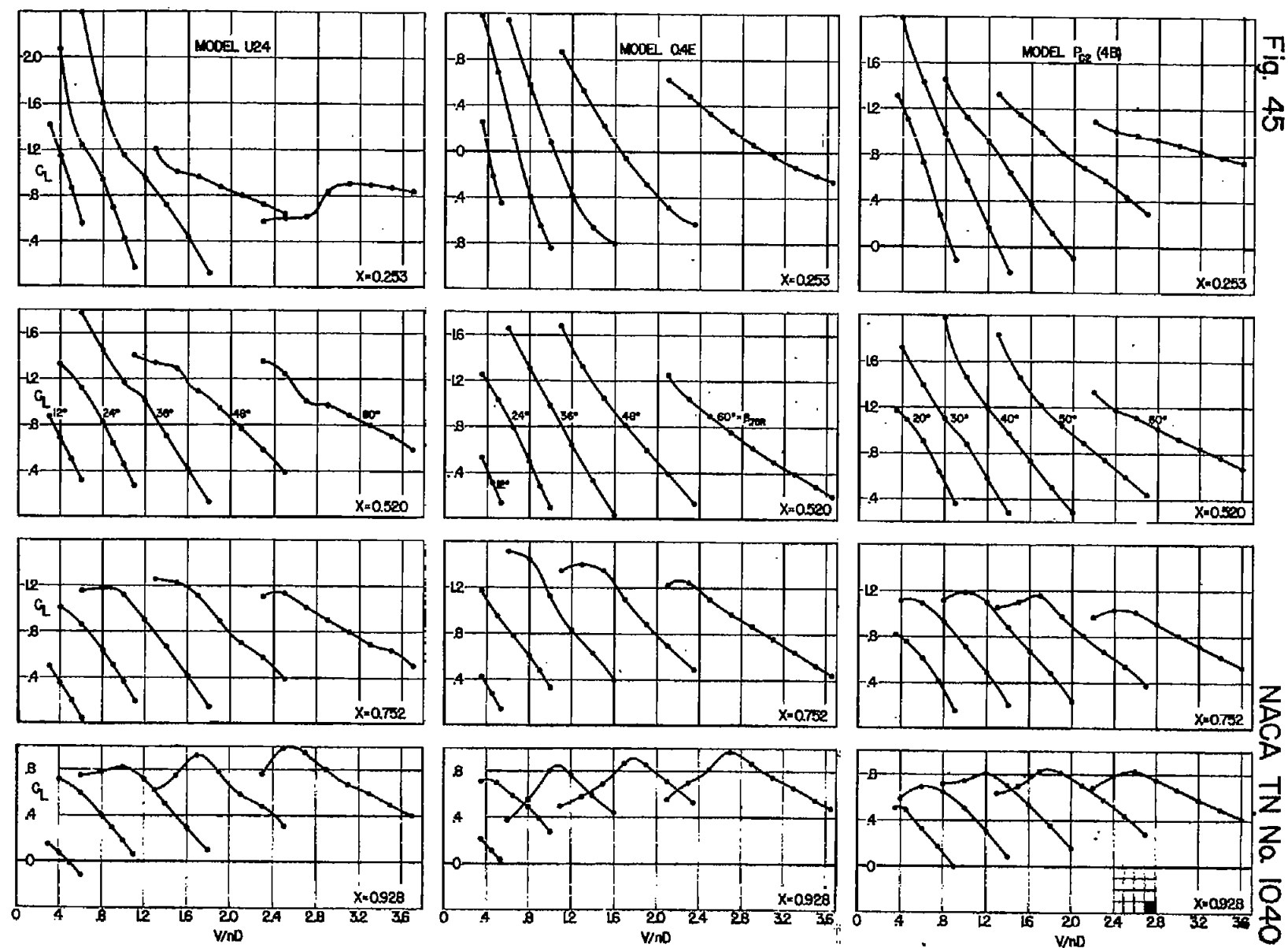
FIG. 45   SECTION·LIFT COEFFICIENTS VS. V/nD
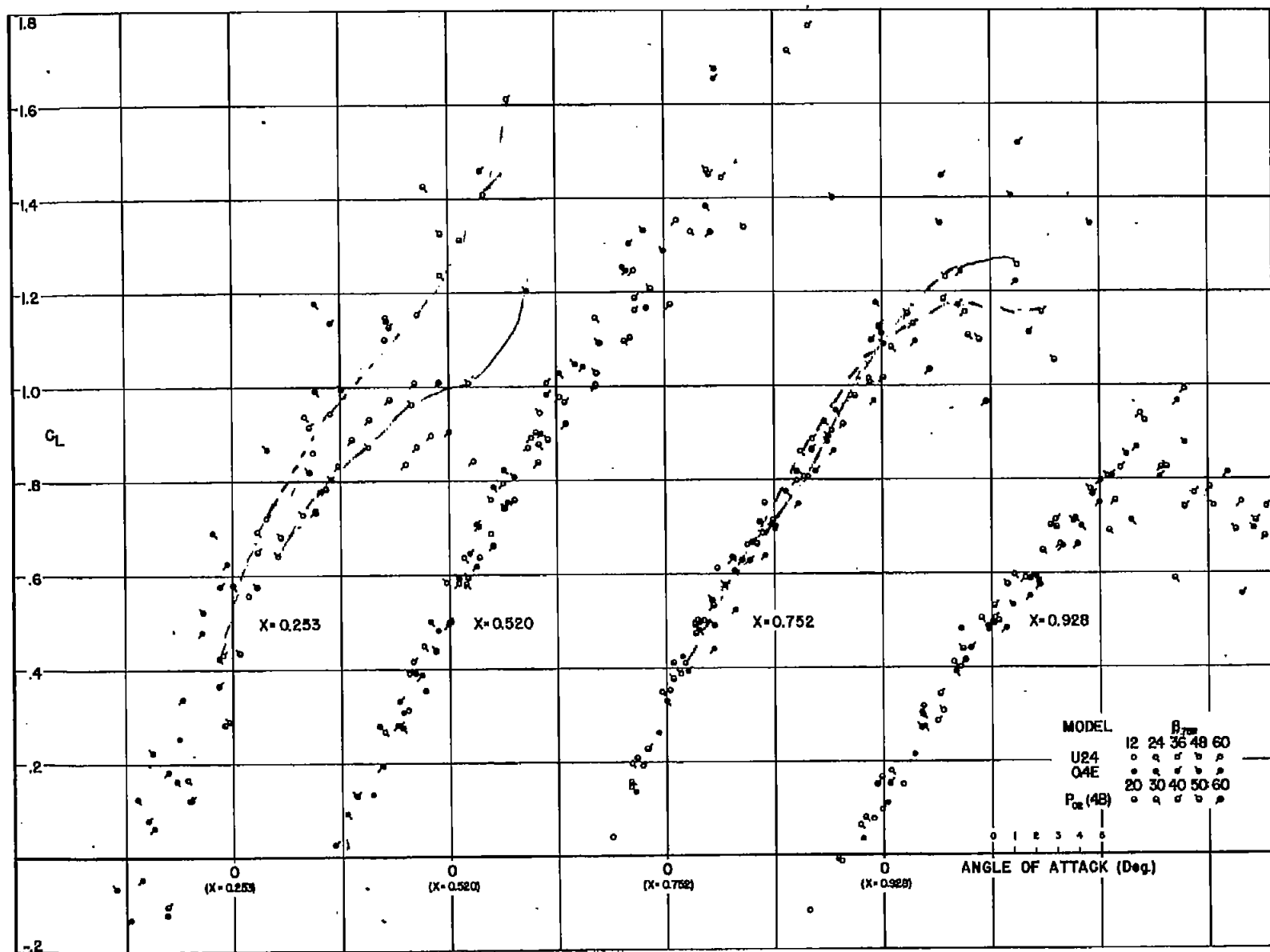
FIG. 46   SECTION LIFT COEFFICIENTS – THREE- AND FOUR-BLADE MODELS.

Fig. 46

Fig. 47

HIGH SPEED (I)

CLIMB (II)

C_L

SPINNER

V/nD = 2.85

$C_P = 0.5$

C_L

SPINNER

V/nD = 1.71

C_L

V/nD = 1.80

$C_P = 0.2$

C_L

V/nD = 1.08

C_L

V/nD = 0.90

$C_P = 0.05$

U24
U60
.4E
.8E

C_L

V/nD = 0.54

X

X
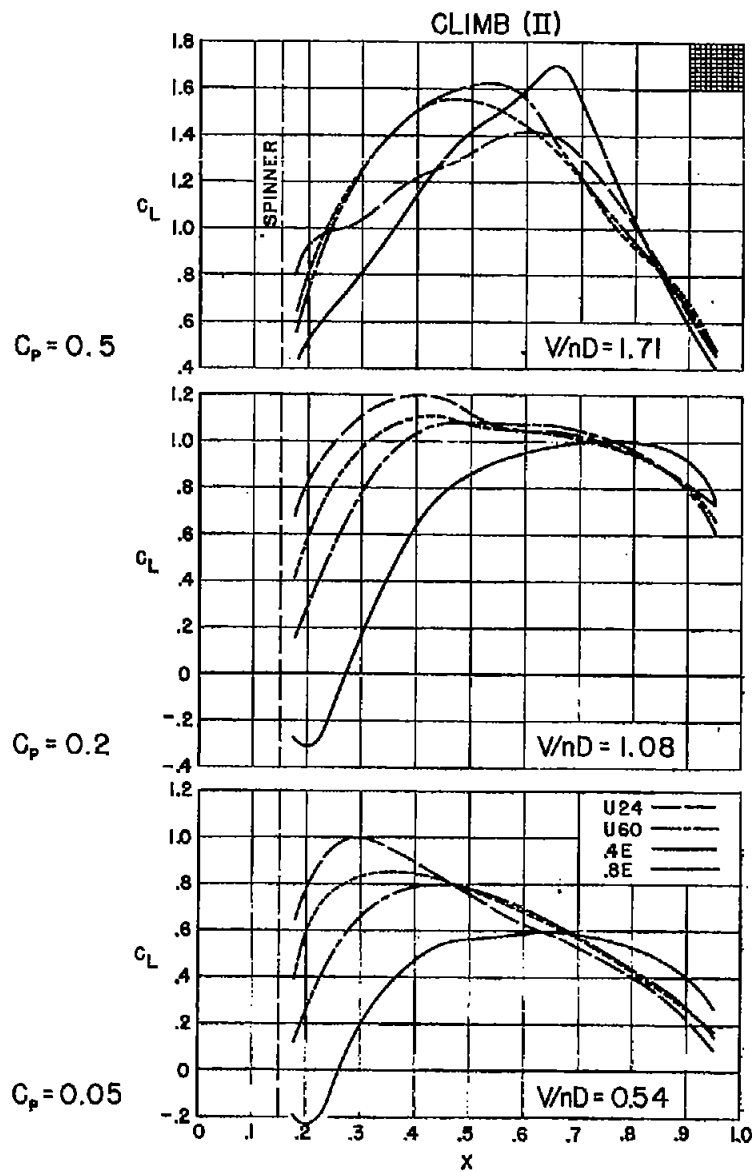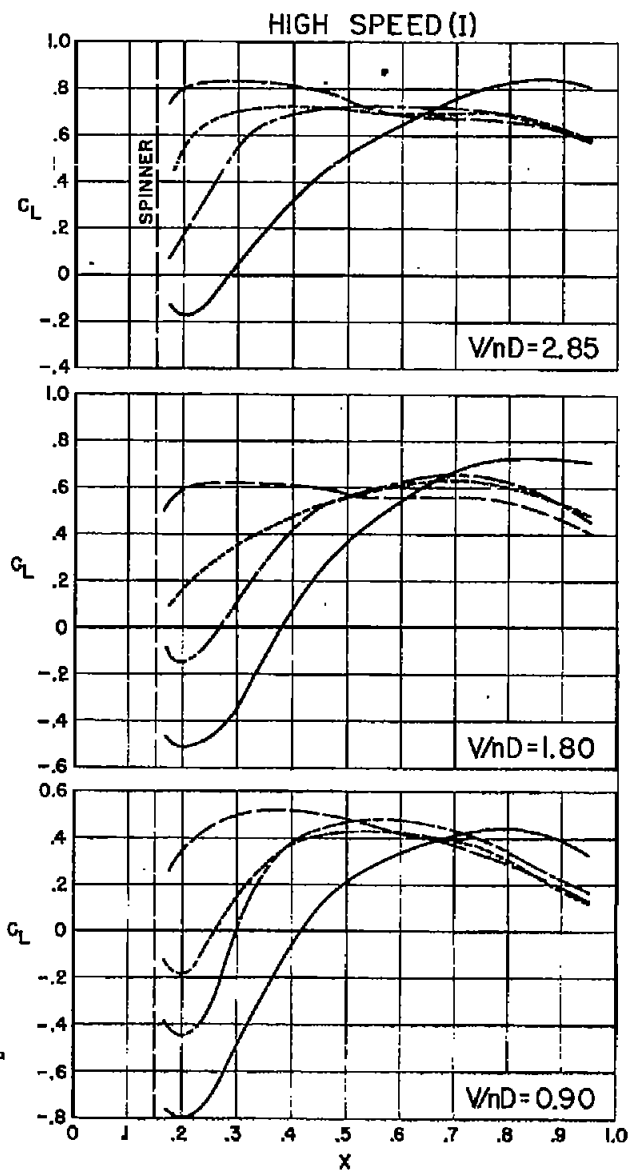
FIG. 47   SECTION LIFT COEFFICIENTS DERIVED FROM FIGURES 41 AND 42
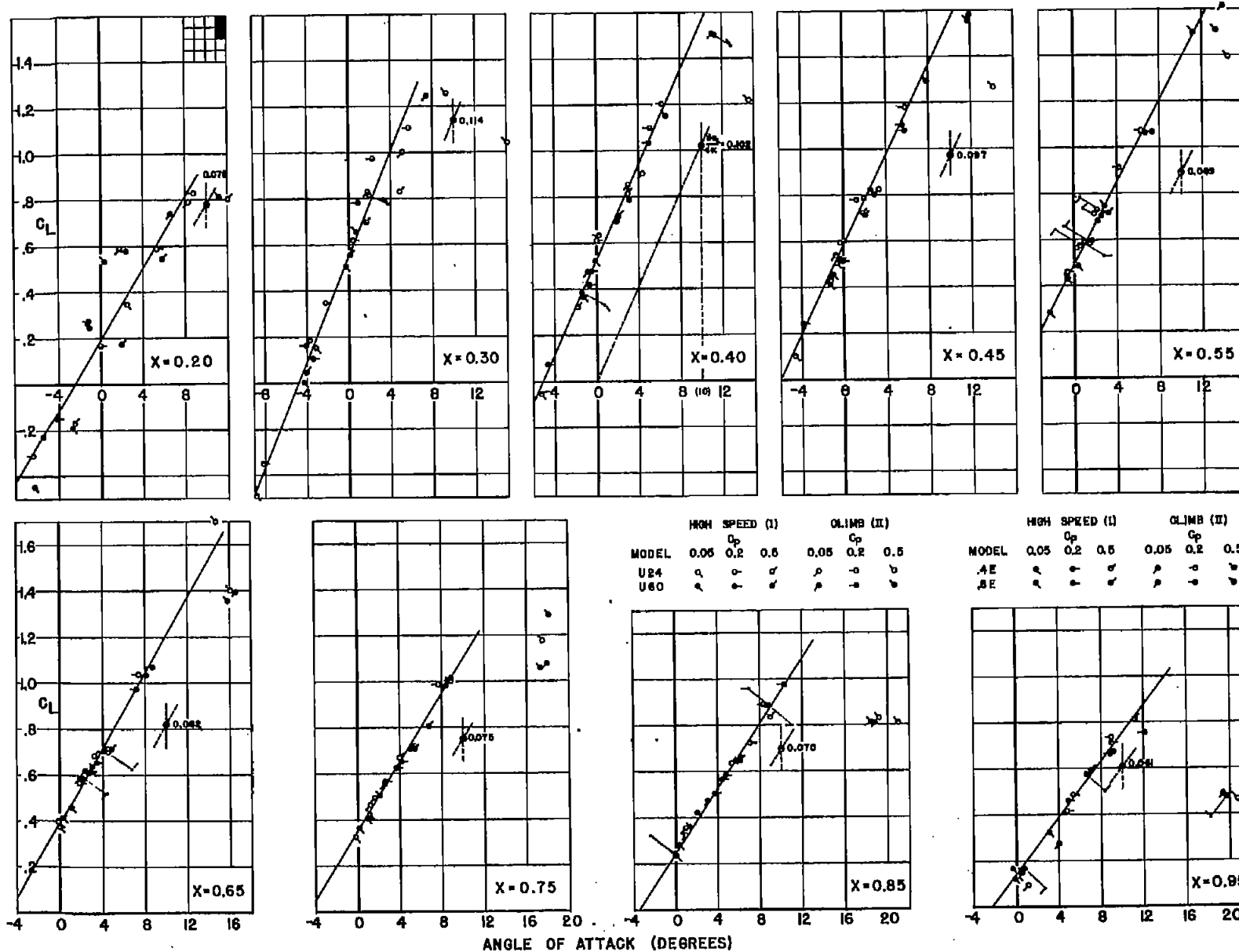
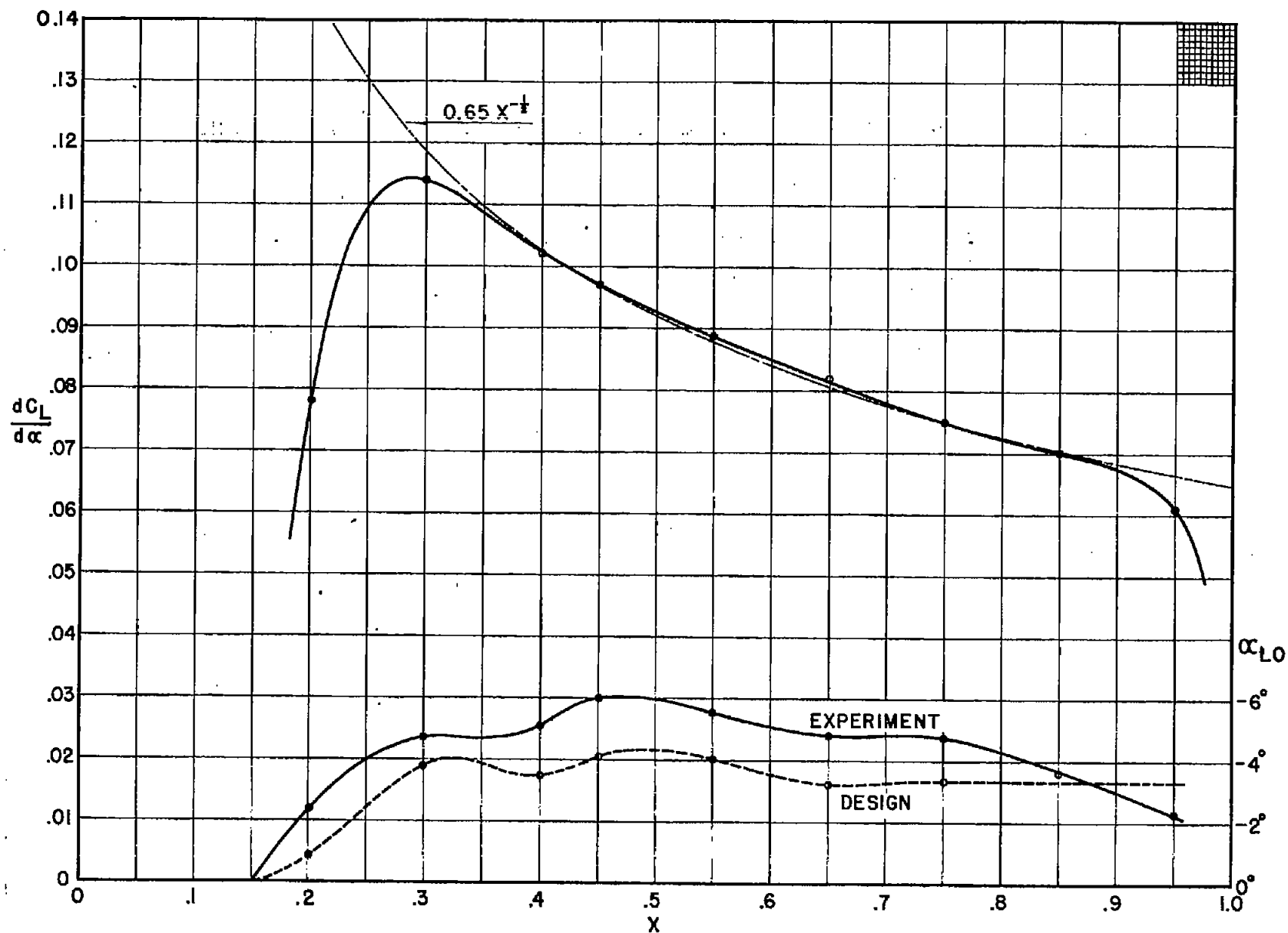FIG. 48   SECTION LIFT COEFFICIENTS DERIVED FROM FIGURES 41 AND 42

Fig. 48
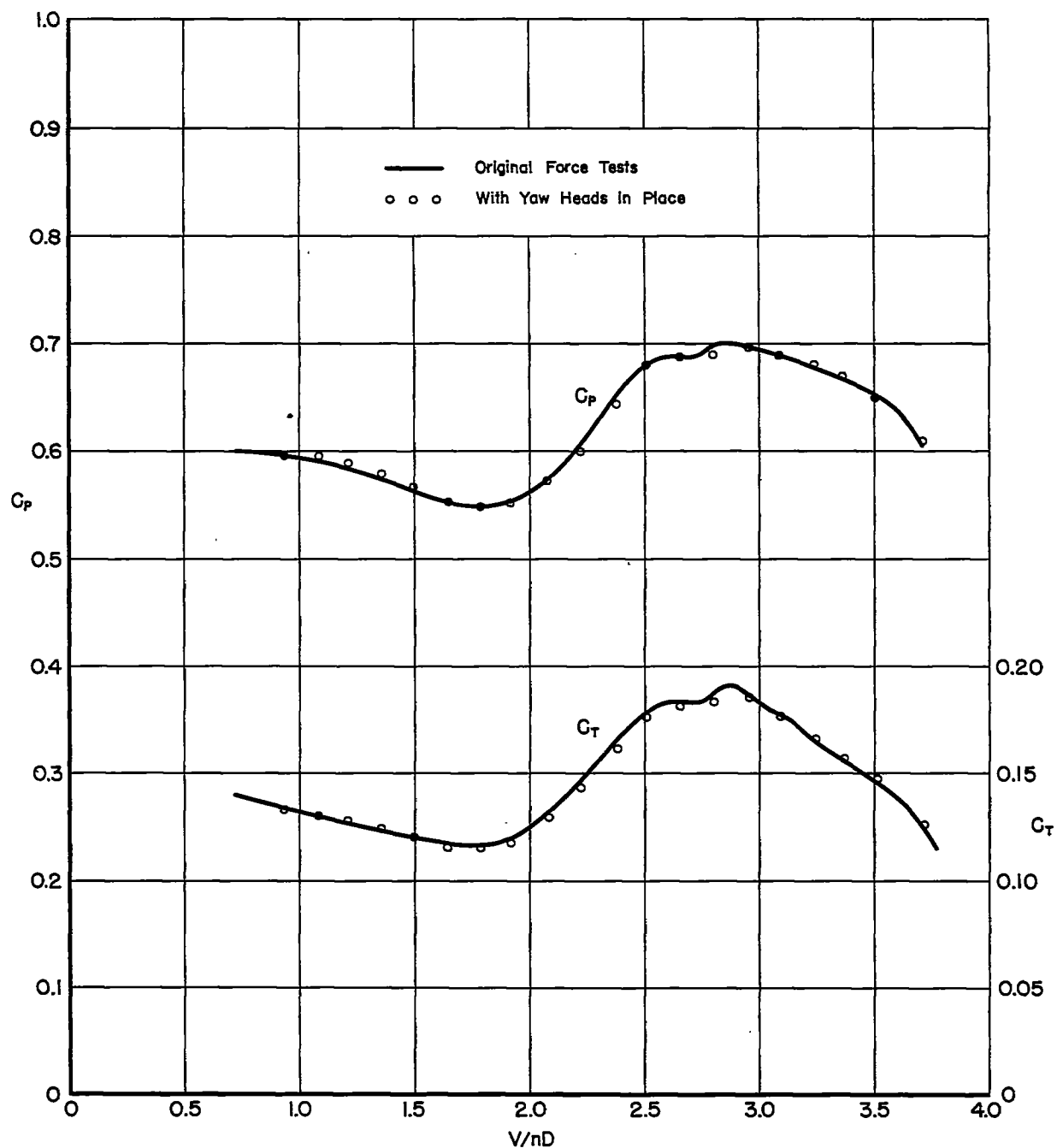
FIG. 49   SECTION CHARACTERISTICS — FROM FIGURE 48

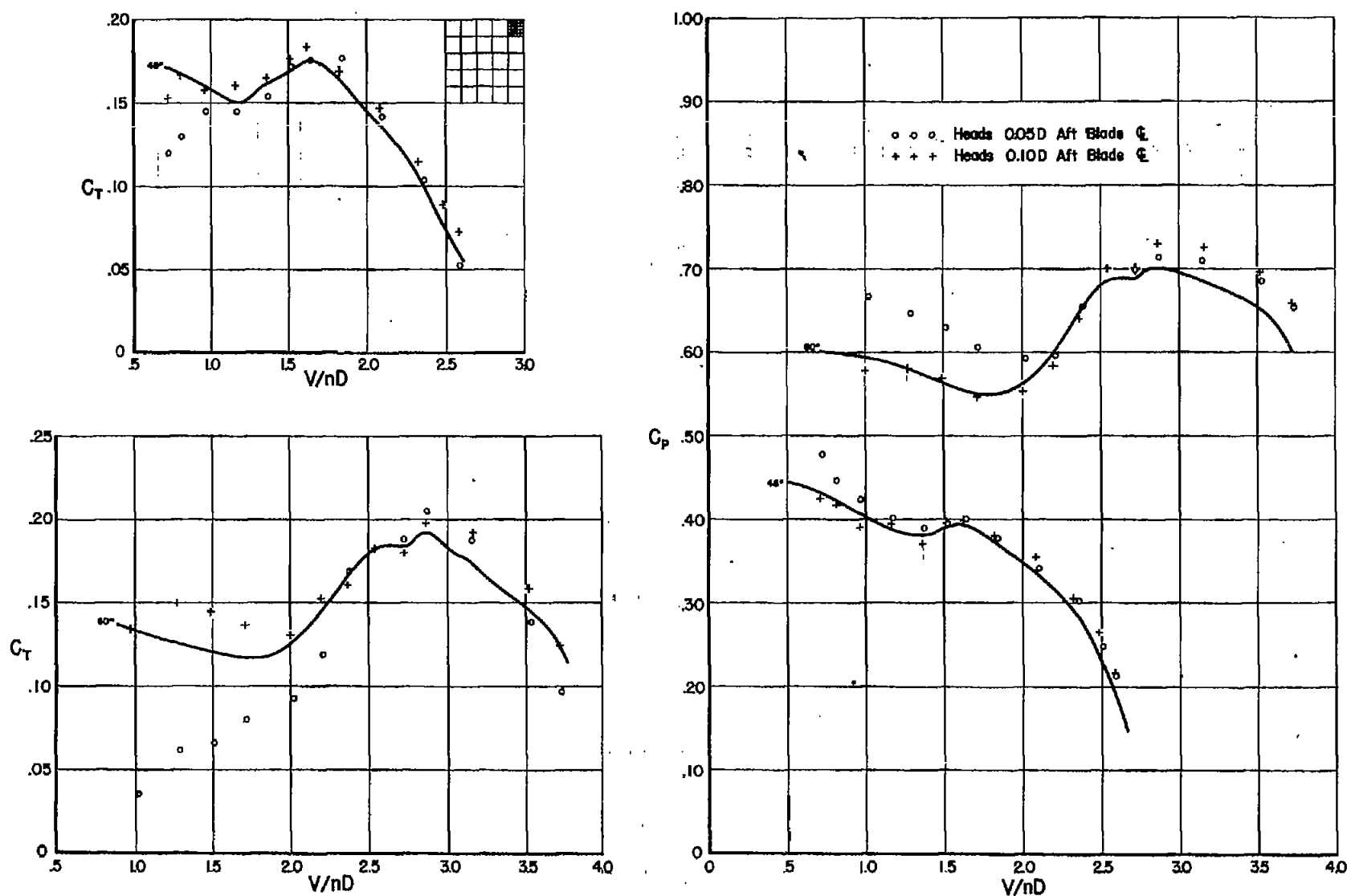FIG. 50   FORCE TESTS OF MODEL U 24 – $\beta_{.75R}$ = 60°

Fig. 51

FIG. 51 EFFECTS OF MOVING YAW HEADS DOWNSTREAM